Lithos 268–271 (2017) 198–224

Contents lists available at ScienceDirect

Lithos

journal homepage: www.elsevier.com/locate/lithos

Invited review article

The role of solid–solid phase transitions in mantle convection

Manuele Faccenda [a,*], Luca Dal Zilio [b]

[a] Dipartimento di Geoscienze, Università di Padova, via Gradenigo 6, 35131 Padova, Italy
[b] Institute of Geophysics, ETH-Zurich, Sonneggstr. 5, 8092 Zurich, Switzerland

ARTICLE INFO

Article history:
Received 4 August 2016
Accepted 3 November 2016
Available online 12 November 2016

Keywords:
Phase transitions
Metastability
Mantle convection
Numerical modelling

ABSTRACT

With changing pressure and temperature conditions, downwelling and upwelling crustal and mantle rocks experience several solid–solid phase transitions that affect the mineral physical properties owing to structural changes in the crystal lattice and to the absorption or release of latent heat. Variations in density, together with phase boundary deflections related to the non-null reaction slope, generate important buoyancy forces that add to those induced by thermal perturbations. These buoyancy forces are proportional to the density contrast between reactant and product phases, their volume fraction, the slope and the sharpness of the reaction, and affect the style of mantle convection depending on the system composition. In a homogeneous pyrolitic mantle there is little tendency for layered convection, with slabs that may stagnate in the transition zone because of the positive buoyancy caused by post-spinel and post-ilmenite reactions, and hot plumes that are accelerated by phase transformations in the 600–800 km depth range. By adding chemical and mineralogical heterogeneities as on Earth, phase transitions introduce bulk rock and volatiles filtering effects that generate a compositional gradient throughout the entire mantle, with levels that are enriched or depleted in one or more of these components.
Phase transitions often lead to mechanical softening or hardening that can be related to a different intrinsic mechanical behaviour and volatile solubility of the product phases, the heating or cooling associated with latent heat, and the transient grain size reduction in downwelling cold material. Strong variations in viscosity would enhance layered mantle convection, causing slab stagnation and plume ponding.
At low temperatures and relatively dry conditions, reactions are delayed due to the sluggish kinetics, so that non-equilibrium phase aggregates can persist metastably beyond the equilibrium phase boundary. Survival of low-density metastable olivine, Ringwoodite, pyroxene and pyrope garnet in the transition zone and uppermost lower mantle produces positive buoyancy forces that decrease the subduction velocity and may lead to slab stagnation in the transition zone. The presence of deep metastable portions is still debated, and should not be associated a-priori with a completely dry slab as field observations suggest that heterogeneously hydrated oceanic plates could contain metastable dry portions surrounded by transformed wet rocks.

Contents

* Corresponding author.
E-mail address: manuele.faccenda@unipd.it (M. Faccenda).

http://dx.doi.org/10.1016/j.lithos.2016.11.007
0024-4937/

1. Introduction

Mantle convection is the main process by which excess heat is extracted from the Earth's interior. One of the most important characteristics of mantle convection is the establishment of ascending hot and descending cold currents that in an ideal viscous fluid layer will encounter no impediment to vertical flow. Seismic tomographies suggest, however, that on Earth the vertical motion of the convective currents is hampered at transition zone and mid-mantle depths, where some slabs and plumes appear to be deflected horizontally (e.g., French and Romanowicz, 2015; Fukao and Obayashi, 2013; Rickers et al., 2013). The nature of these obstacles to vertical flow is debated, although it is commonly related to important variations in the physical properties of mantle minerals (King, 2016) or to the presence of chemically distinct reservoirs (Ballmer et al., 2015).

Over the last few decades, several laboratory and theoretical studies have robustly documented that, as oceanic plates are recycled in the mantle, mafic and ultramafic rocks experience a series of solid–solid phase transformations that tend to thermodynamically re-equilibrate the system with the new pressure and temperature conditions. A reversed series of reactions is expected to occur in upwelling plumes, although with non-negligible dissimilarities due to the different plume temperature (and possibly composition) relative to cold subducting slabs. Solid–solid phase transitions are often accompanied by significant variations in the mineral physical properties such as density and viscous mechanical behaviour. As a result, these phase transformations introduce first-order thermomechanical effects in the convective mantle system that can fundamentally affect the patterns of (layered, intermittent or whole) mantle convection and, consequently, the degree of chemical mixing of the Earth's interior.

Complementing laboratory experiments, numerical simulations have provided a unique tool to explore the thermomechanical and chemical consequences of equilibrium and disequilibrium phase transitions. Several authors have critically assessed the results of both laboratory and numerical studies. For instance, phase equilibria of oceanic crustal and mantle rocks in dry or wet conditions have been reviewed by (Akaogi, 2007; Irifune and Tsuchiya, 2015; Litasov and Ohtani, 2007; Ringwood, 1991; Stixrude and Lithgow-Bertelloni, 2011). A review of numerical experiments that have evaluated the role of olivine phase transitions at transition zone depths can be found in (Christensen, 1995). More recently, (Tackley, 2012) and (Hirose et al., 2015) focused on the effects of phase transformations occurring in the deep lower mantle, while (Tackley, 2015) discussed the chemical layering induced by phase transitions in a compositionally differentiated mantle. (Kirby et al., 1996) have summarized the effects of olivine and pyroxene disequilibrium transformations within the cold lithospheric mantle, although with particular emphasis on deep earthquakes and strain localization.

The aim of this review paper is to provide a comprehensive and updated description of solid–solid phase transformations at equilibrium and disequilibrium conditions and of their effects on mantle convection. In the first part of the review we introduce equilibrium phase transitions in mafic and ultramafic rocks that participate actively to mantle convection (in this respect, solid–solid phase transitions in the continental crust and sediments will be only marginally considered). The second part deals with disequilibrium transformations that are relevant in cold and dry lithospheric environments where metastable phases may survive beyond the equilibrium boundary due to the sluggish reaction kinetics. Here, an additional section regarding the thermokinetic modelling perspective and seismological evidence for the presence of deep metastable regions is provided. For both equilibrium and disequilibrium reactions we discuss the thermomechanical and chemical implications, together with a brief description of the numerical methods commonly employed in mantle convection simulations to account for phase transitions.

2. Equilibrium phase transitions

2.1. Phase equilibria and major solid–solid phase transitions in the oceanic crust and mantle

A widely accepted petrological model for the upper mantle that is used to explain formation by decompressional melting of a petrologically and chemically stratified oceanic plate is pyrolite (Ringwood, 1991). Oceanic plates formed at oceanic ridges with medium to high spreading rates are composed of a 6–7 km thick crust with enriched MORB composition, overlying a 5–20 km thick depleted harzburgitic layer and deeper lherzolitic/pyrolitic layers that have experienced successively smaller degrees of partial melting (Ringwood, 1982). In the following discussion we will review the phase equilibria and the most important phase transitions obtained in laboratory experiments at different mantle depths and for the different oceanic plate bulk rock compositions. We should bear in mind, however, that several discrepancies exist among experimentally determined phase boundaries, since they are affected by the experimental procedure, the kinetics of transformation, pressure standards and equations of state used for pressure calibration (with increasing depth, the predicted pressures can differ by several GPa, yielding different depths and Clapeyron slopes), difficulties in estimating the correction for measured temperatures at high pressure, and different sample composition (Ohtani and Sakai, 2008).

The phase proportions for pyrolite, harzburgite and MORB compositions computed at equilibrium conditions with HeFESTo (Stixrude and Lithgow-Bertelloni, 2011) along the reference 1600 K adiabat are reported in Fig. 1. Density for the different bulk rock compositions and their relative density contrasts are shown in, respectively, Figs. 2 and 3 as a function of P–T conditions of the uppermost 1000 km of the mantle. The reaction slopes for the most important phase transitions are listed in Table 1.

Phase transitions within the thin sedimentary cover atop the subducting oceanic plates will not be discussed in this review article. In brief, they are characterized by a series of devolatilization reactions and solid–solid phase transformations that lead to dry aggregates of clinopyroxene, garnet and high-pressure carbonate phases (Kerrick and Connolly, 2001).

2.1.1. Pyrolitic mantle

At shallow depths, the fertile pyrolitic mantle consists of olivine, diopside, enstatite and pyrope-rich garnet (Fig. 1B). With increasing pressure, the Ca-rich clinopyroxene and the Ca-poor orthopyroxene are gradually dissolved into pyrope-rich garnet to form Al-poor majoritic garnet, which is the most abundant mineral next to Wadsleyite or Ringwoodite in the transition zone (Akaogi, 2007). The incorporation of enstatite and of its high-pressure polymorph (clinoenstatite) in garnet occurs in the upper mantle, while that of diopside in the uppermost transition zone, resulting in a marked density increase of the pyrolitic aggregate (+120 kg/m^3). On the other hand, olivine transforms to Wadsleyite at ~13.5 GPa and further to spinel-structured Ringwoodite at ~18 GPa, causing, respectively, the 410 km and 520 km seismic discontinuities, respectively. Both polymorphic reactions have a positive Clapeyron slope, with the former transformation having a gentler slope (+1–4 MPa/K) but a larger density contrast (+206 kg/m^3) than the Wadsleyite ⇔ Ringwoodite transformation (3–7 MPa/K, +102 kg/m^3) (Table 1). The presence of water decreases the depth of the olivine ⇔ Wadsleyite transformation, modifies its sharpness and increases the Clapeyron slope (Chen et al., 2002a; Litasov and Ohtani, 2003; Smyth and Frost, 2002).

Toward the lower part of the transition zone, the Ringwoodite-majoritic garnet assemblage transforms to a perovskitic assemblage

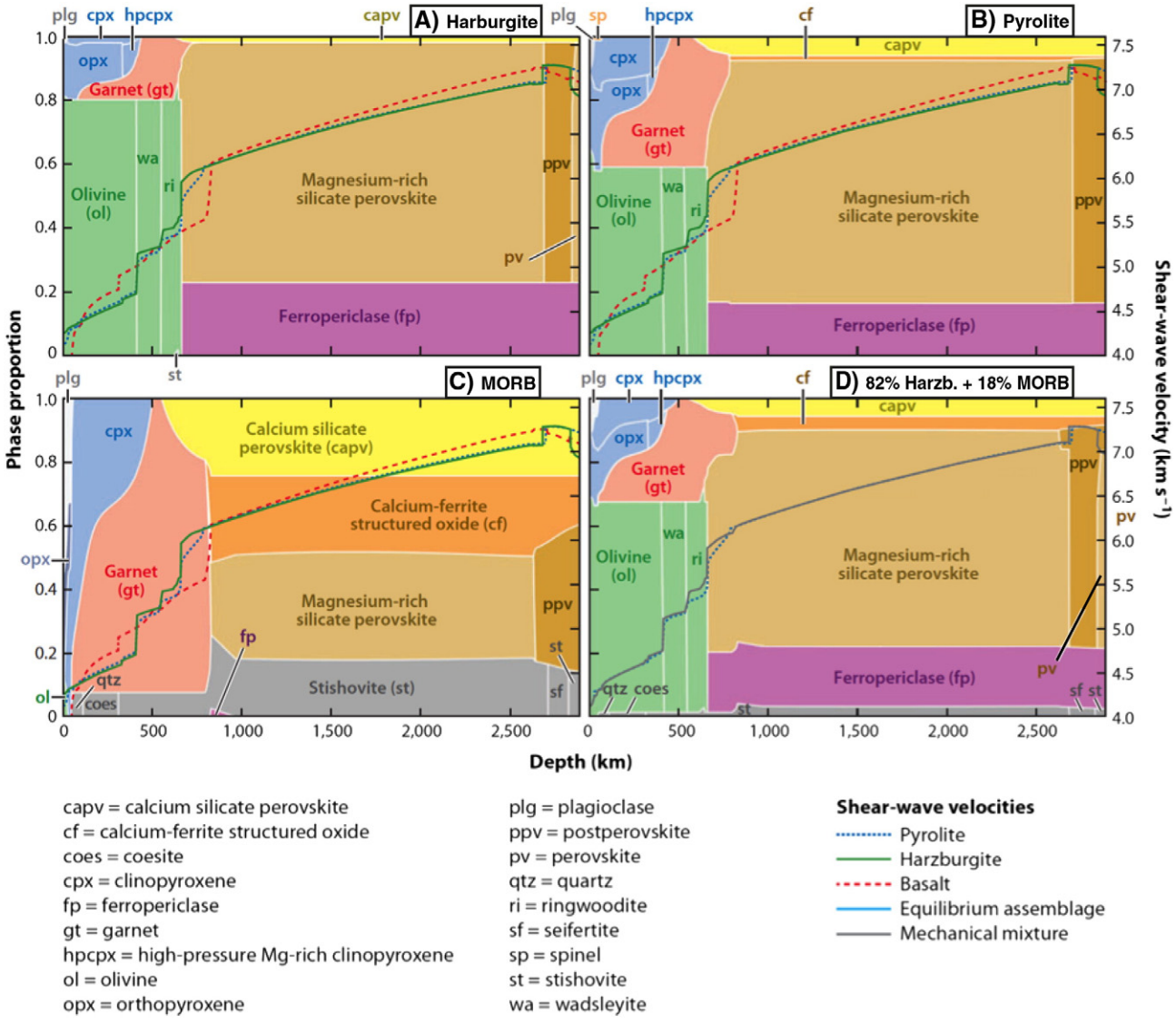

Fig. 1. Phase proportions (atomic fraction) of A) harzburgite, B) pyrolite, C) basalt, and D) a mechanical mixture of 18% basalt and 82% harzburgite equal in overall bulk composition to pyrolite. Superimposed are the shear-wave velocities of pyrolite (dotted blue line), harzburgite (solid green line), basalt (dashed red line), and the mechanical mixture (solid grey line). Curves are repeated in multiple panels to permit direct comparison. Phase proportions and velocity vary with composition in an equilibrium assemblage (solid light blue line) and a mechanical mixture of the end-member compositions (solid grey line). Computed with HeFESTo (Stixrude and Lithgow-Bertelloni, 2011). All bulk compositions are taken from (Xu et al., 2008). From (Stixrude and Lithgow-Bertelloni, 2012).

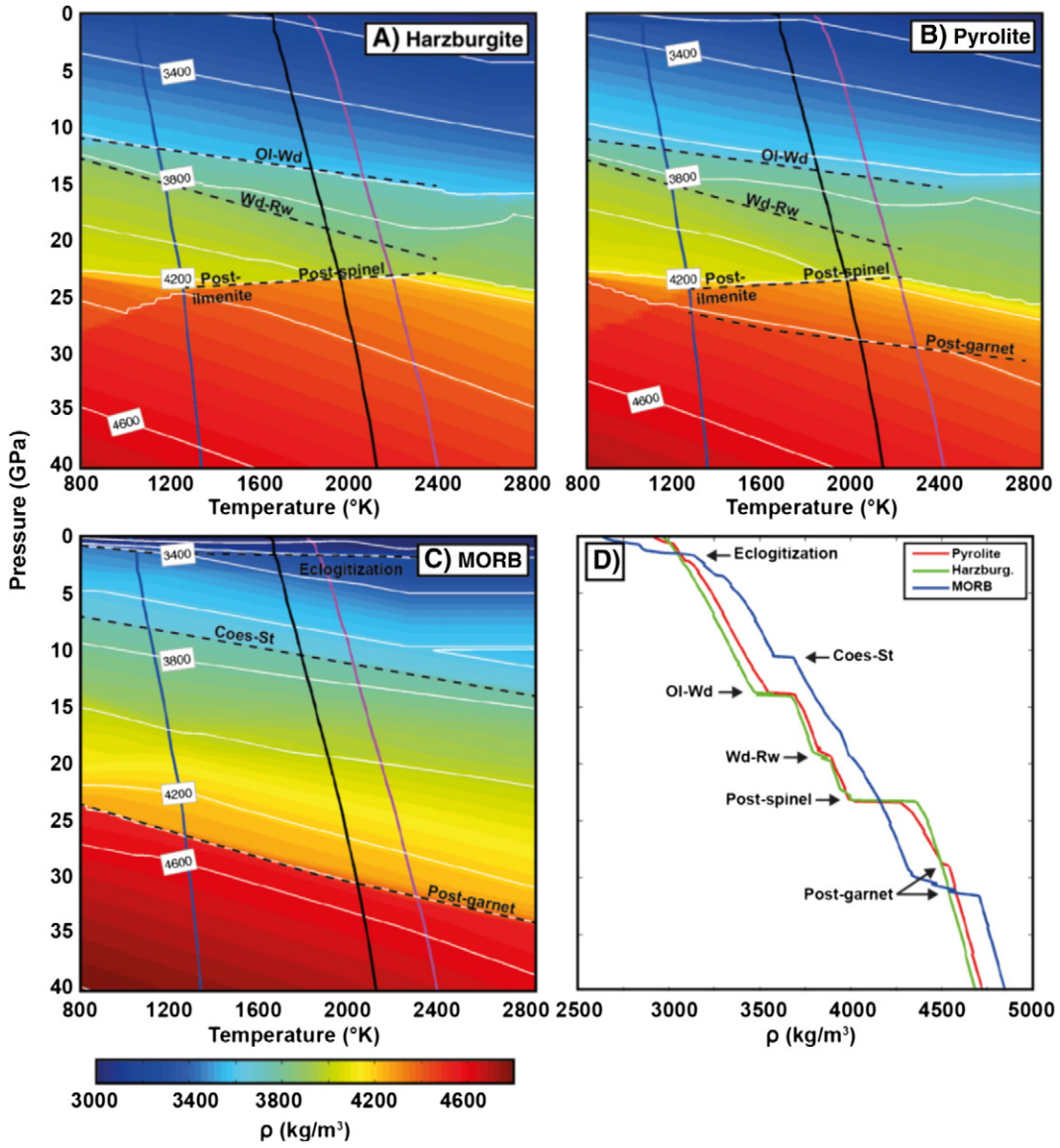

Fig. 2. Density of A) harzburgite, B) pyrolite and C) MORB in the uppermost ~1000 km of the Earth at equilibrium. The blue, black and magenta lines are the 1000, 1600 and 1800 K adiabats, corresponding to approximately the slab interior, ambient mantle and hot plume. Dashed lines indicate major phase transitions associated with large density variations. D) Density profiles along the reference 1600 K adiabat. Computed with HeFESTo (Stixrude and Lithgow-Bertelloni, 2011) for the bulk compositions as in Fig. 1.

(~76% Al-bearing Bridgmanite (Mg-perovksite), ~17% ferropericlase and ~7% Ca-perovskite) via the post-spinel decomposition reaction (Ringwoodite ⇔ Bridgmanite + ferropericlase; +322 kg/m^3) and the gradual disappearance of garnet that culminates with the post-garnet reaction (+480 kg/m^3) (Hirose, 2002; Irifune, 1994; Nishiyama et al., 2004; Stixrude and Lithgow-Bertelloni, 2011). More precisely, Ringwoodite decomposes at about 23–25 GPa either to (i) Akimotoite with ilmenite-type structure and ferropericlase at T < 1100–1400 °C, (ii) Bridgmanite and ferropericlase at T < 1800 °C or (iii) majoritic garnet and ferropericlase for higher temperatures (Hirose, 2002; Ishii et al., 2011; Nishiyama et al., 2004; Yu et al., 2011). In the ambient mantle, the multicomponent majoritic garnet progressively decomposes into Ca-perovskite and Al-bearing Bridgmanite. Ca-perovskite exsolves from majorite in the 20–25 GPa pressure range (Akaogi, 2007), while formation of Al-bearing Bridgmanite from majoritic garnet starts at about 22.5–23 GPa and is smeared out over a pressure interval (1–3 GPa) that increases with temperature (due to the positive slope of the post-garnet reaction) and the Al content (Hirose, 2002; Irifune and Ringwood, 1987; Ishii et al., 2011). At temperatures below 1400–1600 °C, instead, majoritic garnet decomposes into Ca-perovskite and its high-pressure polymorph Akimotoite (+5 MPa/K), which further transforms to Bridgmanite through the post-ilmenite reaction (from −2 to −6 MPa/K) (Hirose, 2002; Ishii et al., 2011; Yu et al., 2011). The relatively sharp post-spinel transition (<1 GPa) is believed to be the main cause of the 660 km seismic discontinuity, while the smeared out transition majorite ⇔ Bridgmanite should produce more gradual density and velocity variations at normal mantle conditions (Hirose, 2002; Ishii et al., 2011; Stixrude and Lithgow-Bertelloni, 2011).

As the negative Clapeyron slope of the post-spinel transformation has important implications for mantle convection, several groups have attempted to investigate its nature by means of laboratory experiments or molecular ab-initio models over the last decades. There are significant discrepancies among different estimates of the negative reaction slope (from −0.5 to −4 MPa/K) and of the depth of the transformation (21–24 GPa). While earlier laboratory studies found a steep negative slope (−2 to −4 MPa/K; Hirose, 2002; Irifune et al., 1998; Ito and Takahashi, 1989; see Table 1), more recent estimates have progressively reduced the slope of the post-spinel transition (−0.5 to −1.3 MPa/K; Fei et al., 2004; Ishii et al., 2011; Katsura et al., 2003; Litasov et al., 2005a, 2005b). (Ohtani and Sakai, 2008) explained this discrepancy by arguing that,

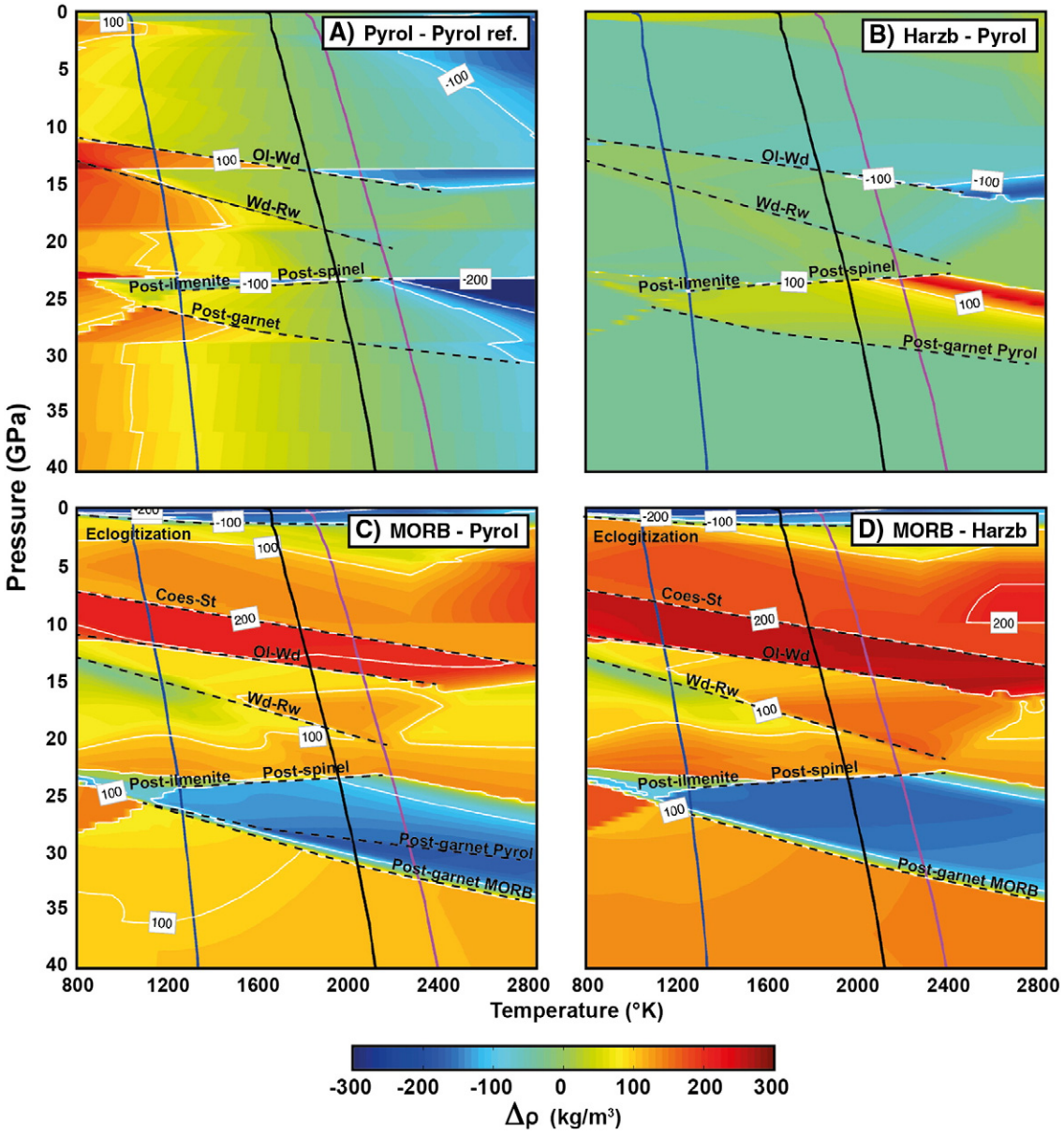

Fig. 3. Density contrasts in the uppermost ~1000 km of the Earth at equilibrium between A) pyrolite and pyrolite along the reference 1600 K adiabat representative of the ambient mantle, B) harzburgite and pyrolite, C) MORB and pyrolite, D) MORB and harzburgite. Density contrasts in A) arise from temperature variations with respect to the reference ambient mantle and phase transitions, while those in B), C) and D) from the difference in composition between the two rock types and phase transitions. The blue, black and magenta lines are the 1000, 1600 and 1800 K adiabats, corresponding to approximately the slab interior, ambient mantle and hot plume. Dashed lines indicate major phase transitions associated with large density variations. Computed with HeFESTo (Stixrude and Lithgow-Bertelloni, 2011) for the bulk compositions as in Fig. 1.

besides the difficulties in determining the correct in-situ P–T conditions, old data might have over-estimated the pressure of the phase transition due to slow transformation kinetics at low temperatures. On the other hand, (Ishii et al., 2011) pointed out that experiments on the olivine Mg_2SiO_4 system yield higher slopes than in the more appropriate pyrolite composition.

Because a small Clapeyron slope cannot account for the observed depth variations of the 660 km discontinuity (+20 to −50 km, requiring a −2.5 or −3 MPa/K slope; Fukao et al., 2009; Lebedev et al., 2002) with a reasonable temperature change at the bottom of the transition zone, (Litasov et al., 2005a) and (Ghosh et al., 2013) suggested that the topography of the 660 km discontinuity can be partly explained by the presence of water yielding more negative Clapeyron slopes (−2 to −3.2 MPa/K). Conversely, recent molecular ab-initio models (Yu et al., 2007) and laser-heated diamond anvil cell experiments (LHDAC) on dry MAS and CFMAS systems (Ye et al., 2014) yielded more negative slopes (−2.5 to −3 MPa/K) for the post-spinel transition that, differently from the results obtained by quench and in-situ multianvil press experiments (Fei et al., 2004; Hirose, 2002; Ishii et al., 2011; Katsura et al., 2003; Litasov et al., 2005b), could explain the observed 660 km topography by temperature variations alone.

(Hirose, 2002) and (Ishii et al., 2011) found that the Clapeyron slope of the transition to the lower mantle perovskitic phase aggregate is temperature dependent. At temperatures below 1800 °C, it is defined by the post-ilmenite and post-spinel reactions with negative Clapeyron slopes. At higher temperatures, however, a substantial fraction of Ringwoodite decomposes into majoritic garnet and ferropericlase with a small density variation and either a slightly negative or, with increasing temperature, positive Clapeyron slope. With increasing pressure, garnet transforms to Bridgmanite with a positive reaction slope (+1.3–4 MPa/K) and a much larger density variation. Thus, at temperatures above 1800 °C typical of upwelling hot plumes, the transition from the

Table 1
Major phase transitions in MORB and pyrolitic/harzburgitic mantle compositions which posses a meaningful Clapeyron slope.

Phase transition	γ (MPa/K)	Composition	Reference
Amphibolite ⇔ Eclogite	1–1.5	MORB + H_2O	Hacker et al. (2003)
P = 1–2 GPa (30–60 km)			
T > 800 K			
$\Delta\rho$ = 200–300 kg/m^3 (6–9%)			
Bluescist ⇔ Eclogite	−30	MORB + H_2O	Hacker et al. (2003)
P = 1–3 GPa (30–90 km)			
T = 740–800 K			
$\Delta\rho$ = 200–300 kg/m^3 (6–9%)			
Coesite ⇔ Stishovite	3.1	SiO_2	Liu et al. (1996)
P = 9–10 GPa (270–300 km)	2.6	SiO_2	Zhang et al. (1996)
T = 1760 K			
$\Delta\rho$ = 1165 (32%)			
Olivine ⇔ Wadsleyite	1.5 ± 0.5	$Fo_{89}Fa_{11}$	Akaogi et al. (1989)
P = 13.5 GPa (410 km)	2.5	$Fo_{89}Fa_{11}$	Katsura and Ito (1989)
T = 1810 K	4	$Fo_{89}Fa_{11}$	Katsura et al. (2004)
$\Delta\rho$ = 206 (5.9%)	2.95 ± 0.05	Fo_{100}	Bina and Helffrich (1994)
	3.6 ± 0.2	Fo_{100}	Morishima et al. (1994)
	2.1–2.4	Fo_{100} (theory)	Yu et al. (2008)
	2.8	Fo_{100} (theory)	Hernandez et al. (2015)
	~5	Pyrolite + H_2O	Litasov and Ohtani (2003)
Wadsleyite ⇔ Ringwoodite	5	$Fo_{89}Fa_{11}$	Katsura and Ito (1989)
P = 18 GPa (520 km)	3	Fo_{100}	Kuroda et al. (2000)
T = 1870 K	7	Fo_{100}	Suzuki et al. (2000)
$\Delta\rho$ = 102 kg/m^3 (2.8%)	4.1	Fo_{100}	Inoue et al. (2006)
	2.8–3.0	Fo_{100}	Yu et al. (2008)
	3.5	Fo_{100} (theory)	Hernandez et al. (2015)
Post-spinel	−2	Fo_{100}	Ito and Yamada (1982)
(Ringwoodite ⇔ Bridgmanite + ferropericlase)	−2.8	Fo_{100}	Ito and Takahashi (1989)
P = 23–24 GPa (650–670 km)	−4 ± 2	Fo_{100}	Ito et al. (1990)
T = 1940 K	−3 ± 1	Fo_{100}	Akaogi and Ito (1993)
$\Delta\rho$ = 322 kg/m^3 (8%)	−2.3 ± 0.8	Fo_{100}	Bina and Helffrich (1994)
	−2.5	Fo_{100}	Chopelas et al. (1994)
	−2.9	Fo_{100}	Irifune et al. (1998)
	−1.2 ± 0.8	Fo_{100}	Katsura et al. (2003)
	−1.3	Fo_{100}	Fei et al. (2004)
	−2	Fo_{100}	Ishii et al. (2011)
	−0.55 ± 0.15	Fo_{100}	Ghosh et al. (2013)
	−2.75 ± 0.15	Fo_{100} (theory)	Yu et al. (2007)
	−3.6	Fo_{100} (theory)	Belmonte (2013)
	−3.9 ± 1.3	Fo_{100} (theory)	Hernandez et al. (2015)
	−3.1	Fo_{100} + 2% H_2O	Ghosh et al. (2013)
	−2.5 ± 0.4	Fo_{100} + 5% Al	Ye et al. (2014)
	−2.8	Pyrolite	Hirose (2002)
	−0.5	Pyrolite	Litasov et al. (2005b)
	−2	Pyrolite + H_2O	Litasov et al. (2005a)
	−1	Pyrolite	Ishii et al. (2011)
	−2.5 ± 0.4	Pyrolite	Ye et al. (2014)
Majorite ⇔ Akimotoite	7.4 ± 0.5	Maj_{100} (theory)	Yu et al. (2011)
P = 15–22.5 GPa (450–640 km)	7.2	Maj_{100} (theory)	Hernandez et al. (2015)
T < 1800 K	~10	Pyrolite	Hirose (2002)
$\Delta\rho$ = 216–230 kg/m^3 (5–6%)	~5	Pyrolite	Ishii et al. (2011)
Post-ilmenite	−2	En_{100}	Ito and Yamada (1982)
(Akimotoite ⇔ Bridgmanite)	−5 ± 2	En_{100}	Ito et al. (1990)
P = 23 GPa (640 km)	−3.4 ± 2	En_{100}	Akaogi and Ito (1993)
T = 1200 K	−4.6	En_{100}	Chopelas (1999)
$\Delta\rho$ = 275 kg/m^3 (6.5%)	−3.2 ± 2	En_{100}	Ono et al. (2001)
	−4 ± 2	En_{100}	Chudinovskikh and Boehler (2004)
	−3.1	En_{100}	Fei et al. (2004)
	−2	En_{100}	Ishii et al. (2011)
	−6 ± 1	En_{100} (theory)	Yu et al. (2011)
	−3.5 ± 0.8	En_{100} (theory)	Hernandez et al. (2015)
Post-garnet	6.4	Natural pyrope	Oguri et al. (2000)
(Garnet ⇔ Bridgmanite)	2.6	Maj_{100}	Chopelas (1999)
P = 21–30 GPa (600–810 km)	1.2 ± 0.3	Maj_{100} (theory)	Yu et al. (2011)
T > 1800 K	1.1	Maj_{100} (theory)	Hernandez et al. (2015)
$\Delta\rho$ = 470–486 kg/m^3 (11–12%)	0.8	MORB	Hirose et al. (1999)

(continued on next page)

Table 1 (*continued*)

Phase transition	γ (MPa/K)	Composition	Reference
	4.1	MORB	Litasov et al. (2004)
	4.9	MORB + H_2O	Litasov and Ohtani (2005)
	1.3	Pyrolite	Hirose (2002)
	0.8	Pyrolite	Hirose and Fei (2002)
	4	Pyrolite	Ishii et al. (2011)
Post-perovskite	7.5	$MgSiO_3$ (theory)	Tsuchiya et al. (2004)
(Bridgmanite ⇔ Mg-post-perovskite)	9.85	$MgSiO_3$ (theory)	Oganov and Ono (2004)
P = 112–122 GPa	7 ± 3	$MgSiO_3$	Ono and Oganov (2005)
(2480–2650 km)	5–11.5	$MgSiO_3$	Hirose et al. (2006)
T = 2500 K	13.3 ± 1	$MgSiO_3$	Tateno et al. (2009)
$\Delta\rho$ = 66 kg/m^3 (1%)	8 ± 5	Pyrolite	Ono and Oganov (2005)
	8 ± 4	Pyrolite	Ohta et al. (2008)
	5.6 ± 0.8	Pyrolite	Grocholski et al. (2012)

Transition to eclogitic aggregates involves a series of devolatilization and solid–solid phase transitions. Theory refers to molecular dynamic simulations. Clapeyron slope values preceded by the "~" symbol were visually calculated from the published phase diagrams, while those with the "±" symbol contain the reported uncertainty. A range of Clapeyron slopes indicates estimates from different pressure calibrations.
Density contrasts of all reactions - except for eclogitization (Hacker et al., 2003) and the post-perovskite reaction (Vilella et al., 2015) — have been estimated with EosFit7 (Angel et al., 2014) by using the THERMOCALC database and a modified Tait EoS (Holland et al., 2013) for Mg-end member phases.

Ringwoodite-majoritic garnet assemblage to the perovskitic assemblage can be assumed to have a positive slope.

Toward the bottom of the lower mantle, Bridgmanite transforms to the high-pressure polymorph Mg-post-perovskite (post-perovskite transition) with a strongly positive Clapeyron slope – estimates vary from +5 to +13 MPa/K depending mostly on the pressure scale – but a small density contrast (+66 kg/m^3) (Murakami et al., 2004; Oganov and Ono, 2004; Tsuchiya et al., 2004). In a pyrolitic mantle, the post-perovskite transformation occurs between 116 and 121 GPa (2550–2640 km) at 2500 K (Hirose et al., 2006; Ohta et al., 2008), although much higher pressures (140–168 GPa at 2500 K) have been reported (Grocholski et al., 2012), implying that Mg-post-perovskite might not exist at all at mantle P–T conditions. The stability field of Bridmanite expands with increasing Al content, while the effect of iron is uncertain (Hirose et al., 2015). If the core-mantle boundary (CMB) temperature is in the post-perovskite stability field, then this phase will exist everywhere in the lowermost mantle. If, however, the CMB temperature is in the Bridgmanite stability field, then the post-perovskite will only exist in colder regions, with a double-crossing of the phase boundary with increasing depth, while in hot areas it would not occur at all (Hernlund et al., 2005). The post-perovskite transition in the lowermost 300–500 km of the mantle is frequently invoked to explain several seismological observations beneath regions of past subduction (e.g., abrupt increases and decreases in velocity, topography of the seismic discontinuity above the "D", increase in seismic anisotropy), which would support the presence of Mg-post-perovskite within colder, deep mantle portions (Hutko et al., 2009; Lay and Garnero, 2013; Sidorin et al., 1999; Wookey et al., 2005).

Two more phase transformations causing, respectively, valence state and spin transitions in iron have been recently proposed to occur in the lower mantle. Upon transition to perovskitic phase aggregate, ferrous iron (Fe^{2+}) in Al-bearing Bridgmanite disproportionates to ferric iron (Fe^{3+}) and iron metal (Fe) (Frost et al., 2004). As a result, the bulk lower mantle could potentially have a Fe^{3+}/total Fe ratio up to 0.4, which is over ten times that of the upper mantle and requires the formation of approximately 1 wt.% of metallic iron-rich alloy. Ferrous iron is likely stabilized in the Bridgmanite structure by energetically favourable coupled substitution with Al (Frost and Myhill, 2016) and can occupy both the large A (Mg^{2+}) and small B (Si^{4+}) cation sites. (Xu et al., 2015) argued, however, that in the uppermost lower mantle, where most Al remains in majoritic garnet, the concentration of Fe^{3+} in Al-poor Bridgmanite and the content of metallic iron are expected to be very low till completion of the post-garnet reaction. The physical consequences of the disproportionation reaction are still poorly understood, and are likely related to the increase in ferric iron content rather than to the formation of minor iron metal.

With increasing pressure, atomic orbitals of iron collapse from the high-spin to the low-spin state, causing a significant ionic volume reduction (up to 52% for Fe^{2+} in ferropericlase) and important changes in the bonding character of one of the Earth's most important elements (Lin et al., 2013; Speziale et al., 2005). As the concentration of iron is approximately 20 mol% in ferropericlase (mostly Fe^{2+}) and about 10 mol% (both Fe^{2+} and Fe^{3+}) in Bridgmanite and Mg-post-perovskite (Lin et al., 2013), this transformation has been the subject of much interest in the last decade since it could have important implications for the seismic and transport properties of mantle silicates. The transition from high spin state to low spin state of the B-site Fe^{3+} in Bridgmanite and Mg-post-perovskite likely occurs in the 15–50 GPa (440–1300 km) pressure interval, while that of Fe^{2+} in ferropericlase between 70 and 125 GPa (1700–2700 km) (Lin et al., 2013). Thus, iron spin transitions in lower mantle minerals appear to take place over a wide depth interval, with physical properties varying smoothly across the transition. The high and low spin states of ferropericlase should exist in the uppermost and lowermost mantle, while low spin state of the B-site Fe^{3+} should be present in the mid and lowermost mantle in Bridgmanite and in the stability field of Mg-post-perovskite. Both Fe^{2+} and Fe^{3+} in the A-site of Bridgmanite and Mg-post-perovskite likely remain in the high spin state through the entire mantle (Lin et al., 2013).

2.1.2. Harzburgitic mantle

Harzburgitic upper mantle is made of ~75–80% olivine and ~20–25% of orthopyroxene, plus a minor amount of clinopyroxene and Cr-spinel (Fig. 1A). Because of the low contents in Al, Ca, and to a less amount in Fe, the phase transitions in the Mg–Fe–O system are thought to be representative of the depleted harzburgitic composition (Irifune and Tsuchiya, 2015). Olivine is subjected to the same polymorphic transformations described for the pyrolitic mantle composition. However, according to (Ishii et al., 2011), the post-spinel reaction has a steeper Clapeyron slope and occurs at shallower depths in comparison to an Al-rich pyrolitic mantle (Table 1). The enstatite dissolution in garnet-poor harzburgite is expected to be minimal, which could lead to the survival of the pyroxene phase down to the transition zone (Ringwood, 1991). Above 8 GPa (about 250 km depth), enstatite transforms to high-pressure clinoenstatite, which has a higher density and seismic velocity of the low-pressure polymorph (Angel et al., 1992; Kung et al., 2005). At about 17 GPa, the high-pressure polymorph of clinoenstatite either dissolves into garnet (T > 1900 K) or decomposes into Wadsleyite and sthishovite (post-pyroxene transformation; Hogrefe et al., 1994). Akimotoite appears at about 19–20 GPa (Chopelas, 1999), although (Irifune and Ringwood, 1987) found that Akimotoite is stable between 22 and 24 GPa in the harzburgite minus olivine system. Decomposition of Ringwoodite and polymorphic transformations of Al-poor garnet and

Akimotoite occur at depths <700 km, and lead to a perovskitic assemblage with Al-poor Bridgmanite (~73%), ferropericlase (~25%) and a minor amount of Ca-perovskite (~2%) that toward the bottom of the lower mantle should transform to a post-perovskitic aggregate. Hence, at lower mantle depths harzburgite contains more ferropericlase than pyrolite. The low Al content in Bridgmanite implies that harzburgite should contain low amounts of ferric iron (Fe^{3+})(Xu et al., 2015).

2.1.3. Oceanic crust: MORB

With increasing pressure, several phase transformations occur within MOR basalts, leading to eclogitic, garnetitic, perovskitic, and post-perovskitic assemblages (Fig. 1C).

Metasomatized basalts and gabbros of the oceanic crust progressively transform to eclogitic phase aggregates via intermediate blueschist (low T), greenschist and amphibolitic (medium to high T) metamorphic facies. Eclogitization of MORB is characterized by the progressive disappearance of plagioclase, substitution of magmatic pyroxene, significant devolatilization of the wet crust related to the decomposition of hydrous phases such as amphibole and lawsonite, and a marked increase in density (+450 kg/m^3) above that of the mantle (Green and Ringwood, 1967; Hacker et al., 2003; Schmidt and Poli, 1998). The set of phase transformations which yield to the eclogitization (and thus to the density crossover) of dry/wet MOR basalts in blueschist or amphibolitic facies occurs between 1 and 3 GPa and above 450 °C at equilibrium. Although not strictly univariant due to solid-solution effects, the transformation from amphibolitic to eclogitic metamorphic facies can be represented by a gentle Clapeyron slope of about 1–1.5 MPa/C for T > 500 °C, while transition from bluescist to eclogitic phase aggregate has a strongly negative Clapeyron slope (Hacker et al., 2003; Schmidt and Poli, 1998) (Table 1).

Eclogites under upper mantle conditions mainly consist of omphacitic pyroxene, pyrope garnet, and ~10% of coesite/stishovite (e.g., Aoki and Takahashi, 2004; Irifune et al., 1986; Okamoto and Maruyama, 2004). Coesite transforms to stishovite at about 9–10 GPa, with a tremendous increase in density (+1165 kg/m^3). The pyroxene components are gradually absorbed into the garnet structure with increasing pressure, forming majoritic garnet. The proportion of garnet increases rapidly above 10 GPa and pyroxene-free majoritic garnetites (+ stihovite) are produced at 14–15 GPa (Irifune et al., 1986). The density of subducting MORB containing 80–90% volume fraction of majoritic garnet (which is denser than the high-pressure olivine polymorphs) increases greatly due to the transformation of eclogite to garnetite, so that at transition zone depths the crust remains negatively buoyant with respect to the surrounding mantle (e.g., Aoki and Takahashi, 2004; Ganguly et al., 2009).

At 600–800 km depth (~21–29 GPa), majoritic garnet progressively decomposes into Ca-perovskite, Bridgmanite and an aluminous phase with $CaFe_2O_4$-type structure (Hirose et al., 1999; Irifune and Ringwood, 1993; Ono et al., 2001). The disappearance of garnet and appearance of Bridgmanite (post-garnet transformation) in MORB occurs within 1 GPa and is characterized by a positive Clapeyron slope, which has been estimated to be either gentle (+0.8 MPa/K; (Hirose et al., 1999) or steep (4.1 MPa/K in dry conditions, (Litasov et al., 2004); 4.0–5.0 MPa/K in wet conditions, but at 1–2 GPa lower pressure, (Sano et al., 2006)). There is also quite a bit of uncertainty in terms of the depth of the post-garnet transformation, with estimates varying from 720 to 800 km in the hot mantle, depending on the Al content and, mostly, on the experimental pressure scale.

Below 720–800 km, MORB composition consists of 35% Bridgmanite, 25% $CaFe_2O_4$-type aluminous phase, 23% Ca-perovskite and 17% stishovite (Hirose et al., 2005; Ono et al., 2001). Stishovite transforms to $CaCl_2$-type SiO_2 above 62 GPa and 2000 K and further to α-PbO_2-type in the 112–118 GPa pressure range at 2500 K. Bridgmanite transform to Mg-post-perovskite in the same pressure range at 2500 K, with the transformation having a strongly positive Clapeyron slope and occurring at 4 GPa lower pressure than that in pyrolitic composition (Grocholski et al., 2012; Ohta et al., 2008). The aluminous phase and Ca-perovskite are stable to the bottom of the mantle.

2.2. Thermomechanical effects and chemical implications

2.2.1. Buoyancy and thermal effects

In the presence of a thermal perturbation, the equilibrium phase boundary of reactions with a positive/negative Clapeyron slope is deflected to different depths with respect to the ambient mantle. For reactions with a positive Clapeyron slope (as the higher density phase is formed, these reactions are exothermic), such as the olivine polymorphic transformations, the garnet ⇔ Akimotoite, the post-garnet and post-perovskite reactions, the high-pressure and denser phase forms at lower depths in cold subducting slabs and deeper in hot upwelling plumes. These transformations provide additional buoyancy forces that favour mantle convection and that are comparable to those arising from thermal contraction or expansion (10^{12}–10^{13} N/m; Billen, 2010; Schubert et al., 1975). The latent heat released during subduction or absorbed during upwelling diminishes the exothermic phase boundary distortion and induces density variations, both partly counteracting the effect due to the positive slope of the phase boundary. On the other hand, phase transformations with a negative Clapeyron slope (as the higher density phase is formed, these reactions are endothermic), hamper mantle convection because of the induced positive and negative buoyancy forces in, respectively, subducting cold slabs (where the post-spinel and the post-ilmenite reactions are effective) and upwelling hot material. Latent heat absorbed during subduction and released during upwelling further distorts the endothermic phase boundary away from their normal depths, and at the same time produces density variations that favour the flow instability (Schubert et al., 1975).

The buoyancy force and latent heat generated by the non-null slope of phase transformations are proportional to the density contrast between the reactant and product phases, their volume fraction and to the steepness of the reaction slope. Buoyancy and thermal effects on mantle convection are maximal for univariant, single-component reactions and progressively diminish with increasing depth interval needed to bring a multicomponent reaction to completion. Phase transitions in the natural rocks are not strictly univariant because minerals are solid solutions. However, many reactions such as the olivine polymorphic transformations and the post-spinel reactions can be approximated as univariant because they occur over a narrow pressure range (<1 GPa). On the other hand, the progressive disappearance of pyroxene and majoritic garnet should be broader in depth-extent by about an order of magnitude than the transitions in olivine and their contributions to local density anomalies and hence buoyancy forces should be considerably more diffuse (Bina et al., 2001). Indeed, the breadth of transitions involving garnet-bearing assemblages reflects their highly multivariant nature, so that in a natural multicomponent system they may not possess meaningful Clapeyron slopes (which are strictly defined only for univariant reactions). Similar arguments can be applied to the iron spin transition occurring over a wide pressure interval. For these reasons, numerical studies of mantle convection have primarily addressed the role of phase transformations that are associated with abundant mineral phases, significant volume changes, and that occur over a narrow pressure interval, such as the early recognized olivine polymorphic and post-spinel reactions. As a result, it was found that the additional buoyancy induced by these phase transformations strongly affects mantle convection. However, recent laboratory and numerical experiments demonstrated that the number and efficiency of the buoyancy perturbations varies considerably with the chosen system composition, as schematically depicted in Fig. 4.

Olivine system (Fig. 4A). The buoyancy and thermal effects of the post-spinel endothermic phase transition has been investigated with 2D and 3D numerical models at the global and regional scale. Isoviscous global convection models with a strongly negative Clapeyron slope of −3 or −4 MPa/K for the post-spinel reaction are characterized by accumulation of downwelling cold material in the transition zone, which eventually sinks rapidly into the lower mantle during episodic avalanche events (Fig. 5). This process generates long-wavelength lateral

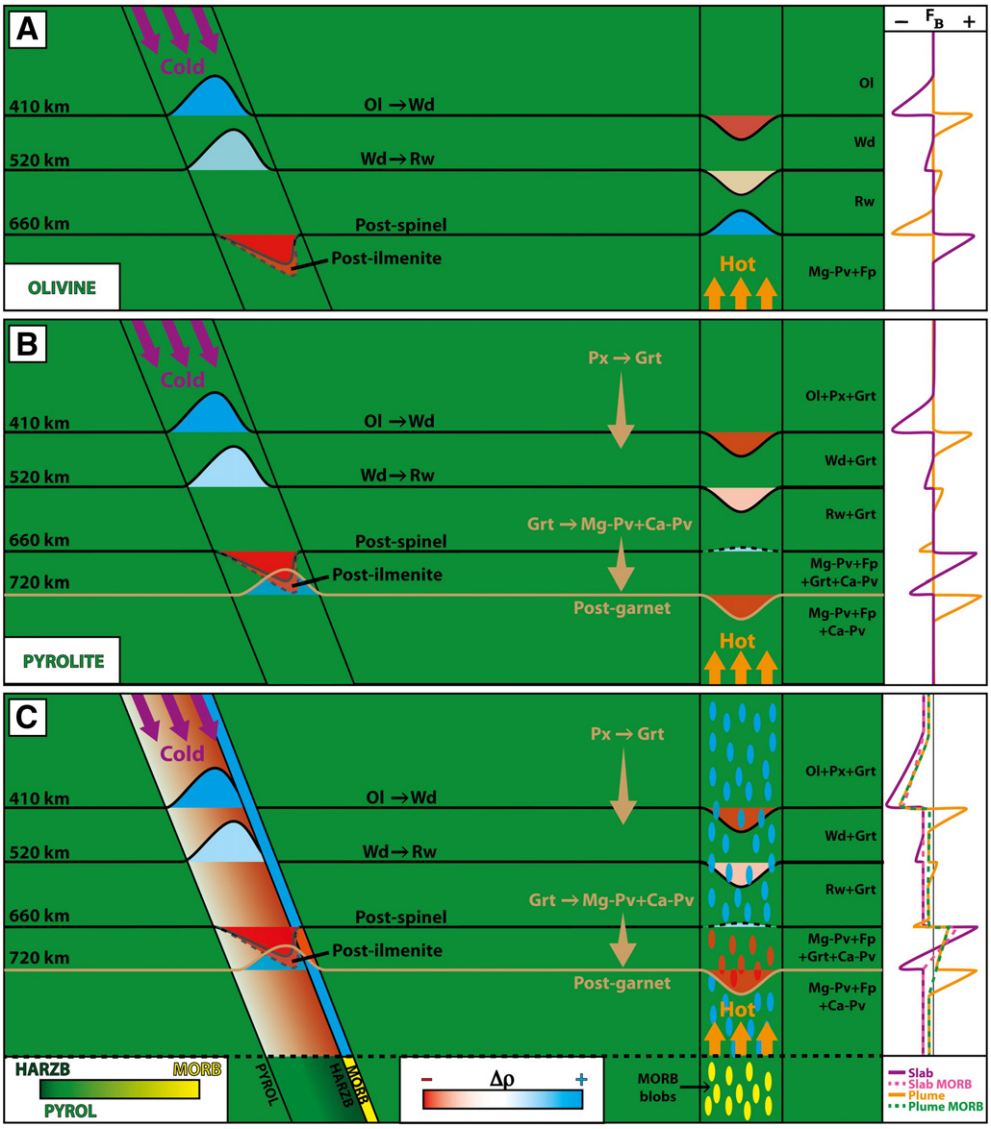

Fig. 4. Schematic representation of the buoyancy effects due to major phase transformations occurring at equilibrium around the transition zone in a subducting cold slab (left) and an upwelling hot plume (right) for different compositional systems. Density contrasts with the ambient mantle are given indicatively by the red-blue colour bar. Buoyancy effects due to thermal contraction or expansion are ignored. Buoyancy force (F_B, kg/m^3) profiles induced by phase transitions and compositional heterogeneities (in panel C) are schematically drawn in the right column. (A) Homogeneous dry olivine system. (B) Homogeneous dry pyrolite system. The brownish arrows indicate the pyroxene to garnet and garnet to perovskite transformations that occur over a broad depth range. The post-garnet reaction is set to occur at 720 km in the ambient mantle. At high temperatures, the post-spinel transition is indicated with a thin dashed line because of the small Clapeyron slope and density contrast (Hirose, 2002). (C) Heterogeneous dry harzburgite–MORB system. Density contrast and buoyancy forces are drawn with respect to a pyrolitic ambient mantle. The upwelling hot plume is pyrolitic in composition and contains a volume fraction of MORB heterogeneities (yellow blobs) smaller than that present in the subducting slab, resulting in smaller compositional buoyancy effects. The post-ilmenite reaction in the cold slab is indicated with a dashed line due to experimental uncertainties.

heterogeneities (reddening effect of the heterogeneity spectrum), intermittent layered convection with reduced mantle mixing efficiency and superadiabatic gradients near the 660 km discontinuity (Bunge et al., 1997; Christensen and Yuen, 1985; Honda et al., 1993; Machetel and Weber, 1991; Peltier and Solheim, 1992; Tackley et al., 1993; van Keken and Ballentine, 1999; Yanagisawa et al., 2011). The intermittent or layered mantle convection behaviour appears to increase with the vigour of convection (thus requiring smaller Clapeyron slopes of the post-spinel reaction for geodynamically relevant Rayleigh numbers; Tackley, 1996, Yanagisawa et al., 2011), while adding the 410 km exothermic phase transition diminishes the propensity to layering by making avalanches smaller and more frequent (Tackley et al., 1994). In simulations with a strongly temperature-dependent viscosity and plate-like behaviour, rigid cold downwellings penetrate more readily in the lower mantle than in isoviscous models, although the overall mass flux between upper and lower mantle does not increase significantly (Zhong and Gurnis, 1994, 1995).

The negative and positive buoyancy forces associated with phase transition in the abundant olivine component could have a first order control on the dynamics of subducting rigid slabs, affecting their sinking rates or promoting stagnation and subsequent rollback. From the analysis of these buoyancy forces and kinematic parameters from the Earth's subduction zones, (Billen, 2010) concluded that the negative buoyancy due to the olivine polymorphic transformations could temporarily double the descent rate of slabs, while the positive buoyancy associated with post-spinel reaction is likely not a good candidate for slab stagnation, although it may cause a slowing of the descent rate. Regional 2D models of subduction show that the post-spinel reaction can promote slab stagnation within the transition zone only for extreme deflections of the reaction boundary and fast trench retreat rates (e.g., Christensen, 1996;

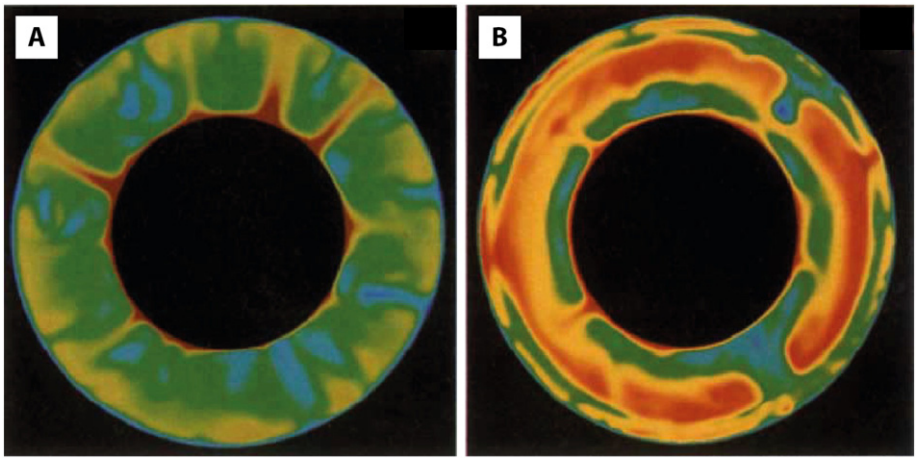

Fig. 5. Cross-sectional slices of the superabiabatic temperature field predicted by one of the earliest 3D global-scale, isoviscous mantle convection simulations. (A) Whole-mantle convection obtained without phase changes switches to (B) intermittent layered convection when adding the post-spinel transition with a strongly negative Clapeyron slope (−4 MPa/K). Scale range from −780 K to +220 K and from −1050 K to +350 K in panels A and B, respectively. From (Tackley et al., 1993).

Davies, 1995; Torii and Yoshioka, 2007). Slab stagnation depends also on trench kinematics because higher rates of trench retreat result in gentler slab dips and a slab negative buoyancy force that is distributed over a larger surface, yielding smaller stresses acting upon the mineralogical discontinuity (Christensen, 1996). When the 410 km discontinuity is included, the slab pull increases, which decreases the rate of trench retreat while increasing the slab dip and the tendency to penetrate into the lower mantle (Čížková and Bina, 2013). Conversely, (Van Hunen et al., 2001) found that the latent heat released during the olivine ⇔ Wadsleyite transformation increases the slab buoyancy and decreases the dip angle. The Wadsleiyte ⇔ Ringwoodite transformation has been traditionally ignored in this type of regional (but also global) numerical simulations because it was assumed that its effect on mantle convection patterns would be minor given the relatively low density contrast between the two phases. It is worth to note, however, that the negative buoyancy associated with this phase transition could be as large as that of the olivine ⇔ Wadsleyite transition due to the strongly positive reaction slope (3–7 MPa/K) (Billen, 2010).

Regional 2D models of plume upwelling suggest that the post-spinel reaction with moderate negative Clapeyron slopes can partially or completely hamper the penetration of low-viscosity plumes with relatively small sizes and large excess temperatures (Davies, 1995; Marquart and Schmeling, 2000; Tosi and Yuen, 2011). The penetration of very hot plumes could be hampered also by the Wadsleyite ⇔ majorite + ferropericlase transformation (Ichikawa et al., 2014), which, according to first principle calculations (Yu et al., 2011), should occur in a pure fosteritic system at T > 2200 K and 500–600 km depth with a small density contrast (1.6%) but a very large negative Clapeyron slope (−22 MPa/K).

Pyrolite system (Fig. 4B). The majority of numerical studies including mantle phase transformations (like those discussed so far) have assumed a 100% olivine composition of the mantle, and often extremely negative Clapeyron slopes for the post-spinel reaction, which causes strongly layered or intermittent convection and slab/plume stagnation. In a pyrolitic system (*pyr*: pyroxene; *ol*: olivine), however, the flow inhibition at the base of the transition zone decreases considerably because the exothermic majorite ⇔ Bridgmanite transition largely compensates the effect of the endothermic post-spinel transition (Tackley et al., 2005). More in detail, the buoyancy induced by phase transitions around 660 km depth appears to be very sensitive to temperature (Hirose, 2002) (Fig. 3*A*). In a cold downwelling mantle, the formation of Bridgmanite is dominated by the post-spinel and post-ilmenite endothermic phase transitions, both of which resist convection. At these cold temperatures, the positive buoyancy generated by the endothermic reactions is only partly compensated by the negative buoyancy associated with the majorite ⇔ Bridgmanite transformation that takes place at similar depths (Hirose, 2002; Hirose et al., 1999). Fig. 6 display results of 3D regional subduction models in a pyrolitc mantle, showing that, similarly to models assuming 100% olivine composition, the endothermic phase transitions can lead to slab stagnation in the transition zone for sufficiently fast rates of trench retreat (e.g., Christensen, 1996).

On the other hand, at high temperatures typical of upwelling hot plumes (T > 1800 °C), Ringwoodite decomposes to majorite and ferropericlase and the formation of Bridgmanite is related mostly to the majorite ⇔ Bridgmanite transition with a positive Clapeyron slope and a large density difference (Hirose, 2002; Ishii et al., 2011). In other words, in upwelling hot material the majorite ⇔ Bridgmanite reaction occurs well below the 660 km discontinuity, generating strong positive buoyancy that favours plume penetration in the transition zone. This is shown in Fig. 7, where the oblique trajectory of the sheared plume becomes vertical and its upwelling velocity increases when the hot material crosses the post-garnet boundary.

Thus, in a pyrolitic mantle phase transformations around the 660 km discontinuity should work as an accelerator rather than a barrier for hot upwelling plumes, while some moderate impediment to penetration in the lower mantle should be effective for subducting slabs. At the larger scale, this would enhance vertical flow with convective patterns characterized by reduced wavelengths (Dal Zilio et al., submitted for publication), which become larger when incorporating self-consistent plate tectonics and depth-dependent viscosity (Nakagawa et al., 2009).

Harzburgite–MORB system (Fig. 4C). Partial melting of the source pyrolitic mantle and subsequent fractional crystallization introduce compositional and mineralogical heterogeneities in the convective system that further complicates the buoyancy effects due to phase transformations. The entire set of compositional flavours arising from magmatic differentiation of pyrolite can be described by a chemical or mechanical mixture of the enriched MORB and depleted harzburgitic end-members.

The enriched MORB is unaffected by the phase transformation in the olivine system and after eclogitization becomes denser than the mantle at any depth, except around the 660 km discontinuity where a density crossover exists due to stability of the Al-rich garnet at depths below the post-spinel reaction (Ganguly et al., 2009; Hirose et al., 1999; Irifune and Ringwood, 1993; Ono et al., 2001; Richard et al., 2005) (Figs. 2D, 3C, D). In the ambient mantle, the density crossover likely exists in the 660–720 km depth interval (Hirose et al., 1999; Ono et al., 2001). However, because of the negative and positive slopes of the post-spinel and post-garnet transformations, respectively, the depth

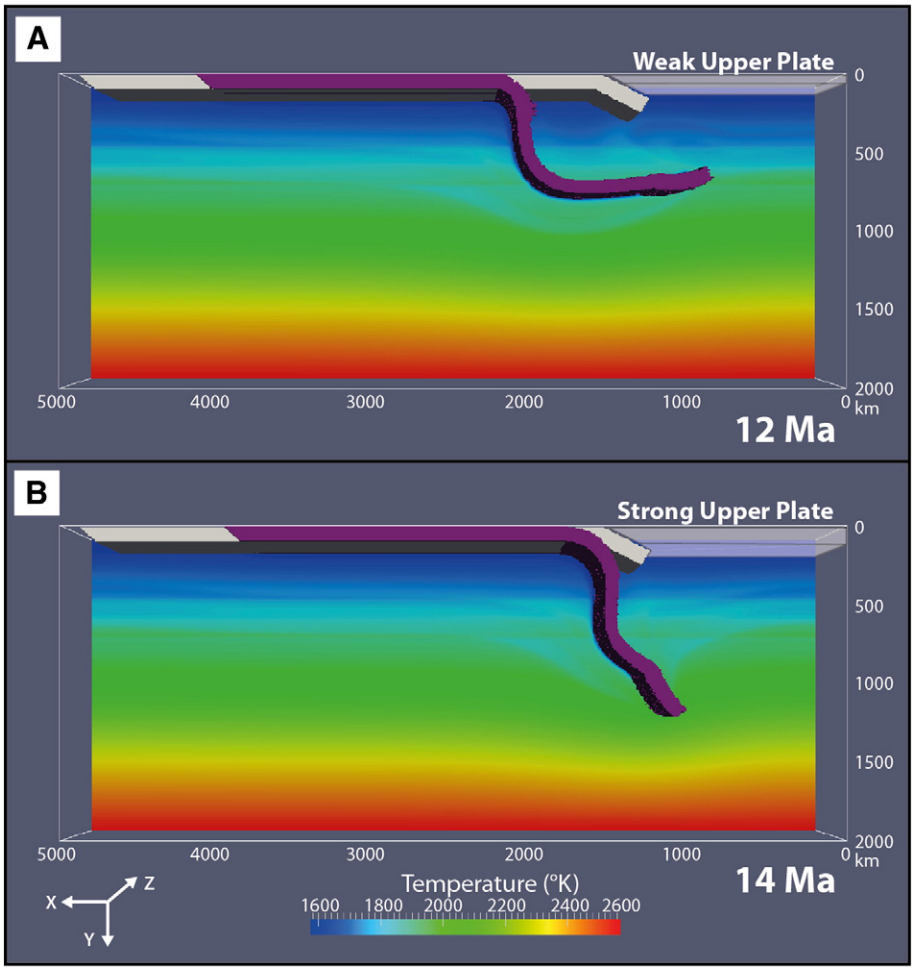

Fig. 6. Snapshots of dynamic thermomechanical models of subduction in a pyrolitic mantle. Phase transitions are included with the self-consistent approach as explained in Section 2.3.3. Subduction initiates spontaneously driven by a 200 km long slab. The white and purple surfaces indicate, respectively, the initial and final positions of the oceanic plate. The initial setup of the two models is similar, except that in (A) the age of the overriding mantle is much younger than in B) (1 Ma vs. 20 Ma). The weak overriding mantle in (A) opposes small resistance to subduction, yielding fast rates of trench retreat and, together with the positive buoyancy generated by the post-spinel and post-ilmenite reactions, slab stagnation (as in (Christensen, 1996)). Cooling of the entrained mantle due to the endothermic post-spinel reaction can be observed in the vertical cross-section of the temperature field at Z = 500 km. Mantle creep is calculated considering the diffusion and dislocation creep flow laws of olivine and activation volume of 12 cm^3, while pseudo-plasticity is defined by the Drucker–Prager yield criterion (as in Faccenda, 2014a). The employed visco-plastic rheological model is characterized by a smooth increase of viscosity with depth that culminates at the cut-off value of $5 \cdot 10^{22}$ Pa s in the lower mantle. Boundary conditions are free slip for all boundaries.

interval of the density crossover becomes small at low temperatures, while it increases at high temperatures. (Litasov et al., 2004) found a strongly positive Clapeyron slope (+4.1 MPa/K) for the post-garnet transformation in dry MORB composition, which would imply that in the cold subducting slab the basaltic component transforms to perovskite at lower pressures than the surrounding mantle. Thus, the positive buoyancy generated by the MORB component around the 660 km discontinuity could be small in subducting plates, while it is likely significant in heterogenous upwelling material.

On the other hand, the depleted harzburgitic mantle is slightly more buoyant than pyrolite and much less dense than MORB due to the smaller amount of garnet and Bridgmanite, and at low temperatures provides only small negative buoyancy (Ganguly et al., 2009) (Figs. 2D, 3B, D). However, when compared to a pyrolitic mantle, the harzburgitic layer of the slab with ~75–80% of olivine component is more affected by the deflections of the olivine polymorphic transformations and post-spinel reaction, and less by those involving pyroxene and garnet. Furthermore, the post-spinel reaction occurs at higher pressures and has a more negative slope in a pure fosteritic component - which is representative of harzburgite - compared to a pyrolitic mantle, even when using the same experimental procedure (Ishii et al., 2011; Litasov et al., 2005a). Also, it is important to note that at low temperatures the presence of Akimotoite in both the olivine and pyroxene-garnet components would generate even larger positive buoyancy forces around 660 km depth due the post-ilmenite polymorphic reaction with a strongly negative Clapeyron slope.

In a hot and chemically heterogeneous upwelling material, enrichment in the MORB component relative to the surrounding mantle decreases the chemical buoyancy through the whole mantle, except within the uppermost lower mantle where strong positive buoyancy is produced in between the post-spinel and post-garnet reactions (Fig. 4C). (Ballmer et al., 2013) and (Dannberg and Sobolev, 2015) showed that by including 15–20% of eclogite decreases the buoyancy of chemically heterogeneous plumes, which, if not sufficiently hot or voluminous, may pond between 300 and 410 km depth. This is because over this depth range the denser majoritic garnet-stishovite aggregate gradually transforms to the lighter pyrope garnet-pyroxene-coesite aggregate in the MORB component, while in the mantle the transformation of Wadsleyite to lighter olivine takes place at about 410 km depth. As a result, a large density contrast exists between MORB and ultramafic rocks at the base of the upper mantle (Figs. 2D, 3C, D, 4C). Enrichment in harzburgitic component would have basically opposite effects, thus increasing the plume chemical buoyancy throughout most of the mantle except in between the post-spinel and the pyrolite post-garnet reaction

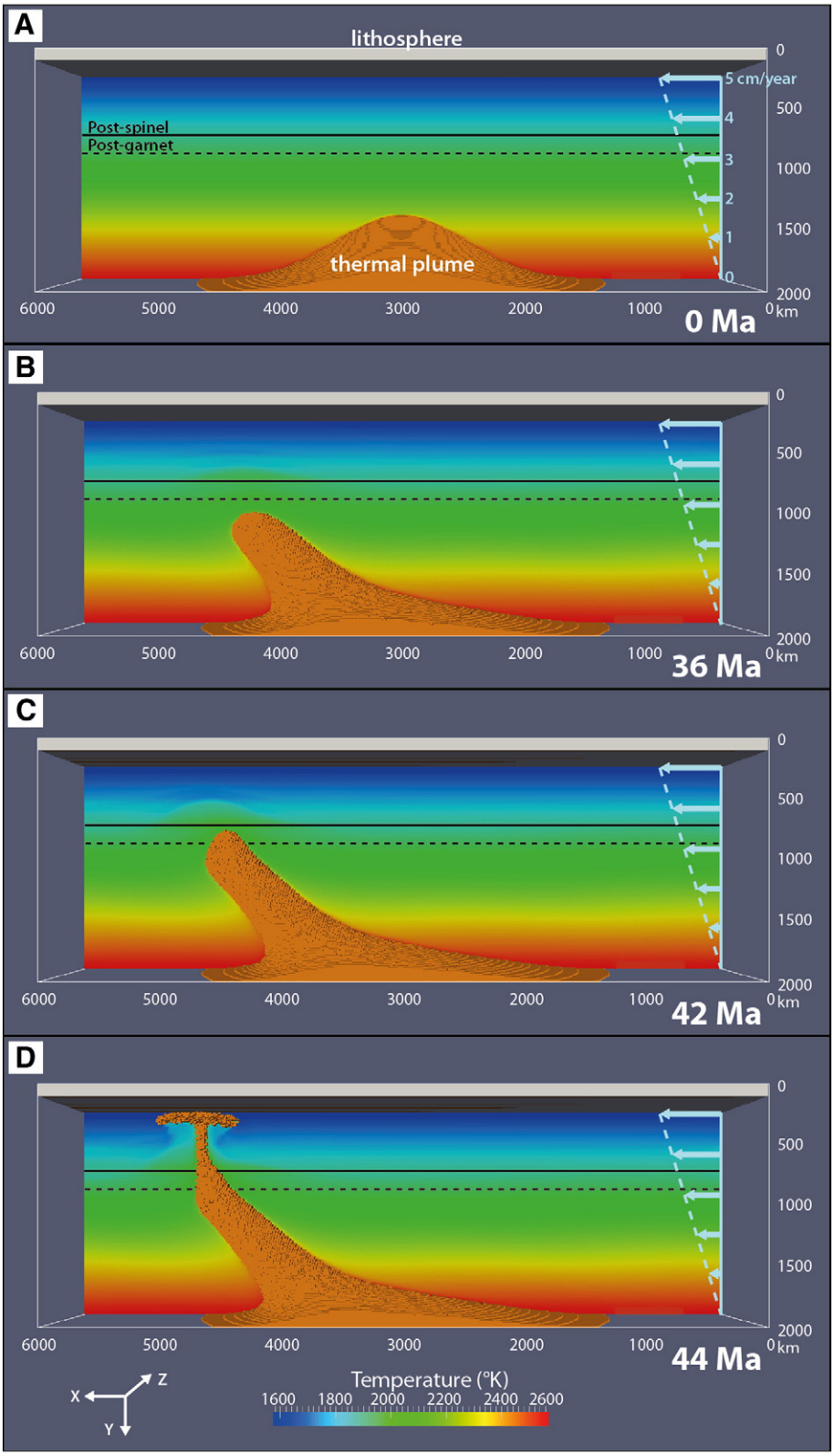

Fig. 7. Snapshots of a thermomechanical model where a thermal plume upwells in a pyrolitic mantle. Phase transitions are included with the self-consistent approach as explained in Section 2.3.3. The initial position of the symmetric plume (orange) is centred with respect to the horizontal coordinates (A) and its initial temperature is set equal to that of the bottom boundary (2555 K). The plume is sheared ($\dot{\varepsilon}_{xy} = 8 \cdot 10^{-16}\ s^{-1}$) by a hypothetical mantle wind with surface velocity of 5 cm/yr that linearly decreases to zero toward the bottom of the model. As the plume penetrates through the post-garnet phase boundary (C), its upwelling velocity increases and its trajectory is deflected toward the vertical due to the increased positive buoyancy. Same rheological model as in Fig. 6. Boundary conditions are free slip for the top, front and back boundaries, no slip at the bottom, while the left and right boundaries are periodic.

boundaries. This is because the transformation of garnet in harzburgite composition completes at shallower depths (<700 km) than in pyrolitic composition (<800 km). As a consequence, harzburgite may pond near the post-garnet phase transition (Figs. 8B, C).

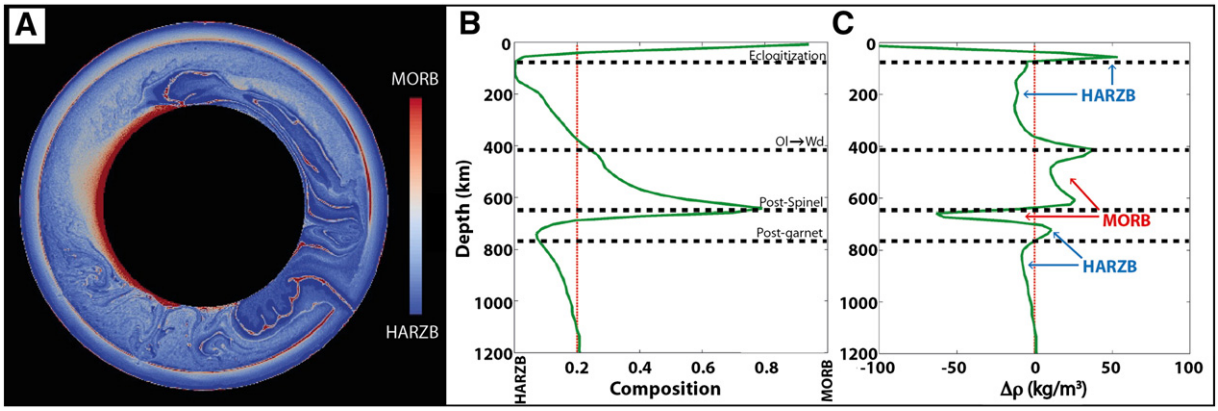

Fig. 8. Compositional mantle layering predicted by global-scale thermochemical mantle-convection model after ~4.6 Gy model time (after Ballmer et al., 2015). (A) Composition in the harzburgite–MORB system. (B) Initial (red dashed line) and final (green line) compositional profiles. (C) Average density contrast profile (green line) between the final and initial (pyrolitic) compositions. Density contrasts generated by enrichments in harzburgite or basalt are indicated.

Global-scale simulations predict that phase transformations in the harzburgitic–MORB system generate a distinct compositional layering in the Earth's mantle, with levels that in average are either more depleted or enriched in the MORB component with respect to the starting pyrolitic composition (Ballmer et al., 2015; Nakagawa and Buffett, 2005) (Fig. 8; see Section 2.2.3 for more details). These results suggest that the ambient mantle is highly heterogeneous and the density contrasts of downwelling and upwelling materials are more complicated than when estimated against a homogeneous pyrolitic mantle (Fig. 8C).

Aside from the phase transitions taking place in the 300–800 km depth interval, phase transformations at mid and lower mantle depths could also affect the Earth's internal dynamics. The post-perovskite transformation has a strongly positive Clapeyron slope, which destabilizes the chemically-dense material piling within the lower thermal boundary, slightly increases the heat flow and the interior mantle temperature, and increases the number and upwelling velocities of plumes (Matyska and Yuen, 2007; Nakagawa and Tackley, 2004, 2005; Tackley et al., 2007; Yuen et al., 2007). However, because of the small density difference (1%), the destabilizing effect is relatively small despite the large Clapeyron slope, so that the post-perovskite transformation has likely less influence than other uncertainties in deep mantle parameters, such as the density of MORB (Tackley, 2012). If the post-perovskite transition indeed occurs at lower pressure in basalts relative to pyrolite (Grocholski et al., 2012; Ohta et al., 2008), the post-perovskite phase may be present everywhere over the CMB, such that the destabilization effect of chemically dense MORB material is eliminated (Tackley et al., 2007). Buoyancy effects of the iron spin transition in ferropericlase add on those due to the post-perovskite transition, enhancing vertical flow and affecting mantle temperatures by more than 10% for relatively large density contrasts (2–4%) and relatively sharp transitions (Bower et al., 2009; Shahnas et al., 2011). When using smaller density variations (<1%) and smoother transitions that are appropriate for, respectively, Al-bearing ferropericlase together with more realistic mantle potential temperatures, the iron spin transition in ferropericlase has a minor impact on mantle dynamics (Vilella et al., 2015).

Eclogitization of the continental mafic crust can also have major effects on the evolution of continental plates. With the progression of the reaction, the eclogitized continental root becomes denser than the surrounding mantle and thus it is prone to foundering (Kay and Kay, 1993). Numerical models predict that high-density eclogite accelerates the development of Rayleigh–Taylor instabilities (Jull and Kelemen, 2001), affects the orogeny evolution (Doin and Henry, 2001; Krystopowicz and Currie, 2013) and, if sufficiently weak, can lead to delamination of the continental plate (Krystopowicz and Currie, 2013).

2.2.2. Rheological effects

The newly formed mineral assemblage often possesses different mechanical properties with respect to the parental phase aggregate, which produces a variation in the rheological behaviour of the transformed material (Karato, 1989b).

Within the oceanic crust, field observations suggest that dry gabbroic rocks are stiffer than wet eclogitized rocks where the weak omphacite accommodates most of the deformation (Bjørnerud et al., 2002). On the other hand, the progressive dehydration of hydrothermally altered gabbroic and eclogitic aggregates should lead to an increase in viscous strength. As garnet is stronger than omphacite (Jin et al., 2001), a further strengthening of the crust is expected with its gradual garnetization in the 300–450 km depth range. It is worth to note that omphacitic pyroxene has a very low thermal conductivity, so that the eclogitic crust could thermally insulate to some extent the underlying harzburgitic layer, which could be about 50 °C colder (and thus stiffer) than previously modelled (Wang et al., 2014). It is unclear to what extent the transition to a perovskitic assemblage affects the rheological behaviour of the MORB aggregate, as the strength of its four main phases at lower mantle conditions is poorly understood.

In the mantle, the abundant olivine and its high-pressure polymorphs control the rheological behaviour of mantle down to the base of the transition zone, while the role of garnet is predominant within the garnetitic crust and becomes progressively important in the mantle as its volume fraction increases with depth. Laboratory experiments indicate that olivine is slightly weaker than its high-pressure polymorphs (Chen et al., 1998; Karato et al., 2001; Nishihara et al., 2008). Furthermore, water weakens olivine dramatically but only slightly weakens Wadsleyite and Ringwoodite (Chen et al., 1998). In dry conditions, garnet appears to be harder than any other abundant mineral phases of the upper mantle and transition zone (Jin et al., 2001; Karato et al., 1995). In wet conditions, however, garnet becomes progressively weaker than olivine with increasing water content (Katayama and Karato, 2008). Thus, in dry conditions transition from upper mantle to transition zone aggregates in the mantle and progressive garnetization of the crust should result in a viscosity increase. This type of radial viscosity structure of the Earth's mantle has been obtained by several studies (e.g., Hager and Richards, 1989; Ricard and Wuming, 1991; Steinberger and Calderwood, 2006), while others predict low viscosity within the whole or part of the transition zone (e.g., King and Masters, 1992; Liu and Zhong, 2016; Mitrovica and Forte, 2004; Rudolph et al., 2015) (Fig. 9). A low viscosity transition zone might be related to the presence of water which would enhance the creep mechanisms of all mantle and crust silicates.

A more consistent result across different radial viscosity profiles is the increase in viscosity by 1 or 2 orders of magnitude at lower mantle depths, which often culminates in correspondence of a viscosity hill

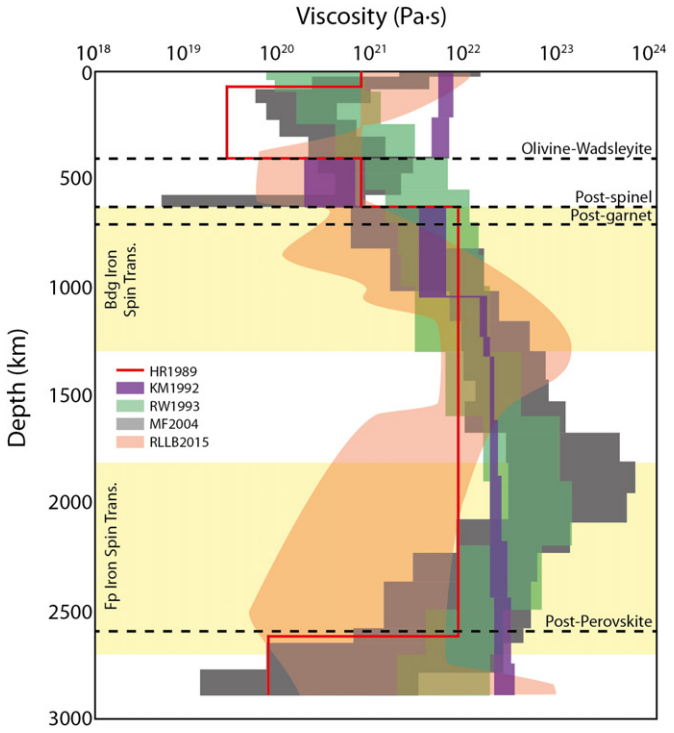

Fig. 9. Patterns of radial viscosity profiles with superimposed major mantle phase transitions. HR1989: (Hager and Richards, 1989); KM1992: (King and Masters, 1992); RW1991: (Ricard and Wuming, 1991); MF2004: (Mitrovica and Forte, 2004); RLLB2015: (Rudolph et al., 2015). The reference viscosity for HR1989, KM1992 and RLLB2015 profiles is taken as 10^{21} Pa·s. The pale yellow areas indicate the inferred regions of Bridgmanite and ferropericlase iron spin transition (Lin et al., 2013). Post-perovskite refers to the transformation of Bridgmanite into post-perovskite.

in the 1000–1500 km depth range (Rudolph et al., 2015) or at about 2000 km depth (Mitrovica and Forte, 2004; Ricard and Wuming, 1991). The viscosity jump at the 660 km discontinuity indicated by some inversions (Hager and Richards, 1989; King and Masters, 1992; Liu and Zhong, 2016; Mitrovica and Forte, 2004) could be attributed to a higher resistance to creep of lower mantle aggregates than that of transition zone aggregates - for example, (Chen et al., 2002b) found that the viscosity of Bridgmanite is one order of magnitude higher than that of Ringwoodite at 1073 K and 20 GPa in relaxation stress experiments. However, because no major phase transitions have been experimentally found at mid-lower mantle conditions, alternative rheological mechanisms are required in order to explain the existence of a viscosity hill (i.e., hardening of both Bridgmanite and ferropericlase with increasing pressure (Ammann et al., 2010; Ito and Toriumi, 2007; Marquardt and Miyagi, 2015); increase in volume fraction of Bridgmanite relative to that of the weaker ferropericlase (Girard et al., 2016) as shown by (Ballmer et al., 2015); decrease in water solubility of nominally anhydrous minerals as proposed by (Rudolph et al. 2015)).

The reduction in viscosity toward the bottom of the mantle could be attributed to the iron spin transition in ferropericlase (Marquardt and Miyagi, 2015), which may lead to an increase in atoms diffusivity (Wentzcovitch et al., 2009) and/or to the appearance of potentially weak post-perovskitic aggregates, together with strong temperature gradients toward the core-mantle boundary. Indeed, from the theoretical point of view, post-perovskite is weaker than Bridgmanite during diffusion and dislocation creep (Ammann et al., 2010; Carrez et al., 2007), and a reduction in viscosity has been observed in analogue material $CaIrO_3$ after the post-perovskite transformation (Hunt et al., 2009). Thus, the post-perovskite transformation might be accompanied by rheological weakening of the lower mantle aggregate. Although the iron spin transition induces a weakening of the bulk modulus in Bridgmanite (Hsu et al., 2011), it is unclear whether it would affect also creep mechanisms in the lower mantle.

From the numerical perspective, a viscosity contrast of 1 to 2 orders of magnitude has frequently been assumed in order to model the transition from the mantle transition zone to the lower mantle (e.g., Hager and Richards, 1989). In global convection models, such viscosity stratification increases the wavelength of the convective flow patterns (the reddening effect of the convective spectrum; Bunge et al., 1996; Tackley, 1996), decreases the lateral motion of hotspots (Bunge et al., 1996) and enhances mantle degassing rates (van Keken and Ballentine, 1998). Two-dimensional simulations of dynamic subduction indicate that, with increasing viscosity contrast between the upper and lower mantle, the slab retreat increases and sinking rates decrease - because of the decrease of effective Rayleigh number -, with slabs that tend to stagnate in the transition zone and eventually penetrate in the lower mantle (Čížková and Bina, 2013; Garel et al., 2014; Torii and Yoshioka, 2007).

The effects of a weak post-perovskitic mantle assemblage have been investigated both in 2D Cartesian and 3D spherical calculations. A low-viscosity post-perovskite in subducting cold material enhances deformation and mechanical unmixing of the compositionally stratified slab above the CMB, with slab material that is able to spread more effectively and larger amounts of MORB settling at the CMB (Čížková et al., 2010; Nakagawa and Tackley, 2011; van den Berg et al., 2010). Furthermore, such local rheological weakening can substantially increase the convective vigour, yielding faster secular core cooling rates, higher global heat fluxes, higher mantle temperatures and a smaller CMB topography (Benesova and Čížková, 2013; Li et al., 2014; Nakagawa and Tackley, 2011; Samuel and Tosi, 2012; Tosi et al., 2010).

(Matyska et al., 2011) explored the rheological effects due to the softening of the bulk modulus and activation energy during the iron spin transition set to occur around 1600 km depth in both Bridgmanite and ferropericlase, and found that a low-viscosity channel in the mid-mantle enhances horizontal flow.

2.2.3. Chemical implications

The density crossover between the crust and the mantle in the 660–720 km depth interval – at ambient mantle conditions – caused by different depths of the post-spinel and post-garnet transitions can generate a chemical stratification across the 660 km boundary (Tackley, 2015; Tackley et al., 2005). It has been originally proposed that this density crossover would cause the separation of the different slab components and the accumulation of the positively buoyant crust around the 660 km discontinuity to form garnetite megaliths (Ringwood, 1991). However, (van Keken et al., 1996) demonstrated that this mechanism can operate only when the strong garnetitic crust and the underlying lithospheric mantle are separated by a soft layer, whose origin is doubtful (but see Section 3.2.3). Furthermore, it should be considered that the depth interval of the density crossover progressively reduces with decreasing temperatures (e.g., Litasov et al., 2004), implying that crust delamination from the slab likely does not take place at the base of the transition zone during slab penetration in the lower mantle.

Separation of the crust and of the underlying depleted components can occur when the density contrasts are non-zero and the slab viscosity is sufficiently low. This situation could establish, for example, in the transition zone due to both thermal relaxation and superplastic behaviour of stagnating slabs (Motoki and Ballmer, 2015). In this case, the lighter harzburgitic component rises toward the upper mantle, while the heavier MORB component sinks into the lower mantle. Unmixing of the slab components may occur also in the deep mantle owing to the progressive conductive warming of the slab material and/or its transformation into weak post-perovskite (Ammann et al., 2010). The separated components can be subsequently entrained in upwelling hot material and entrapped around the 660 km discontinuity, where the density crossover exists over a sufficiently wide depth interval. As a result, a strong compositional gradient is formed around the 660 km discontinuity, with MORB material accumulating at the bottom of the

transition zone, the depleted harzburgitic component accumulating in the uppermost lower mantle, and a chemical gradient present throughout the entire mantle (Fig. 8) (Armann and Tackley, 2012; Ballmer et al., 2015; Davies, 2008; Nakagawa et al., 2009; Tackley et al., 2005). It is worth noting that small variations in MORB composition strongly affect the degree of layering due to such a basalt filter effect (Nakagawa et al., 2010). (Ballmer et al., 2015) have shown that the presence of a strong compositional gradient within the mantle introduces additional buoyancy forces able to neutralize the negative buoyancy of subducting slabs, which may then stagnate at about 1000 km depth.

A similar filtering mechanism could lead to the accumulation of the continental crust and terrigenous sediments at the base of the transition zone. Felsic material can be transported at mantle depths by crustal delamination, continental collision, or subduction of sediments, volcanic arcs/ridges and upper plate material tectonically eroded by the descending slab along ocean-continent convergent plate boundaries (Clift et al., 2009; Ichikawa et al., 2016; Stern and Scholl, 2010). Upon deep subduction, granitic rocks experience several phase transitions, becoming denser than the mantle below 270 km depth, where coesite transforms to stishovite (Irifune et al., 1994). As no further major densification reactions occur, the continental crust density becomes lower than that of the mantle at 660 km depth. Based on these two density crossovers and on published global rates of sediments subduction and continental crust material eroded by the underlying oceanic plate, (Kawai et al., 2013) proposed that up to six times the volume of surface continental crust could be present in the transition zone, which they refer to as "*the second continent*".

Intrinsic structural changes of the mineral phases are associated with variations on volatiles solubility, with some volatile species being more prone to be incorporated into certain minerals than others. For example, it is well established that solubility of water (as hydrogen) varies considerably in mantle minerals, with transition zone olivine polymorphs capable of storing 1–3 wt.% H_2O in contrast to mineral phases of the upper and lower mantle where less than 1 wt.% H_2O can be incorporated (Karato, 2015). Such differences in water and other volatiles solubility in nominally anhydrous minerals of the mantle can lead to the formation of chemically distinct reservoirs, deep partial melting and further chemical differentiation. (Bercovici and Karato, 2003) have proposed that slowly upwelling mantle in response to the cold slab downwellings may be wetted through a water-rich transition zone by chemical diffusion. When such an upwelling wet mantle subsequently transforms to upper mantle mineral aggregates, exsolution of water will generate partial melting and sequestration of incompatible elements that will then accumulate at the bottom of the upper mantle due to the negative melt buoyancy. This enriched molten layer could be subsequently dragged downward by subducting slabs and incorporated in the mantle transition zone. As a result, the transition zone could be enriched in water and incompatible elements that are progressively filtered out from the slowly upwelling and progressively depleted mantle material. Similar arguments could be applied in the future to other volatile species. For instance, (Roberge et al., 2015) have found experimentally that a large fraction of the Earth's fluorine could be hosted in the transition zone minerals. They have also suggested that other heavy halogens elements (chlorine, bromine and iodine) would also likely be stored in the mineral assemblage of the transition zone, although their real contents in deep mantle minerals remain poorly constrained.

2.3. Numerical implementation

The effects of phase transformations can be investigated with compressible mantle convection simulations that incorporate energetic effects due to released or absorbed latent heat and progressive variations in physical properties of the transforming mineral aggregate. Two different approaches have been traditionally employed to incorporate equilibrium phase transitions in mantle convection simulations: 1) via parameterization of phase boundaries, and 2) through internally-consistent thermodynamic datasets that allow to calculate the physical properties of the equilibrium phase assemblages at different pressure and temperature conditions and for a given bulk chemical composition.

2.3.1. Governing equations of compressible mantle convection

The equations of conservation of mass, momentum and energy which govern convection in a compressible fluid with infinite Prandtl number are (Gerya, 2010; Ita and King, 1994; Jarvis and McKenzie, 1980):

$$\nabla\cdot\vec{v} = -\frac{D\ln(\rho)}{Dt} \tag{1}$$

$$\nabla\cdot\tau_{ij} - \nabla P = -\rho\,\vec{g} \tag{2}$$

$$\rho C_P\frac{DT}{Dt} = \nabla\cdot(K\nabla T) + H_R + H_S + H_A \tag{3}$$

where D/Dt is material time derivative and H_R is the internal heat source due to radiogenic elements. The frictional and adiabatic heat source terms are:

$$H_S = \tau_{ij}\frac{\partial v_i}{\partial x_j} \tag{4}$$

$$H_A = \alpha T\frac{DP}{Dt} \tag{5}$$

In these equations, ρ is density, $\vec{v}$ is the velocity vector, τ is the deviatoric stress tensor, P is pressure, $\vec{g}$ is the gravity acceleration vector, C_P is the isobaric specific heat capacity, K is thermal conductivity and α is thermal expansivity.

This set of base equations for compressible mantle convection is then modified to incorporate phase transformations as discussed below.

2.3.2. Parameterized phase boundaries

Phase transitions can be parameterized as a function of thermodynamic state variables (P, T, V) and composition by using polynomials to interpolate the reaction boundary. For instance, the olivine polymorphic transformations and the post-spinel reaction are frequently parameterized with the linear P–T relationship:

$$P = P_0 + \frac{\partial P}{\partial T}\Delta T = P_0 + \gamma\Delta T \tag{6a}$$

where γ is the Clapeyron slope of the reaction, P_0 is the pressure at reference temperature T_0, and $\Delta T = T - T_0$. As an example, substituting data derived by (Fei et al., 2004) for the post-spinel reaction in the Mg_2SiO_4 system, Eq. (6a) becomes:

$$P(GPa) = 25.12 - 0.0013T(C) \tag{6b}$$

Reactions involving production or consumption of a fluid phase are more commonly characterized by non-linear reaction boundaries due to the P–T dependency of the fluid phase compressibility, and thus their parameterization requires higher order polynomials (e.g., Faccenda et al., 2012; Gerya and Yuen, 2003). One of most sophisticated reaction parameterizations is the one presented by (Katz et al. 2003), which allows to calculate the melt fraction during hydrous melting of peridotites as a function of pressure, temperature, water content and modal clinopyroxene.

The progress of the reaction Γ – which varies from 0 to 1 and indicates the volume fraction of the product phase(s) – has been typically modelled with either a step function when considering the phase transition as univariant (Bunge et al., 1997; Christensen, 1984; Krystopowicz and

Currie, 2013; Tackley et al., 1993), or by means of a hyperbolic tangent function to simulate the range of P–T conditions through which divariant phase transitions take place (Christensen and Yuen, 1985; Nakagawa et al., 2009; Peltier and Solheim, 1992; Richter, 1973; Zhong and Gurnis, 1994).

Latent heat released or absorbed during the transformation can be included explicitly in the right term of the heat conservation equation (Eq. (3); by adding $H_L = \rho DQ_L/Dt$ or $H_L = \rho Q_L D\Gamma/Dt$ for univariant and divariant transformations, respectively. Q_L is the latent heat per unit mass of the total transformation) or implicitly by calculating the effective thermal expansivity and heat capacity as (Gerya, 2010; Schubert et al., 1975):

$$C_{Peff} = C_P + Q_L\left(\frac{\partial\Gamma}{\partial T}\right)_P \tag{7}$$

$$\alpha_{eff} = \alpha + \rho_{RP}\frac{Q_L}{T}\left(\frac{\partial\Gamma}{\partial P}\right)_T \tag{8}$$

where ρ_{RP} is the average density of the reactant and product phases. Variations in bulk rock physical properties $\overline{q}$ (i.e., density, thermal conductivity, isobaric heat capacity) in the two-phase mixture are modelled with the weighted arithmetic average:

$$\overline{q} = q_R(1-\Gamma) + q_P\Gamma \tag{9}$$

where q_R and q_P are the given physical property of the reactant and product phases. Variations in viscosity are better modelled with the weighted harmonic average that emphasizes the contribution of the weaker phase. The non-dimensional formulations of the equations of conservation of mass, momentum and energy accounting for parameterized phase transitions are reported in several articles (e.g., Christensen and Yuen, 1985; Ita and King, 1994; Nakagawa et al., 2009).

This approach has the advantage of being computationally efficient and easy to implement, but it becomes inconvenient in multi-variant systems where several reactions take place over finite P–T ranges. As a matter of fact, reaction parameterization has been widely used to study the effects of only few phase transitions which have major effects on specific geological processes, such as solid–solid (see references above), melting/crystallization (Ballmer et al., 2013; Faccenda et al., 2009b; Gerya and Yuen, 2003; Gerya et al., 2008) and hydrothermal metamorphic reactions (e.g., Faccenda et al., 2012).

2.3.3. Self-consistent approach: Isochemical pseudo-sections

An alternative approach is to use internally-consistent thermodynamic dataset for mineral end-members and activity composition models for assembling endmembers into solid-solutions in order to calculate the stable mineral assemblage as a function of pressure, temperature, and composition via Gibbs free-energy minimization (Holland et al., 2013). This approach has been recently used by several groups (Gerya et al., 2006; Kerrick and Connolly, 2001; Mishin et al., 2008; Nakagawa et al., 2009, 2010; Piazzoni et al., 2007; Ricard et al., 2005; Stixrude and Lithgow-Bertelloni, 2011) to calculate gradual variations in bulk rock properties such as density, enthalpy, elastic moduli, and free fluid components (for example, free water or melt). As an example, the stable phase equilibria and density as a function of pressure and temperature calculated with HeFESto (Stixrude and Lithgow-Bertelloni, 2011) for pyrolite, harzburgite and MORB compositions are shown in Figs. 1–3. Other widely used and publicly available software are THERMOCALC (Powell et al., 1998) and Perple_X (Connolly, 2005). To incorporate phase transitions in mantle convection simulations, density and enthalpy (H) maps are then used to compute density, effective heat capacity and energetic (both adiabatic and latent heating) effects for adiabatic (de)-compression (Gerya, 2010):

$$C_{Peff} = \left(\frac{\partial H}{\partial T}\right)_P \tag{10}$$

$$H_A = \left(1-\rho\frac{\partial H}{\partial P}\right)_T\frac{DP}{Dt} \tag{11}$$

The numerical models in Figs. 6 and 7 account for phase transitions in a pyrolitic mantle using this approach.

3. Disequilibrium phase transitions

3.1. Low temperature reaction kinetics of major solid–solid phase transitions in the oceanic crust and mantle

The phase diagrams discussed in Section 2 illustrate the mineral phases coexisting at different P–T conditions at equilibrium for a given composition. This is equivalent assuming that reactions across phase boundaries are instantaneous or that the mineral phases had time to completely re-equilibrate with the changing P–T conditions. However, if the rate of material advection through the P–T space is faster than the reaction rate, non-equilibrium phase aggregates can persist beyond the equilibrium phase boundaries. Reaction rates can be particularly sluggish when temperatures are insufficient to overcome the activation energy barrier to transformation and catalytic fluids are absent. These conditions are simultaneously met in the cold and dry portions of slabs, where, for current subduction rates, the high-pressure transformations of crust and mantle minerals can be kinetically hindered.

More in detail, because temperature and pressure dependencies are different between nucleation and growth kinetics, three types of high-pressure transformations are expected in the subducting slabs (Kubo et al., 2009) (Fig. 10). In the cold centre of slabs untransformed regions are formed due to slow growth kinetics at low temperatures (G type: growth-controlled transformation). Untransformed regions are also formed under relatively warmer and smaller overpressure conditions where the growth rate is fast enough but nucleation cannot occur (N

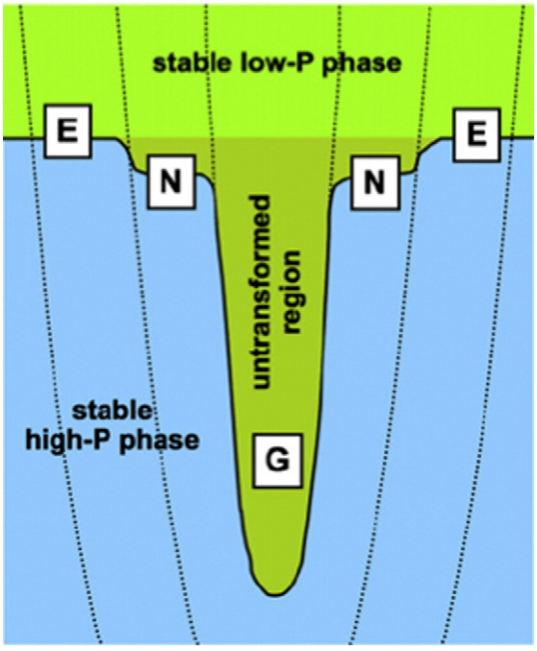

Fig. 10. Schematic figure showing three types of high-pressure transformation expected in subducting slabs with an equilibrium phase boundary with zero Clapeyron slope. Dotted lines show isotherms. Untransformed regions are formed due to slow growth kinetics at low temperature conditions (G type, growth-controlled transformation) and due to slow nucleation kinetics at small overpressure conditions (N type, nucleation controlled transformation). At higher temperatures the transformation front can ascend against the downgoing current to the equilibrium boundary where the nucleation does not occur, because of the fast growth kinetics (E type, equilibrium transformation). From (Kubo et al., 2009).

type: nucleation-controlled transformation). When the growth rate is faster than the subduction rate at higher temperatures, the transformation front can ascend against the downgoing current to the equilibrium boundary where nucleation does not occur, because of the fast growth kinetics (E type: equilibrium transformation).

The nucleation and growth kinetics of high-pressure phase transitions vary with the changing P–T conditions of the subducting slab, increasing exponentially with temperature (T) and overpressure or pressure beyond equilibrium (ΔP). They are also promoted by introducing shear stresses, diminishing grain-size, and adding water or other catalysts to the reactants. On the other hand, the elastic strain due to the large volume reduction (for example, 16% in the post-pyroxene transformation; Hogrefe et al., 1994), if not relaxed plastically in the aggregate at low-T, results in a decrease of the growth rate.

Besides thermodynamic ambient conditions, reaction rates depend also on the type of transformation: polymorphic reactions are relatively fast because of the short range atomic diffusion at the scale of the crystal interface (2–3 nm). In contrast, decompositional reactions with 2 or more product phases require long-range diffusion of atoms that decreases the rate of transformation. Because of the smaller growth distance, intra-granular nucleation of the product phases considerably speeds up reaction rates in comparison to cases where nucleation occurs along grain-boundaries. Kinetics studies of high-pressure mineral transformations in multiphase aggregates have shown that the presence of secondary phases can influence reaction rates (e.g., Hogrefe et al., 1994).

Below we report a compilation of reaction kinetics experiments for the major phase transformations occurring within the slab, and that are frequently employed in numerical models to predict the extent of metastable portions in subducting oceanic plates (Fig. 11).

3.1.1. Olivine polymorphic transformations

Olivine may persist at transition zone depths in the cold interior of the slab forming a metastable wedge that progressively transforms to either Wadsleyite or Ringwoodite. At low temperatures and low differential stresses, the most likely growth mechanism of the olivine polymorphic transformation is grain boundary nucleation, in which grains of the product phase nucleate along pre-existing olivine grain boundaries and grow afterwards at the expense of the host olivine (Rubie and Ross, 1994). (Sharp and Rubie, 1995) demonstrated that high-pressure clinoenstatite (cEns) can catalyse the olivine polymorphic transformation by enhancing nucleation kinetics. (Kerschhofer et al., 1996, 2000) found that the olivine polymorphic transformation can occur also by intra-granular nucleation at low to moderate differential stresses and pressures greater than 17 GPa (about 520 km), which significantly speeds up the reaction.

(Hosoya et al., 2005) measured growth rates of the olivine ⇔ Wadsleyite transformation in experiments with relatively high concentrations of water (660–5000 wt. ppm), and found that the reaction kinetics is proportional to the amount of dissolved OH to the power of ~3. Subsequently, (Diedrich et al., 2009) and (Du Frane et al., 2013) found low activation enthalpies in hydrous conditions for the olivine ⇔ Ringwoodite transformation, yielding fast reaction rates for relatively low amounts of water. Furthermore, as the growth rates appear to be independent to the concentration of OH at low water contents, they argued that the growth-controlled reaction rate with water dependence from (Hosoya et al., 2005) (Eq. (15)) cannot be extrapolated to water contents less than 300 wt. ppm. According to (Du Frane et al., 2013), the metastable wedge of olivine could exist only in a lithospheric mantle with less than 75 wt. ppm H_2O.

3.1.2. Ringwoodite transformation

The reaction kinetics of $(Mg,Fe)_2SiO_4$ Ringwoodite dissociation into $(Mg,Fe)SiO_3$ perovskite and (Mg,Fe)O ferropericlase have been poorly constrained. The post-spinel transformation is a eutectoid-type transformation that is characterized by the formation at low T of alternating lamellae of Bridgmanite and ferropericlase, which display topotactic relations with the reactant Ringwoodite (Kubo et al., 2002a; Poirier et al., 1986; Wang et al., 1997). For longer duration and higher temperature, the texture becomes more uniform and most of the grains are equigranular (Poirier et al., 1986; Yamazaki et al., 1996).

The lamellar growth kinetics was examined at low temperatures and relatively wet conditions (1000–2000 wt. ppm H_2O) by (Kubo et al., 2002a, 2008). In these experiments the lamellar spacing decreases with increasing overpressure, promoting higher reaction rates and smaller grain-sizes, which in turn induce rheological weakening.

(Wang et al., 1997) qualitatively suggested a kinetic blocking temperature of about 700 °C for the reaction, while (Kubo et al., 2002a) estimated that at that temperature an overpressure greater than 1 GPa is needed to complete the reaction in the cold slab.

3.1.3. Pyroxene dissolution in garnet

The kinetics of pyroxene dissolution into pyrope-rich garnet to form Al-poor majoritic garnet is controlled by the rate of diffusion of the majoritic component ($Mg_4Si_4O_{12}$, same stoichiometry as $MgSiO_3$ cEns) in pyrope garnet ($Mg_3Al_2Si_3O_{12}$) (van Mierlo et al., 2013). Diffusion experiments on majorite-natural pyrope garnet diffusion couples indicate that the majoritic component in garnet is one of the slowest diffusing components in the Earth's mantle and that, for realistic subduction rates, a temperature of at least 1500 °C is needed to complete the dissolution of pyroxene into garnet (Nishi et al., 2008, 2013; van Mierlo et al., 2013). This temperature is much higher than the temperature needed for olivine transformation (about 600–700 °C), implying that pyroxene and pyrope garnet could survive metastably at higher P–T conditions than olivine.

A sluggish diffusion of pyroxene into garnet has been measured also in wet pyrolitic compositions (CMAS system + 700–4000 wt. ppm H_2O) with two pyroxenes (diopside + enstatite) and pyrope garnet (Nishi et al., 2008). Despite the relatively high water content, the measured rate of dissolution of pyroxenes into garnet is much slower on experimental timescales than that of the dry olivine ⇔ Wadsleyite and post-garnet transformations at the same P–T conditions. In the basaltic crust, where Ca–Fe–Na-rich clinopyroxene coexist with pyrope garnet and minor coesite/stishovite at upper mantle conditions, pyroxene transformation

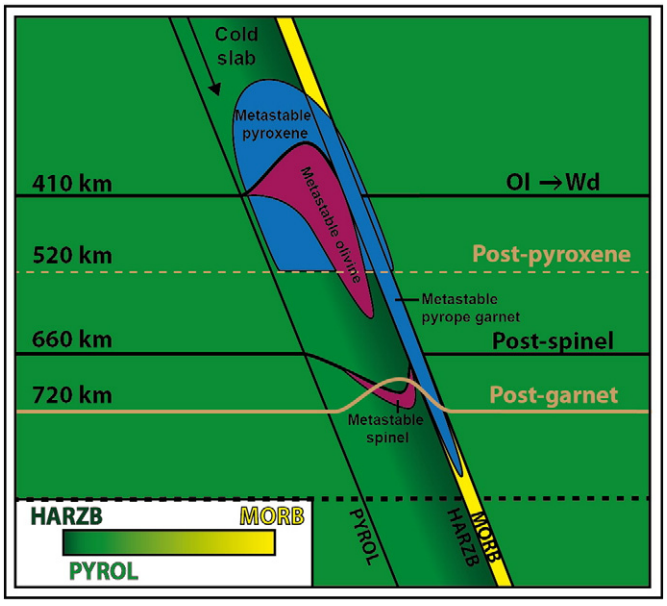

Fig. 11. Schematic representation of potential metastable fields for the olivine (purple) and non-olivine (blue) components within a compositionally stratified cold slab. The olivine ⇔ Wadsleyite, post-spinel and post-garnet reactions (continuous horizontal lines) are drawn at equilibrium, while the post-pyroxene reaction (dashed horizontal line) is effective in both equilibrium and metastable aggregates.

proceeds by an early exsolution of majoritic garnet along clinopyroxene grain boundaries at about 14–15 GPa, and a subsequent slow diffusion of pyroxene into garnet, which impedes the complete pyroxene transformation (Nishi et al., 2009, 2011). At T < 800 °C majoritic garnet exsolution is kinetically hindered for geological timescales, even with 1000 wt. ppm H_2O. It is worth nothing, however, that intracrystalline nucleation of majoritic garnet in clinopyroxene could occur in the subducting plate as observed in natural samples, where the actual grain-size of clinopyroxene is much larger. Intracrystalline nucleation would reduce the exsolution lamellae distance and diffusion length, so that the reaction could proceed even if the temperature is 800 °C (Nishi et al., 2011).

The remnant pyroxene phases, which kinetically failed to be accommodated in the garnet, eventually transform to their own high-pressure phases while keeping their original chemical compositions at about 18–20 GPa (post-pyroxene transformations). For instance, Ca-rich metastable clinopyroxene dissociates into Ca-perovskite, Wadsleyite and stishovite at about 18 GPa (Nishi et al., 2008). In the sub-Moho harzburgitic mantle high-P cEns transform directly to its high-pressure polymorphs Akimotoite or majorite, because decomposition of pyroxene to Wadsleyite and stishovite requires higher long-range diffusion and higher temperatures (Bina, 2013; Hogrefe et al., 1994).

3.1.4. Pyrope garnet transformation

The post-garnet transformation in pyrope garnet proceeds by nucleation on grain boundaries followed by sluggish growth of decomposed phases (Kubo et al., 2002b, 2008). Because the decomposition kinetics of pyrope garnet is significantly slower than for the post-spinel transformation, a significantly large amount of metastable garnet is predicted to exist in the cold crust of the subducting plate (Kubo et al., 2002b; Nishi et al., 2012). (Kubo et al., 2008) reported that the post-garnet transformation cannot complete at less than 1730 K with 400 wt. ppm H_2O for geological timescales, which is much higher than the approximate 900 K for the olivine ⇔ Wadsleyite transformation with a higher water content (Hosoya et al., 2005). Reaction kinetics experiments on decomposition of majoritic garnet have not been carried out, probably because it is assumed that pyroxene dissolution in pyrope garnet is very slow under low T conditions. However, (Litasov et al., 2004) argued that the kinetics of pyrope is not applicable for the transformation of the basaltic crust component, since metastable CaMg-perovskite (which forms around 22–23 GPa and 1300 K in dry conditions) enhances the kinetics of the post-garnet transformation. Under large overpressure conditions (31–38 GPa), metastable post-garnet transformation would eventually proceed by intracrystalline nucleation (Nishi et al., 2012).

3.1.5. Eclogitization

(Ahrens and Schubert, 1975) showed experimentally that for T < 600–800 °C the gabbro to eclogite transformation in the upper mantle cannot occur for geological timescales of subduction due to the slow diffusion of ions, and that water is needed to catalyse the reaction. There is indeed widespread field evidence for disequilibrium textures of incomplete reactions, and metastabilities due to sluggish nucleation or slow diffusion rate and kinetics of reactions in mafic rocks from low-T/high-P environments (Austrheim, 1987; Bjørnerud et al., 2002; John and Schenk, 2003; Pennacchioni, 1996). Interestingly, in these units eclogitization is observed only along those portions where fluid infiltration in previously dry and unusually strong mafic complexes has catalysed the reaction. Hence, differently from the deep phase transformations previously discussed, the occurrence of dry metastable rock units within both the continental and oceanic mafic crust at shallow upper mantle depths is supported by several field observations suggesting that the process of eclogitization is limited by reaction kinetics and dissolution–precipitation rates rather than by the metamorphic P–T conditions (John and Schenk, 2003).

3.2. Thermomechanical effects and chemical implications

3.2.1. Buoyancy and thermal effects

Metastable persistence of low-pressure phases, and the resulting spatial variations in mineralogy produce petrological buoyancy forces that affect the net buoyancy of slabs (Bina et al., 2001) (Fig. 12, Table 2). Spatial and temporal variations in the net buoyancies of slabs may be reflected in varying subduction rates and may affect slab morphology. Faster and older slabs with larger metastable wedges are decelerated more efficiently, and tend to be deflected toward the horizontal due to a parachute effect (Kirby et al., 1996; Marton et al., 1999; Schmeling et al., 1999). For sufficiently large metastable wedges of low-pressure phases, slab material may stagnate in the transition zone until thermal erosion of the positively buoyant metastable wedge allows the slab to resume sinking under the influence of its residual negative thermal buoyancy (Agrusta et al., 2014; Bina et al., 2001; King et al., 2015; Tetzlaff and Schmeling, 2000).

On the other hand, smaller sinking rates expose slabs to greater conductive warming, which thermally erodes their metastable wedges and damps the parachute effect. Although such feedback damping may act to narrow the range of feasible subduction rates, the net effect of the metastable wedge is to retard the penetration into the lower mantle (Bina et al., 2001; Tetzlaff and Schmeling, 2009). In the long-term, subduction velocities and the size of the metastable wedge should approach – paradoxically – an equilibrium state, with small cyclic variation (Tetzlaff and Schmeling, 2009).

Although the largest thermomechanical effects are often considered as related to the survival of olivine, other sluggish reactions can significantly influence the dynamic of subducting plates (Fig. 11). For instance, (Kubo et al., 2009) argued that the ~1 GPa overpressure needed for the post-spinel transformation at relatively low T would affect, together with the negative Clapeyron slope of the equilibrium boundary, the depression of 660 km seismic discontinuity, thus increasing the positive buoyancy forces within the peridotitic layer of the slab.

(Agrusta et al., 2014) and (King et al., 2015) have demonstrated that the extremely slow dissolution rate of pyroxene into garnet could lead to the formation of a buoyant metastable wedge of pyroxene in the cold slab and surrounding entrained mantle that is much broader than the one with metastable olivine, causing slab stagnation in the transition zone. Although both studies have likely overestimated the

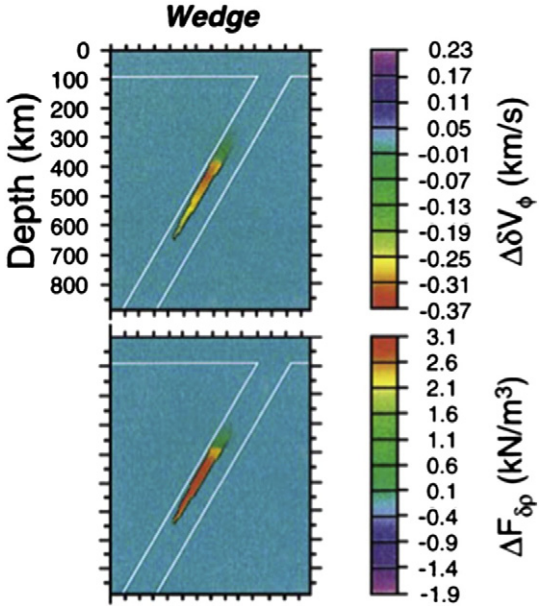

Fig. 12. Differential bulk sound velocity anomalies (top) and buoyancy anomalies (bottom) between disequilibrium and equilibrium cases, showing predicted effect of metastable olivine wedge. The slab boundary is also shown. From (Bina et al., 2001).

Table 2
Density and bulk sound velocity anomalies of major metastable phases with respect to the ambient mantle.

Low-P phase (High-P phase)	P (GPa)	T (K)	$\Delta\rho$ (kg/m^3)	$\Delta V\phi$ (km/s)
Ol (Wd)	13.5	1000 (1810)	−202 (−125)	−0.63 (−0.42)
	18	1000 (1870)	−188 (−110)	−0.60 (−0.40)
Ol (Rw)	23	1000 (1934)	−262 (−195)	−0.76 (−0.55)
Rw (Bdg + Fp)	23.5	1000 (1940)	−344 (−255)	−0.16 (0.08)
Hcen (Maj)	13.5	1000 (1810)	−226 (−169)	0.20 (0.39)
	18	1000 (1870)	−230 (−174)	0.28 (0.47)
Pyr (Bdg)	28	1300 (1990)	−465 (−408)	−0.62 (−0.46)

The densities and bulk sound velocities ($V\phi^2 = Vp^2 - 4/3Vs^2$) have been calculated with EosFit7 (Angel et al., 2014) by using the THERMOCALC database and a modified Tait EoS (Holland et al., 2013) for Mg-end member phases (except for pyrope: $Mg_3Al_2Si_3O_{12}$). The anomalies associated with the metastable phase in the cold slab interior are computed as differences relative to the high-P phase at both the slab and the ambient mantle (in brackets) temperatures. Abbreviations: Ol = Olivine; Wd = Wadsleyite; Rw = Ringwoodite; Bdg = Bridgmanite; Fp = Ferropericlase; Hcen = High-P clinoenstatite; Maj = Majorite; Pyr: Pyrope.

buoyancy induced by the metastable pyroxene ((King et al., 2015) assumed 50% average volume fraction of pyroxene for the slab instead of a more appropriate 30–40%, while (Agrusta et al., 2014) set the depth of post-pyroxene transformation to 670 km, instead of ~550 km (Hogrefe et al., 1994)), these results suggest that the presence of metastable pyroxene in the transition zone could be as important as that of metastable olivine. As the harzburgitic mantle contains only up to 20–25% of pyroxene, the positive buoyancy due to metastable pyroxene is larger in the oceanic crust, which could be slightly buoyant with respect to the ambient mantle in the transition zone (Nishi et al., 2011). Transformation of relict pyroxene via post-pyroxene reactions at P = 18–20 GPa (Hogrefe et al., 1994; Nishi et al., 2008) would then switch again the buoyancy to negative within both the crust and underlying harzburgitic mantle.

Metastable pyrope garnet at lower mantle depths also causes positive buoyancy forces within the basaltic crust at less than about 1730 K and the underlying peridotitic layer at about 1400–1600 K (Nishi et al., 2008).

While latent heats of phase transitions in subducting slabs under equilibrium conditions are simply manifested by refraction of adiabats along phase boundaries, latent heat release from exothermic phase transformations under disequilibrium conditions results in isobaric superheating above the equilibrium adiabat. The additional energy (converted into heat or dissipated by mechanical deformation or recrystallization processes) is given by the difference in Gibbs free energy that is zero at equilibrium conditions, and negative (energy is released) for transformations of metastable rock assemblages (Kirby et al., 1996). Indeed, even nominally endothermic transitions can yield heating under sufficient metastable overpressure (Bina, 1998). Thus, eventual transformation of any pods of metastable material should lead to local superheating which can increase the reaction rate.

3.2.2. Rheological effects

An important phenomenon associated with sluggish phase transitions is the grain-size reduction of the newly formed aggregate, which can lead to the activation of grain-size sensitive creep and to a transient rheological weakening of the transformed material. The initial grain-size of the product phase depends on the competition between the rate of nucleation and that of growth (Riedel and Karato, 1997). In the hot mantle, growth of the new crystals is fast, and thus minor variations in grain-size are expected after a phase transformation. In growth-controlled reactions such as the olivine polymorphic transformations occurring in cold core of old and fast slabs, instead, nucleation is very fast and therefore the size of the new grains tends to be small (Karato et al., 2001; Rubie, 1984; Vaughan and Coe, 1981). For instance, the grain-size of Ringwoodite in the cold subducting slab could be less than 100 μm according to the grain growth rates measured by (Yamazaki et al., 2005). Significant grain-size reduction is expected also in nucleation-controlled eutectoid (decomposition) reactions such as the post-spinel, the post-(Ca–Na-rich)-pyroxene and post-(pyrope)-garnet transformations, because of the formation of two or more product phases (Zener pinning effect) (Kubo et al., 2000, 2008; Kubo et al., 2009). A sluggish grain growth at relatively low temperature (≤1773 K) has been observed also in $CaIrO_3$ post-perovskite due to its strong anisotropic shape (Yoshino and Yamazaki, 2007), which may suggest that small grain-size and transient rheological weakening could occur after the material analogue post-pervoskite transition in the lowermost mantle.

The initial grain-size tends to decrease with the pressure overstep of metastable reactions (Kubo et al., 2000; Riedel and Karato, 1997). The subsequent crystal growth, which progressively erases such a rheological weakening effect, increases exponentially with temperature (and thus the rate of thermal relaxation of the slab) and the presence of water (Nishihara et al., 2006). Conversely, the presence of a secondary phases in decomposition reactions retards grain growth by the Zener pinning effect so that grain-sizes of multiphase rocks are several orders of magnitude smaller than those of monophase rocks in the geological time scale (Kubo et al., 2000; Yamazaki et al., 2010) (Fig. 13*A*). Hence, the product aggregates of the olivine polymorphic transformations and of the post-spinel, post-pyroxene and post-garnet reactions should be characterized by small grain-sizes in a cold and dry slab. For sufficiently small crystals, such grain-size reduction mechanism occurring below the tip of metastable portions can significantly affect the mechanical strength of cold rigid slabs, which paradoxically could be weaker than hotter and/or wet oceanic plates.

The mechanical effects induced by grain-size reduction in subducting slabs have been addressed by few studies. (Karato et al., 2001) estimated 1 to 2 orders of magnitude decrease of the flexural rigidity in cold slabs by this mechanism after the olivine polymorphic transformations, and proposed that such rheological weakening could promote slab stagnation (Fig. 13*B*). (Čížková et al., 2002) and (Tagawa et al., 2007) tested different amounts of grain-size reduction and subsequent temperature-dependent growth associated with the olivine polymorphic transformations in 2D dynamic models of subduction, and concluded that four to six orders of magnitude grain-size reduction in the central portion of the slab can induce significant slab weakening, favouring stagnation in the transition zone. (Kubo et al., 2009) predicted the amount of rheological weakening in the Mariana slab after the olivine polymorphic and post-spinel reactions, suggesting that the observed deformation and thickening at the top of the lower mantle could be related to the strong grain-size reduction associated with the post-spinel reaction.

3.2.3. Chemical implications

The buoyancy forces and rheological weakening associated with metastable phases and their subsequent transformation may lead to crustal delamination from the compositionally stratified slab. (Kubo et al., 2008) and (Nishi et al., 2012) suggested that either a buoyant garnetitic basaltic crust or a weak oceanic crust resulting from the decomposition of metastable post-garnet assemblages under large overpressure conditions could separate from the slab and accumulate at the top of the lower mantle, explaining the seismic discontinuities at depths of 900–1080 km observed beneath subduction zones (Kawakatsu and Niu, 1994; Niu and Kawakatsu, 1997; Vanacore et al., 2006).

Another important implication of metastability concerns the slab volatile content. Because water greatly enhances the reaction kinetics, (e.g., Hosoya et al., 2005; Kubo et al., 1998), the existence of metastable phases is often taken as evidence for a dry slab environment with less than 75 wt. ppm H_2O (Du Frane et al., 2013; Green et al., 2010). However, we should bear in mind that hydration of oceanic plates is highly heterogeneous, occurring principally along normal faults activated during bending-related deformation at the trench outer-rise system (Faccenda, 2014b; Faccenda et al., 2009a). Thus, similarly to what is

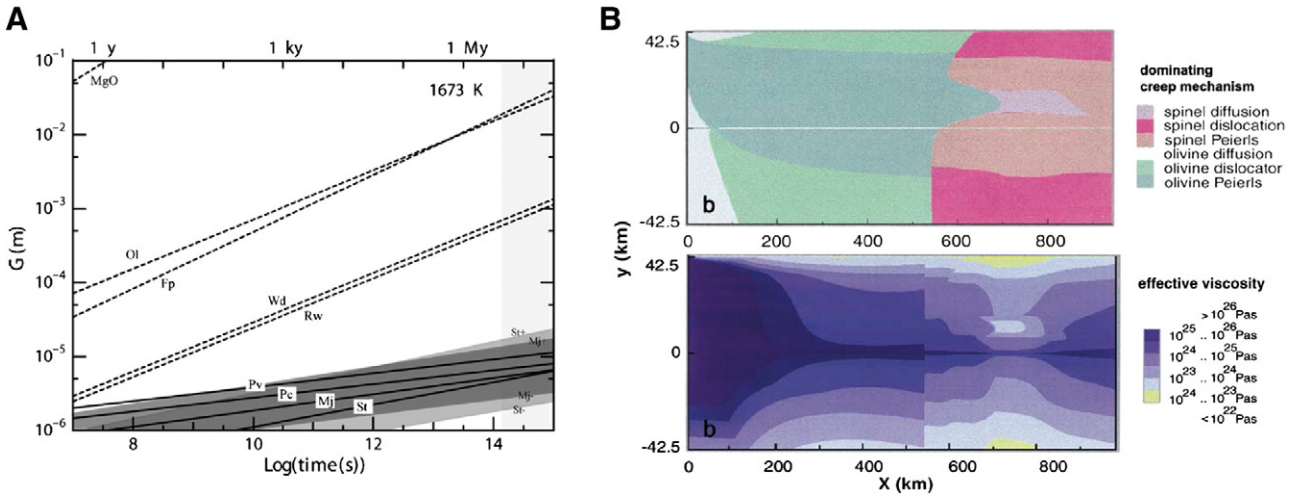

Fig. 13. (A) Comparison of experimental data of grain growth for various mantle materials for geological time scales at 1673 K and with initial grain size, $G_0 = 0$. Ol: olivine at 300 MPa (Karato, 1989a), MgO at ambient pressure (Kapadia and Leopold, 1974), Fp: ferropericlase at 18 GPa (Tsujino and Nishihara, 2009), Wd: Wadsleyite at 15 GPa (Nishihara et al., 2006), Rw: Ringwoodite at 21 GPa (Yamazaki et al., 2005), Pc: periclase and Pv: $MgSiO_3$ perovskite at 25 GPa (Yamazaki et al., 1996), Mj: majorite and St: stishovite at 18 GPa (Yamazaki et al., 2010). Dotted lines indicate the grain growth in the single phase, whereas solid lines indicate the grain growth in the multiphase. Meshed time range corresponds to the timescales of the transition zone residence of subducting slab for subduction velocity of 1–10 cm/y. Uncertainties of grain size of majorite and stishovite are shown as dark meshed areas indicated by "Mj+", "Mj−", "St+" and "St−" for the upper and lower bounds, respectively. From (Yamazaki et al., 2010). (B) Dominant deformation mechanism (top) and effective viscosity (bottom) in a subducting slab with initial temperature distribution corresponding to that for a 100 Myr oceanic lithosphere of 85 km thickness. X and Y coordinates indicate distance along and across the slab, respectively, with Y = 0 being the slab centre. Subduction velocity is 10 cm/yr. In high stress, low temperature regions, the Peierls mechanism dominates. In moderate stress, moderate to large grain-size regions, power-law creep dominates. Diffusion creep plays an important role in cold, fine-grain regions in the centre of slabs after a phase transformation, resulting in a low viscosity. This low viscosity region recovers its strength due to progressive grain-growth of spinel at greater depths. Modified after (Karato et al., 2001).

observed in exhumed low-T/high-P mafic complexes (Austrheim, 1987; Bjørnerud et al., 2002; John and Schenk, 2003; Pennacchioni, 1996), an alternation of wet transformed and dry metastable regions could exist in the cold portion of old and fast subducting oceanic plates at transition zone depths, provided that water released during decomposition of hydrous phase is not homogeneously redistributed within the slab.

3.3. Do deep metastable regions exist in subducting slabs?

3.3.1. Thermo-kinetic modelling perspective

Thermo-kinetic numerical models have been extensively used to predict the presence of metastable untransformed regions within subducting slabs with different ages and subduction rates. (Sung and Burns, 1976) were the first to argue that metastable olivine could persist into the Wadsleyite or Ringwoodite stability field based on results from a kinetic model which employs a standard Avrami equation at isothermal and isobaric conditions. Although no reaction kinetic data for olivine polymorphic transformations were available, they proposed a characteristic temperature of 700 °C below which these reactions are virtually blocked.

About two decades later, (Rubie and Ross, 1994) and (Kirby et al., 1996) employed a kinetic rate equation for phase interface-controlled growth occurring under non-isothermal, non-isobaric conditions, together with kinetic data of the olivine polymorphic transformations estimated empirically from reactions of minerals with analogue compositions. They predicted a wedge of metastable olivine extending to 700 km depth where slab temperatures remains below 600 °C. These predictions were used to infer a widespread presence of metastable wedges of olivine in old and fast subducting slabs, and, through the transformational faulting mechanism occurring during metastable phase transformations, provided a common explanation for the whole set of deep seismicity.

After these preliminary studies, however, which used simplified rock parameters and ignored intra-crystalline nucleation and other important thermo-kinetic effects, successive thermo-kinetic models have progressively reduced the extent of the metastable wedge of olivine. (Devaux et al., 1997) showed that by including thermal feedbacks, due to heat conduction and thermokinetic coupling (latent heat release and adiabatic heating effects), the metastable olivine wedge is considerably reduced.

(Mosenfelder et al., 2001) improved on previous work of (Rubie and Ross, 1994) and (Kirby et al., 1996) by incorporating experimental kinetic data of the olivine ⇔ Wadsleyite transformation from realistic mantle compositions $(Mg,Fe)_2SiO_4$ rather than analogue systems (which are 5 times slower), by accounting for intra-crystalline nucleation (together with grain boundary nucleation) and for latent heat effects in both the transformation kinetics (as (Kirby et al., 1996)) and the conservation of energy equation. The models predict significantly smaller wedges of metastable olivine than those from (Kirby et al., 1996) and a maximum depth extent of 500–550 km for the coldest slab.

(Marton et al., 2005) solved the conservation of energy equation by using realistic thermal conductivities, densities and isobaric heat capacities function of pressure, temperature and mineralogy. When radiative heat transfer is included, thermal conductivities are considerably higher and the slab interior is 50–100 °C warmer. The metastable wedge is reduced by 30–50 km, with a maximum depth of 550 km for the coldest Pacific slab subducting beneath Tonga.

The quotations of the metastable wedge model have recently surged following the quantification of the extremely slow dissolution of pyroxene into garnet by (Nishi et al., 2013) and (van Mierlo et al., 2013). For instance, (King et al., 2015) have used a simplified kinetic growth model in which the pyroxene to majoritic garnet transformation is set to occur rapidly across a transition temperature of 1000–1200 °C and at a maximum pressure of 18 GPa (post-pyroxene transformation) to show that a large metastable wedge of pyroxene forms within old slabs in the upper transition zone. Analogous results were found by (Agrusta et al., 2014) that modelled the pyroxene to majorite garnet transformation using the diffusion model and kinetic data from (van Mierlo et al., 2013). Although (Bina, 2013) pointed out that complex natural pyroxenes may be more reactive than the magnesium-rich variety used in the diffusion experiments, several experiments demonstrated that dissolution of pyroxene in garnet is much slower than the olivine polymorphic transformations (e.g., Nishi et al., 2008), suggesting that the presence of metastable wedges of pyroxene is more likely than that of any other mineral phase.

3.3.2. Seismological evidence

Low-pressure metastable phases can be detected by seismic surveys, as their seismic velocities are usually lower than those of the equilibrium aggregates at the same P–T conditions (but see (Koper et al., 1998)). Consequently, an untransformed region within the slab should be associated with low seismic velocities and depressed seismic discontinuities (Fig. 12). For example, metastable gabbros in the 60–150 km depth range displays 7–8% lower Vp than the equilibrium eclogitic assemblage (Hacker et al., 2003). At lower mantle depths, metastable pyrope has significantly lower seismic velocities than, for example, Bridgmanite (Table 2). In the cold slab mantle, metastable olivine at transition zone depths would be associated with lower seismic velocities only partly compensated by the less abundant metastable clinoenstatite that is characterized by faster seismic wave propagation. Indeed, in contrast to other metastable phases, a metastable wedge of high-P clinoenstatite would increase the seismic velocities while decreasing the slab density.

Accordingly, several seismic observations have been attributed to the existence of metastable phases in some subduction zones. Metastable dry gabbros have been proposed to explain the low velocity zones in the 50–150 km depth range (Abers, 2005). Seismic low-velocity zones and depressed 410 km discontinuities in the Pacific, Mariana, and Kuril slabs have been interpreted as metastable olivine (Jiang et al., 2015; Kaneshima et al., 2007; Kawakatsu and Yoshioka, 2011; Pankow et al., 2002). Seismic anisotropy in the subducting Tonga–Fiji slab and below Northeast Asia has been interpreted as resulting from lattice preferred orientation of metastable olivine (Chen and Brudzinski, 2003; Liu et al., 2008). The presence of metastable Ringwoodite could explain the strong depression of the 660 km discontinuity in correspondence of the slabs ponding beneath Mariana (Kubo et al., 2009) and southern Europe (Cottaar and Deuss, 2016).

Because the transformation of metastable phases normally occurs with large reduction in volume, causing large stresses, and release of latent heat, deep earthquakes triggered by the transformational faulting mechanism is often taken as a further evidence for the presence of metastable regions (Kirby et al., 1996). Indeed, deep focus earthquake hypocentres (300–700 km depth) occur most frequently in the coldest, oldest slabs with high subduction rates, which suggests a possible link to the presence of metastable olivine (Kirby et al., 1996). This hypothesis appears to be confirmed by deep double seismic zones found in the Tonga, Izu–Bonin, and Pacific slabs that have been attributed to delayed, seismogenic transformation at the boundaries of a metastable olivine wedge (Guest et al., 2004; Iidaka and Furukawa, 1994; Wiens et al., 1993).

These sets of observations are contrasting with other regional seismic surveys that have failed to detect the presence of metastable wedges in other segments of the Western Pacific subduction zones. For example, an elevated 410 km discontinuity has been observed in the cold slab at the Izu-Bonin and Japan trenches (Collier and Helffrich, 1997; Gao et al., 2010). At the global scale, several studies show a thickened transition zone in and around subduction systems, including those on the Western Pacific (Deuss, 2009; Gu et al., 2003; Houser et al., 2008; Lawrence and Shearer, 2008). Furthermore, an anomalously depressed 660 km discontinuity around subducting slabs could be explained without invoking the presence of metastable Ringwoodite given (i) the large experimental range of equilibrium Clapeyron slopes for the post-spinel phase transition and (ii) the strongly negative slope of the post-ilmenite transition (Cottaar and Deuss, 2016) (Table 1). The low velocity layer atop the subducting slabs in the 50–150 km depth range can also be interpreted as due to the presence of hydrous phase (Abers, 2005). Finally, alternative triggering mechanisms that do not require metastability have been proposed to explain deep seismicity, such as adiabatic shear instabilities (Karato et al., 2001) and dehydration embrittlement caused by decomposition of deep hydrous phases (Omori et al., 2004).

In summary, although some convincing seismological evidence has been provided for the presence of relatively small, deep metastable portions within cold slabs (e.g., Jiang et al., 2015; Kawakatsu and Yoshioka, 2011), more geophysical observations are needed to better constrain the extent of untransformed regions that, at present, appear to be not as widespread as initially proposed.

3.4. Numerical implementation

The effects of metastable phase transitions can be investigated by simulating the reaction kinetics, the initial grain size of the product phase and its subsequent growth. Below we provide a concise description of the relevant equations and methods that have been traditionally employed to model these processes.

3.4.1. Reaction kinetics

The transformation kinetics at constant P–T conditions is described by the Avrami equation:

$$\xi = 1 - exp(-k \cdot t^n) \tag{12a}$$

$$k = \frac{\pi \dot{N} \dot{G}^3}{3} \tag{12b}$$

where ξ is the volume fraction of the product phase, $\dot{N}$ and $\dot{G}$ are the nucleation and growth rates, while k and n are assumed to be constants.

However, because the P–T conditions are continuously changing within the subducting slab, the nucleation and growth rates, together with k and n, are also changing during the transformation (Rubie and Ross, 1994). A better growth rate model that takes into account the time-dependent P–T conditions of the metastable reaction front is (Cahn, 1956; Rubie and Ross, 1994):

$$\xi = 1 - exp\left(-2S\int_0^t \dot{x}(\theta) d\theta\right) \tag{13}$$

where $S = 3.35/d$, d is the grain diameter of the reactant phase and $\dot{x}(\theta)$ is the growth rate at timestep θ. Assuming nucleation site saturation (no nucleation), Eq. (5) becomes (Hosoya et al., 2005):

$$\xi = 1 - exp\left(-\frac{6.7}{d}\dot{x}t\right) \tag{14}$$

with

$$\dot{x} = k_g T C_{OH}^r exp\left(-\frac{H + PV}{RT}\right)\left[1 - exp\left(\frac{\Delta G}{RT}\right)\right] \tag{15}$$

where k_g is a constant, C_{OH} is the concentration of hydroxils to the power r, H and V are the activation enthalpy and the activation volume for growth, R is the gas constant, and ΔG is the Gibbs free energy change of reaction. This equation is normally used to model interface-controlled reactions, such as polymorphic olivine transformations. Intracrystalline nucleation can be modelled by taking small grain-sizes (Nishi et al., 2009).

The lamellar, diffusion-controlled growth rate in decomposition reaction such the post-spinel transformation is (Nishi et al., 2009):

$$\dot{x} = B\frac{1}{l} exp\left(-\frac{\Delta E^*}{RT}\right)\left(\Delta G_v - 2\frac{\gamma}{l}\right) = B'\Delta P^2 exp\left(-\frac{\Delta E^*}{RT}\right) \tag{16}$$

where B and B' are constants, ΔE^* is the activation energy, ΔG_v is the free energy change of reaction per unit volume, γ is interfacial energy per unit area, l is the lamellae spacing, and ΔP is the overstep in pressure to which ΔG_v and $1/l$ are proportional, yielding the rightmost formulation.

The diffusion of pyroxene components into pyrope garnet is (Nishi et al., 2013; van Mierlo et al., 2013):

$$D = D_0 exp\left(-\frac{\Delta H_{px-grt}}{RT}\right) \tag{17}$$

where D_0 is a pre-exponential constant and ΔH_{px-grt} is the activation enthalpy of the reaction. The volume fraction of dissolved pyroxene can be calculated assuming a spherically symmetric grain, whose size decreases as a function of time (Nishi et al., 2013):

$$d(t) = d_0 - \frac{k_d Dt}{2d_0} - k_d\sqrt{\frac{Dt}{\pi}} \tag{18}$$

where d_0 is the initial grain-size and k_d is approximately 2 in the mantle transition zone. Alternatively, the volume fraction of dissolved pyroxene as proposed by (van Mierlo et al., 2013) is:

$$\xi = \frac{t}{t_{diff}}; \tag{19a}$$

$$t_{diff} = \frac{1}{4}\frac{d^2}{D} \tag{19b}$$

where t_{diff} is the time necessary to diffuse the pyroxene component at a distance of a half the grain size d.

3.4.2. Grain size reduction and subsequent growth

(Riedel and Karato, 1997) developed a theory for estimating the grain-size of the product phases, taking into account thermal feedbacks. The initial grain-size d_0 of the product phase depends on the competition between the rate of nucleation and that of growth:

$$d_0 \cong \left[\frac{\dot{G}_0}{\dot{N}_0}\right]^{1/3} exp\left(\frac{c_1}{T\Delta\mu^2}\right) \tag{20}$$

where c_1 is a constant and $\Delta\mu$ is the thermodynamic driving force proportional to the overstep pressure. In growth-controlled reactions as those occurring at T < 900 K, nucleation is very fast and therefore d_0 is very small. Also, the higher the pressure overstep, the smaller the grain-size. Eq. (20) does not contemplate the presence of secondary phases that retard grain growth by the Zener pinning effect (Yamazaki et al., 2010). As it is difficult to estimate d_0, numerical studies have systematically tested different amounts of grain size reduction (Čížková et al., 2002; Tagawa et al., 2007). Subsequent grain growth can be estimated as (Nishihara et al., 2006):

$$d^n - d_0^n = k_n t; k_n = k_{n0}\, exp\left(-\frac{H^*}{RT}\right) C_{OH}^r \tag{21}$$

where k_{n0} is a pre-exponential factor, $H^*$is the activation enthalpy for grain growth and the last term on the right-hand side describes the enhanced growth rates in presence of water.

4. Conclusions and perspectives

Solid–solid phase transitions play a fundamental role in the Earth's internal dynamic, with the main implications that can be summarized as follows:

- Phase transitions directly affect mantle convection by generating buoyancy forces that arise from deflections of the phase boundary from its normal depth and, to a minor extent, from the release or absorption of latent heat (Christensen, 1995; Schubert et al., 1975). The buoyancy forces increase with the density contrast between the reactant and product phases, their volume fraction, the steepness of the reaction slope, and are progressively mitigated with increasing finite width of multivariant phase transition fields due to solid-solution effects.
- In a homogeneous pyrolitic mantle, the buoyancy effects due to the endothermic post-spinel transformation depend on temperature and can largely be compensated by the exothermic garnet-to-perovskite reaction (Figs. 3A, 4B). At low temperatures where both the endothermic post-spinel and post-ilmenite reactions take place, slabs may stagnate at the 660 km discontinuity for sufficiently fast trench retreat rates (Fig. 6). At high temperatures, instead, upwelling plumes are accelerated by the set of transformations occurring in the 600–800 km depth range (Fig. 7).
- In a compositionally heterogeneous system, additional buoyancy forces are generated by the vertical shift of phase transformations that affect distinct petrological components at different mantle depths and to different extents – given the varying abundances in the olivine and pyroxene components – (Figs. 3B, C, D, 4C). As a consequence, phase transitions enhance density differences between different lithological components and promote their mechanical separation (unmixing). This results in a chemical stratification of the Earth's interior characterized by an enrichment of the MORB component toward the bottom of the transition zone and of the lower mantle (e.g., Ballmer et al., 2015) (Fig. 8). In this system, large positive buoyancy forces are generated within cold slabs with an olivine-rich harzburgitic mantle around the 660 km discontinuity, while MORB-rich plumes may pond in the 300–410 km depth range due to their higher density with respect to a pyrolitic ambient mantle.
- Several metastable phases can potentially survive beyond the equilibrium reaction boundary within cold and dry slabs (Fig. 11), providing additional and positive buoyancy forces that resist subduction. Among these, a metastable wedge of abundant olivine would produce the largest positive buoyancy within the harzburgitic slab mantle at transition zone depths. However, increasingly sophisticated thermo-kinetic models have progressively reduced the size of the olivine metastable field. On the other hand, it has been recently found that the rate of high-pressure transformations of the less abundant non-olivine component such as garnet and pyroxenes is much slower than that of the olivine component, yielding much broader metastable portions. This suggests that, despite their smaller volume fraction, the buoyancy effects induced by the metastable non-olivine component might be as large as those due to metastable olivine.
- The presence of low-density, low-seismic velocity metastable wedges is still debated, as contrasting seismological observations are frequently reported from the same subduction systems. Field observations (e.g., Bjørnerud et al., 2002) and numerical modelling results (Faccenda et al., 2009a) suggest that heterogeneously hydrated slabs could contain metastable dry portions surrounded by transformed wet rocks. Hence, the paradigm according to which presence of metastable portions is indicative of a completely dry slab (<75 wt. ppm H_2O; Du Frane et al., 2013; Green et al., 2010) might not be valid.
- Another important effect associated with phase transformations is the change in transport properties (e.g., viscosity, thermal conductivity, electrical conductivity) of the transformed material. Of particular interest is the change in rheological properties that can be related to the different intrinsic mechanical behaviour of the newly formed mineralogical assemblage, the heating or cooling associated with latent heat and the transient grain size reduction in downwelling cold material (e.g., Karato et al., 2001). Strong gradients in radial viscosity profiles induced by phase transformations, including low-viscosity channels and viscosity hills, would enhance horizontal flow, causing slab stagnation and plume ponding.
- Tendency to layered mantle convection is likely ascribable to variations in viscous mechanical behaviour of the minerals, as buoyancy forces due to changes in density appear to be insufficient to promote layering for realistic mantle compositions.
- Phase transformations in minerals are frequently associated with a change in solubility of volatiles (water — as hydrogen, halogens, sulphur, noble gases), a process that can lead to the formation of deep reservoirs, partial melting and additional variations in the rock mechanical behaviour (e.g., Bercovici and Karato, 2003).

Beside these general and often widely accepted conclusions, there are several issues and open questions that should be further addressed

in the future in order to improve our capability to reproduce and understand mantle convection patterns in our planet:

- There is still no broad consensus on the nature and geodynamic significance of several important phase transformations occurring at transition zone and lower mantle P–T conditions (e.g., the post-spinel, post-garnet, post-perovskite and iron spin transitions), with estimated Clapeyron slopes and depths that vary substantially as a function of the used sample composition, pressure standards and experimental apparatus (Table 1). Large experimental uncertainties exist also about the variation in physical properties and volatile solubility of mineral phases across and away from phase transitions, and about reaction kinetics and subsequent grain growth at low temperatures. These experimental uncertainties cause substantially different numerical model predictions of mantle convection, which, together with conflicting seismological observations, lead to a non-unique and at times biased interpretation of Earth's internal dynamics and evolution.
- Discrepancies among mantle convection predictions often depend exclusively on model assumptions. Ignoring phase transitions in the pyroxene-garnet component of the mantle would represent a major pitfall of any mantle convection numerical simulation, which would likely overestimate the layered or intermittent convective behaviour of the Earth's mantle. Hence, we encourage future numerical studies of global mantle convection to take into account these important phase transformations together with magmatic differentiation processes that allow reproducing compositional heterogeneities characteristic of the Earth's interior. Likewise, metastability is often not contemplated in most numerical simulations, despite the fact it could play an important role in the dynamics of subducting slabs.
- Recent global seismological models indicate that several structures interpreted as ascending plumes and descending slabs appear to be deflected or stagnate around 1000 km depth and away from major phase transitions (French and Romanowicz, 2015; Fukao and Obayashi, 2013; Rickers et al., 2013). These observations have been the subject of great attention over the last few years, as they appear to indicate that other mechanisms different from those related to phase transitions should be considered (intrinsic variation with depth of the lower mantle minerals mechanical behaviour, yielding a mid-mantle viscosity hill (Ammann et al., 2010; Ito and Toriumi, 2007; Marquardt and Miyagi, 2015; Rudolph et al., 2015); gradual enrichment in the heavier and harder MORB component in the lower mantle that would decelerate subducting slabs (Ballmer et al., 2015)). The role of the iron disproportionation reaction and of the iron spin transition in Bridgmanite occurring around these depths is still uncertain, and it is unclear whether they could affect significantly mantle dynamics. More in general, the set physical and chemical processes taking place in the uppermost lower mantle is still not well constrained, and a thorough experimental and numerical investigation could provide the key to the interpretation of these enigmatic observations.

Acknowledgements

Manuele Faccenda is indebted to editors Tim Horscroft and Marco Scambelluri for this review invitation. This article has benefited from fruitful discussions with our colleagues Roberto Agrusta, Ross Angel, Maxim Ballmer, Fabio Capitanio, Taras Gerya, Shun-ichiro Karato, Carolina Lithgow-Bertelloni, Takashi Nakagawa, Giorgio Pennacchioni, Alex Song and Paul Tackley. Carolina Lithgow-Bertelloni kindly provided the density lookup tables plotted in Figs. 2 and 3, while Takashi Nakagawa the data plotted in Fig. 8. Maxim Ballmer and an anonymous reviewer have greatly improved the manuscript with detailed comments and suggestions. The authors were supported by the Progetto di Ateneo FACCPRAT2012 granted by the Università di Padova to M.F.

References

Abers, G.A., 2005. Seismic low-velocity layer at the top of subducting slabs: observations, predictions, and systematics. Physics of the Earth and Planetary Interiors 149, 7–29.
Agrusta, R., Van Hunen, J., Goes, S., 2014. The effect of metastable pyroxene on the slab dynamics. Geophysical Research Letters 41, 8800–8808.
Ahrens, T.J., Schubert, G., 1975. Gabbro-eclogite reaction rate and its geophysical significance. Reviews of Geophysics 13, 383–400.
Akaogi, M., 2007. Phase transitions of minerals in the transition zone and upper part of the lower mantle. In: Ohtani, E. (Ed.), Advances in High-pressure MineralogyGeological Society of America Special Paper Vol. 421. Geological Society of America, pp. 1–13.
Akaogi, M., Ito, E., 1993. Refinement of enthalpy measurements of $MgSiO_3$ perovskite and negative pressure–temperature slopes for perovskite-forming reactions. Geophysical Research Letters 20, 1839–1842.
Akaogi, M., Ito, E., Navrotsky, A., 1989. Olivine-modified spinel–spinel transitions in the system Mg_2SiO_4–Fe_2SiO_4: CALORIMETRIC measurements, thermochemical calculation, and geophysical application. Journal of Geophysical Research 94, 15671–15685.
Ammann, M.W., Brodholt, J.P., Wookey, J., Dobson, D.P., 2010. First-principles constraints on diffusion in lower mantle minerals and a weak D″ layer. Nature 465, 462–465.
Angel, R.J., Chopelas, A., Ross, N.L., 1992. Stability of high-density clinoenstatite at upper-mantle pressures. Nature 358, 322–324.
Angel, R.J., Gonzalez-Platas, J., Alvaro, M., 2014. EosFit-7c and a Fortran module (library) for equation of state calculations. Zeitschrift für Kristallographie 229, 405–419.
Aoki, I., Takahashi, E., 2004. Density of MORB eclogite in the upper mantle. Physics of the Earth and Planetary Interiors 143-144, 129–143.
Armann, M., Tackley, P.J., 2012. Simulating the thermo-chemical magmatic and tectonic evolution of Venus' mantle and lithosphere: two-dimensional models. Journal of Geophysical Research 117. http://dx.doi.org/10.1029/2012JE004231.
Austrheim, H., 1987. Eclogitization of lower crustal granulites by fluid migration through shear zones. Earth and Planetary Science Letters 81, 221–232.
Ballmer, M., Ito, G., Wolfe, C.J., Solomon, S.C., 2013. Double layering of a thermochemical plume in the upper mantle beneath Hawaii. Earth and Planetary Science Letters 376, 155–164.
Ballmer, M.D., Schmerr, N.C., Nakagawa, T., Ritsema, J., 2015. Compositional mantle layering revealed by slab stagnation at ~1000-km depth. Science Advances 1, e1500815.
Belmonte, D., 2013. Ab initio Thermodynamics of Deep Mantle Minerals: The System MgO–SiO_2. (PhD Thesis). Università di Genova .
Benesova, N., Čížková, H., 2013. Effect of post-perovskite rheology on the thermal evolution of the Earth. Physics of the Earth and Planetary Interiors 251, 1–10.
Bercovici, D., Karato, S., 2003. Whole-mantle convection and the transition-zone water filter. Nature 425, 39–44.
Billen, M.I., 2010. Slab dynamics in the transition zone. Physics of the Earth and Planetary Interiors 183, 296–308.
Bina, C.R., 1998. A note on latent heat release from disequilibrium phase transformations and deep seismogenesis. Earth, Planets and Space 50, 1029–1034.
Bina, C.R., 2013. Garnet goes hungry. Nature Geoscience 6, 335–336.
Bina, C.R., Helffrich, G.R., 1994. Phase transition Clapeyron slopes and transition zone seismic discontinuity topography. Journal of Geophysical Research 99, 15,853–15,860.
Bina, C.R., Stein, S., Marton, F.C., van Ark, E.M., 2001. Implications of slab mineralogy for subduction dynamics. Physics of the Earth and Planetary Interiors 127, 51–66.
Bjørnerud, M.G., Austrheim, H., Lund, M.G., 2002. Processes leading to eclogitization (densification) of subducted and tectonically buried crust. Journal of Geophysical Research 107. http://dx.doi.org/10.1029/2001JB000527.
Bower, D.J., Gurnis, M., Jackson, J.M., Sturhahn, W., 2009. Enhanced convection and fast plumes in the lower mantle induced by the spin transition in ferropericlase. Geophysical Research Letters 36. http://dx.doi.org/10.1029/2009GL037706.
Bunge, H.P., Richards, M.A., Baumgardner, J.R., 1996. Effect of depth-dependent viscosity on the planform of mantle convection. Nature 379, 436–438.
Bunge, H.P., Richards, M.A., Baumgardner, J.R., 1997. A sensitivity study of three-dimensional spherical mantle convection at 10^8 Rayleigh number: effects of depth-dependent viscosiy, heating mode and an endothermic phase change. Journal of Geophysical Research 102, 11,991–12,007.
Cahn, J.W., 1956. The kinetics of grain boundary nucleated reactions. Acta Metallurgica 4, 449–459.
Carrez, P., Ferre, D., Cordier, P., 2007. Implications for plastic flow in the deep mantle from modelling dislocations in $MgSiO_3$ minerals. Nature 446, 68–70.
Chen, W., Brudzinski, M.R., 2003. Seismic anisotropy in the mantle transition zone beneath Fiji-Tonga. Geophysical Research Letters 30. http://dx.doi.org/10.1029/2002GL016330.
Chen, J., Inoue, T., Weidner, D.J., Wu, Y., Vaughan, M.T., 1998. Strength and water weakening of mantle minerals, olivine, wadsleyite and ringwoodite. Geophysical Research Letters 25, 575–578.
Chen, J., Inoue, T., Yurimoto, H., Weidner, D.J., 2002a. Effect of water on olivine-wadsleyite phase boundary in the $(Mg, Fe)_2SiO_4$ system. Geophysical Research Letters 29. http://dx.doi.org/10.1029/2001GL014429.
Chen, J., Weidner, D.J., Vaughan, M.T., 2002b. The strength of $Mg_{0.9}Fe_{0.1}SiO_3$ perovskite at high pressure and temperature. Nature 419, 824–827.
Chopelas, A., 1999. Estimates of mantle relevant Clapeyron slopes in the $MgSiO_3$ system from high-pressure spectroscopic data. American Mineralogist 84, 233–244.
Chopelas, A., Boehler, R., Ko, T., 1994. Thermodynamics and behavior of γ-Mg_2SiO_4 at high pressure: implications for Mg_2SiO_4 phase equilibrium. Physics and Chemistry of Minerals 21, 6351–6359.
Christensen, U.R., 1984. The interaction of a subducting lithospheric slab with a chemical or phase boundary. Journal of Geophysical Research 89, 4389–4402.

Christensen, U.R., 1995. Effects of phase transitions on mantle convection. Annual Review of Earth and Planetary Sciences 23, 65–87.

Christensen, U.R., 1996. The influence of trench migration on slab penetration into the lower mantle. Earth and Planetary Science Letters 140, 27–39.

Christensen, U.R., Yuen, D.A., 1985. Layered convection induced by phase-transition. Journal of Geophysical Research 90, 291–300.

Chudinovskikh, L., Boehler, R., 2004. $MgSiO_3$ phase boundaries measured in the laser-heated diamond cell. Earth and Planetary Science Letters 219, 285–296.

Čížková, H., Bina, C.R., 2013. Effects of mantle and subduction-interface rheologies on slab stagnation and trench rollback. Earth and Planetary Science Letters 379, 95–103.

Čížková, H., Van Hunen, J., van der Berg, A.P., Vlaar, N.J., 2002. The infuence of rheological weakening and yield stress on the interaction of slabs with the 670 km discontinuity. Earth and Planetary Science Letters 199, 447–457.

Čížková, H., Cadek, O., Matyska, C., Yuen, D.A., 2010. Implications of post-perovskite transport properties for core–mantle dynamics. Physics of the Earth and Planetary Interiors 180, 235–243.

Clift, P., Vannucchi, P., Morgan, J.P., 2009. Crustal redistribution, crust–mantle recycling and Phanerozoic evolution of the continental crust. Earth-Science Reviews 97, 80–104.

Collier, J.D., Helffrich, G.R., 1997. Topography of the "410" and "660" km seismic discontinuities in the Izu–Bonin subduction zone. Geophysical Research Letters 24, 1535–1538.

Connolly, J.A.D., 2005. Computation of phase equilibria by linear programming: a tool for geodynamic modeling and its application to subduction zone decarbonation. Earth and Planetary Science Letters 236, 524–541.

Cottaar, S., Deuss, A., 2016. Large-scalemantle discontinuity topography beneath Europe: signature of akimotoite in subducting slabs. Journal of Geophysical Research 121, 279–292.

Dal Zilio, L., Faccenda, M., Capitanio, F.A., 2016. The role of Deep Subduction in Supercontinent Breakup (submitted for publication).

Dannberg, J., Sobolev, S.V., 2015. Low-buoyancy thermochemical plumes resolve controversy of classical mantle plume concept. Nature Communications 6. http://dx.doi.org/10.1038/ncomms7960.

Davies, G.F., 1995. Penetration of plates and plumes through the mantle transition zone. Earth and Planetary Science Letters 133, 507–516.

Davies, G.F., 2008. Episodic layering of the early mantle by the 'basalt barrier' mechanism. Earth and Planetary Science Letters 275, 382–392.

Deuss, A., 2009. Global observations of mantle discontinuities using SS and PP precursors. Surveys in Geophysics 30, 301–326.

Devaux, J.P., Schubert, G., Anderson, C., 1997. Formation of a metastable olivine wedge in a descending slab. Journal of Geophysical Research 102, 24,627–24,637.

Diedrich, T., Sharp, T.G., Leinenw, K., Holloway, J.R., 2009. The effect of small amounts of H_2O on olivine to ringwoodite transformation growth rates and implications for subduction of metastable olivine. Chemical Geology 262, 87–99.

Doin, M., Henry, P., 2001. Subduction initiation and continental crust recycling: the roles of rheology and eclogitization. Tectonophysics 342, 163–191.

Du Frane, W.L., Sharp, T.G., Mosenfelder, J.L., Leinenweber, K., 2013. Ringwoodite growth rates from olivine with 7 ppmw H_2O: metastable olivine must be nearly anhydrous to exist in the mantle transition zone. Physics of the Earth and Planetary Interiors 219, 1–10.

Faccenda, M., 2014a. Mid mantle seismic anisotropy around subduction zones. Physics of the Earth and Planetary Interiors 227, 1–19.

Faccenda, M., 2014b. Water in the slab: a trilogy. Tectonophysics 614, 1–30.

Faccenda, M., Gerya, T.V., Burlini, L., 2009a. Deep slab hydration induced by bending-related variations in tectonic pressure. Nature Geoscience 2, 790–793.

Faccenda, M., Minelli, G., Gerya, T.V., 2009b. Coupled and decoupled regimes of continental collision: numerical modeling. Earth and Planetary Science Letters 278, 337–349.

Faccenda, M., Gerya, T.V., Mancktelow, N.S., Moresi, L., 2012. Fluid flow during slab unbending and dehydration: implications for intermediate-depth seismicity, slab weakening and deep water recycling. Geochemistry, Geophysics, Geosystems 13. http://dx.doi.org/10.1029/2011GC003860.

Fei, Y., van Orman, J., Li, J., van Westrenen, W., Sanloup, C., Minarik, W., Hirose, K., Komabayashi, T., Walter, M., Funakoshi, K., 2004. Experimentally determined postspinel transformation boundary in Mg_2SiO_4 using MgO as an internal pressure standard and its geophysical implications. Journal of Geophysical Research 109. http://dx.doi.org/10.1029/2003JB002562.

French, S.W., Romanowicz, B., 2015. Broad plumes rooted at the base of the Earth'smantle beneath major hotspots. Nature 525, 95–99.

Frost, D.J., Myhill, R., 2016. Chemistry of the lower mantle. In: Terasaki, H., Fisher, R.A. (Eds.), Deep Earth Physics and Chemistry of the Lower Mantle and Core. American Geophysical Union, Washington DC, pp. 225–240.

Frost, D.J., Liebske, C., Langenhorst, F., McCammon, C.A., Trønnes, R.G., Rubie, D.C., 2004. Experimental evidence for the existence of iron-rich metal in the Earth's lower mantle. Nature 428, 409–412.

Fukao, Y., Obayashi, M., 2013. Subducted slabs stagnant above, penetrating through, and trapped below the 660 km discontinuity. Journal of Geophysical Research 118, 5920–5938.

Fukao, Y., Obayashi, M., Nakakuki, T., the Deep Slab Project Group, 2009. Stagnant slab: a review. Annual Review of Earth and Planetary Sciences 37, 19–46.

Ganguly, J., Freed, A.M., Saxena, S.K., 2009. Density profiles of oceanic slabs and surrounding mantle: integrated thermodynamic and thermal modeling, and implications for the fate of slabs at the 660 km discontinuity. Physics of the Earth and Planetary Interiors 172, 257–267.

Gao, Y., Suetsugu, D., Fukao, Y., Obayashi, M., Shi, Y., Liu, R., 2010. Seismic discontinuities in the mantle transition zone and at the top of the lower mantle beneath eastern China and Korea: influence of the stagnant Pacific slab. Physics of the Earth and Planetary Interiors 138, 288–295.

Garel, F., Goes, S., Davies, D.R., Davies, J.H., Kramer, S.C., Wilson, C.R., 2014. Interaction of subducted slabs with the mantle transition-zone: a regime diagram from 2-D thermo-mechanical models with a mobile trench and an overriding plate. Geochemistry, Geophysics, Geosystems 15, 1739–1765.

Gerya, T.V., 2010. Introduction to Numerical Geodynamical Modelling. Cambridge University Press .

Gerya, T.V., Yuen, D.A., 2003. Rayleigh–Taylor instabilities from hydration and melting propel 'cold plumes' at subduction zones. Earth and Planetary Science Letters 212, 47–62.

Gerya, T.V., Connolly, J.A.D., Yuen, D.A., Gorczyk, W., Capel, A.M., 2006. Seismic implications of mantle wedge plumes. Physics of the Earth and Planetary Interiors 156, 59–74.

Gerya, T.V., Perchuk, L.L., Burg, J., 2008. Transient hot channels: perpetrating and regurgitating ultrahigh-pressure, high-temperature crust–mantle associations in collision belts. Lithos 103, 236–256.

Ghosh, S., Ohtani, E., Litasov, D.K., Suzuki, A., Dobson, D., Funakoshi, K., 2013. Effect of water in depleted mantle on post-spinel transition and implication for 660 km seismic discontinuity. Earth and Planetary Science Letters 371-372, 103–111.

Girard, J., Amulele, G., Farla, R., Mohiuddin, A., Karato, S., 2016. Shear deformation of bridgmanite and magnesiowüstite aggregates at lower mantle conditions. Science 351, 144–147.

Green, D.H., Ringwood, A.E., 1967. An experimental investigation of the gabbro to eclogite transformation and its petrological applications. Geochimica et Cosmochimica Acta 31, 767–833.

Green, H.W., Chen, W., Brudzinski, M.R., 2010. Seismic evidence of negligible water carried below 400-km depth in subducting lithosphere. Nature 467, 828–831.

Grocholski, B., Catalli, K., Shim, S., Prakapenka, V., 2012. Mineralogical effects on the detectability of the postperovskite boundary. Proceedings of the National Academy of Sciences 109, 2275–2279.

Gu, Y., Dziewonski, A.M., Ekström, G., 2003. Simultaneous inversion for mantle shear wave velocity and topography of transition zone discontinuities. Geophysical Journal International 154, 559–583.

Guest, A., Schubert, G., Gable, C.W., 2004. Stresses along the metastable wedge of olivine in a subducting slab: possible explanation for the Tonga double seismic layer. Physics of the Earth and Planetary Interiors 141, 253–267.

Hacker, B.R., Abers, G.A., Peacock, S.M., 2003. Subduction factory 1. Theoretical mineralogy, densities, seismic wave speeds, and H_2O contents. Journal of Geophysical Research 108. http://dx.doi.org/10.1029/2001JB001127.

Hager, B.H., Richards, M.A., 1989. Long-wavelength variations in Earth's geoid: physical models and dynamical implications. Philosophical Transactions of the Royal Society of London. Series A 328, 309–327.

Hernandez, E.R., Brodholt, J., Alfè, D., 2015. Structural, vibrational and thermodynamic properties of Mg_2SiO_4 and $MgSiO_3$ minerals from first-principles simulations. Physics of the Earth and Planetary Interiors 240, 1–24.

Hernlund, J.W., Thomas, C., Tackley, P.J., 2005. A doubling of the post-perovskite phase boundary and structure of the Earth's lowermost mantle. Nature 434, 882–886.

Hirose, K., 2002. Phase transitions in pyrolitic mantle around 670-km depth: implications for upwelling of plumes from the lower mantle. Journal of Geophysical Research 107. http://dx.doi.org/10.1029/2001JB000597.

Hirose, K., Fei, Y., 2002. Subsolidus and melting phase relations of basaltic composition in the uppermost lower mantle. Geochimica et Cosmochimica Acta 66, 2099–2108.

Hirose, K., Fei, Y., Ma, Y., Mao, H., 1999. The fate of subducted basaltic crust in the Earth's lower mantle. Nature 397, 53–56.

Hirose, K., Takafuji, N., Sata, N., Ohishi, Y., 2005. Phase transition and density of subducted MORB crust in the lower mantle. Earth and Planetary Science Letters 237, 239–251.

Hirose, K., Sinmyo, R., Sata, Y., Ohishi, Y., 2006. Determination of postperovskite phase transition boundary in $MgSiO_3$ using Au and MgO pressure standards. Geophysical Research Letters 33. http://dx.doi.org/10.1029/2005GL024468.

Hirose, K., Wentzcovitch, R.M., Yuen, D.A., Lay, T., 2015. Mineralogy of the deep mantle — the post-perovskite phase and its geophysical significance. second edition Treatise of Geophysics Vol. 2.05. Elsevier, pp. 85–105.

Hogrefe, A., Rubie, D.C., Sharp, T.G., Seifert, F., 1994. Metastability of enstatite in deep subducting lithosphere. Nature 372, 351–353.

Holland, T.J.B., Hudson, N.F.C., Powell, R., Harte, B., 2013. New thermodynamic models and calculated phase equilibria in NCFMAS for basic and ultrabasic compositions through thetransition zone into the uppermost lower mantle. Journal of Petrology 54, 1901–1920.

Honda, S., Yuen, D.A., Balachandar, S., Reuteler, D., 1993. Three-dimensional instabilities of mantle convection with multiple phase transitions. Science 259, 1308–1311.

Hosoya, T., Kubo, T., Ohtani, E., Sano, A., Funakoshi, K., 2005. Water controls the fields of metastable olivine in cold subducting slabs. Geophysical Research Letters 32.

Houser, C., Masters, G., Flanagan, M., Shearer, P., 2008. Determination and analysis of long-wavelength transition zone structure using SS precursors. Geophysical Journal International 174, 178–194.

Hsu, H., Blaha, P., Cococcioni, M., Wentzcovitch, R.M., 2011. Spin-state crossover and hyperfine interactions of ferric iron in $MgSiO_3$ perovskite. Physical Review Letters 106, 118501.

Hunt, S.A., Weidner, D.J., Li, L., Wang, L., Walte, N.P., Brodholt, J.P., Dobson, D.P., 2009. Weakening of calcium iridate during its transformation from perovskite to postperovskite. Nature Geoscience 2, 794–797.

Hutko, A.R., Lay, T., Revenaugh, J., 2009. Localized double-array stacking analysis of PcP: D″ and ULVZ structure beneath the Cocos Plate, Mexico, central Pacific and north Pacific. Physics of the Earth and Planetary Interiors 173, 60–74.

Ichikawa, H., Kameyama, M., Senshu, H., Kawai, K., Maruyama, S., 2014. Influence of majorite on hot plumes. Geophysical Research Letters 41, 7501–7507.

Ichikawa, H., Yamamoto, S., Kawai, K., Kameyama, M., 2016. Estimate of subduction rate of island arcs to the deep mantle. Journal of Geophysical Research 121, 5447–5460.

Iidaka, T., Furukawa, Y., 1994. Double seismic zone for deep earthquakes in the Izu–Bonin subduction zone. Science 263, 1116–1118.

Inoue, T., et al., 2006. The phase boundary between wadsleyite and ringwoodite in Mg_2SiO_4 determined by in-situ X ray diffraction. Physics and Chemistry of Minerals 33, 106–114.
Irifune, T., 1994. Absence of an aluminous phase in the upper part of the Earth's lower mantle. Nature 370, 131–133.
Irifune, T., Ringwood, A.E., 1987. Phase transformations in a harzburgite composition to 26 GPa: implications for dynamical behaviour of the subducting slab. Earth and Planetary Science Letters 86, 365–376.
Irifune, T., Ringwood, A.E., 1993. Phase transformations in subducted oceanic crust and buoyancy relationships at depths of 600–800 km in the mantle. Earth and Planetary Science Letters 117, 101–110.
Irifune, T., Tsuchiya, T., 2015. Phase transitions and mineralogy of the lower mantle. Treatise of Geophysics Vol. 2.03. Elsevier, pp. 33–60.
Irifune, T., Sekine, T., Ringwood, A.E., Hibberson, W.O., 1986. The eclogite-garnetite transformation at high-pressure and some geophysical implications. Earth and Planetary Science Letters 77, 245–256.
Irifune, T., Ringwood, A.E., Hibberson, W.O., 1994. Subduction of continental crust and terrigenous and pelagic sediments: an experimental study. Earth and Planetary Science Letters 126, 351–368.
Irifune, T., Nishiyama, N., Kuroda, K., Inoue, T., Isshiki, M., Utsumi, W., Funakoshi, K., Urakawa, S., Uchida, T., Katsura, T., Ohtaka, O., 1998. The postspinel phase boundary in the Mg_2SiO_4 determined by in-situ X-ray diffraction. Science 279, 1698–1701.
Ishii, T., Kojitani, H., Akaogi, M., 2011. Post-spinel transitions in pyrolite and Mg_2SiO_4 and akimotoite–perovskite transition in $MgSiO_3$: precise comparison by high-pressure high-temperature experiments with multi-sample cell technique. Earth and Planetary Science Letters 309, 185–197.
Ita, J., King, S.D., 1994. Sensitivity of convection with an endothermic phase change to the form of governing equations, initial conditions, boundary conditions, and equation of state. Journal of Geophysical Research 99, 15,919–15,938.
Ito, E., Takahashi, E., 1989. Post-spinel transformation in the system Mg_2SiO_4–Fe_2SiO_4 and some geophysical implications. Journal of Geophysical Research 94, 10,637–10,646.
Ito, Y., Toriumi, M., 2007. Pressure effect of self-diffusion in periclase (MgO) by molecular dynamics. Journal of Geophysical Research 112. http://dx.doi.org/10.1029/2005JB003685.
Ito, E., Yamada, H., 1982. Stability relations of silicate spinels, ilmenites, and perovskites. In: Akimoto, S., Manghnani, M.H. (Eds.), High-Pressure Research in Mineral Physics. Center Acad. Publ, Tokyo, Japan, pp. 441–464.
Ito, E., Akaogi, M., Topor, L., Navrotsky, A., 1990. Negative pressure–temperature slopes for reactions forming $MgSiO_3$ perovskite from calorimetry. Science 249, 1275–1278.
Jarvis, G.T., McKenzie, D.P., 1980. Convection in a compressible fluid with infinite prandtl number. Journal Fluid Mechanics 9 (6), 515–583.
Jiang, G., Zhao, D., Zhang, G., 2015. Detection of metastable olivine wedge in the western Pacific slab and its geodynamic implications. Physics of the Earth and Planetary Interiors 238, 1–7.
Jin, Z., Zhang, J., Grenn II, H.W., Jin, S., 2001. Eclogite rheology: implications for subducted lithosphere. Geology 29, 667–670.
John, T., Schenk, V., 2003. Partial eclogitisation of gabbroic rocks in a late Precambrian subduction zone (Zambia): prograde metamorphism triggered by fluid infiltration. Contributions to Mineralogy and Petrology 146, 174–191.
Jull, M., Kelemen, P.B., 2001. On the conditions for lower crustal convective instability. Journal of Geophysical Research 106, 6423–6446.
Kaneshima, S., Okamoto, T., Takenaka, H., 2007. Evidence for a metastable olivine wedge inside the subducted Mariana slab. Earth and Planetary Science Letters 258, 219–227.
Kapadia, C.M., Leopold, M.H., 1974. Grain growth in pure dense MgO. Journal of the American Ceramic Society 57, 41–42.
Karato, S., 1989a. Grain growth kinetics in olivine aggregates. Tectonophysics 168, 255–273.
Karato, S., 1989b. Plasticity—crystal structure systematics in dense oxides and its implications for the creep strength of the Earth's deep interior: a preliminary result. Physics of the Earth and Planetary Interiors 55, 234–240.
Karato, S., 2015. Water in the evolution of the Earth and other terrestrial planets. In: Schubert, G. (Ed.), Treatise of Geophysics, second edition Elsevier, pp. 105–144.
Karato, S., Wang, Z., Liu, B., Fujino, K., 1995. Plastic deformation of garnets: systematics and implications for the rheology of the mantle transition zone. Earth and Planetary Science Letters 130, 13–30.
Karato, S., Ridel, M.R., Yuen, D.A., 2001. Rheological structure and deformation of subducted slabs in the mantle transition zone: implications for mantle circulation and deep earthquakes. Physics of the Earth and Planetary Interiors 127, 83–108.
Katayama, I., Karato, S., 2008. Effects of water and iron content on the rheological contrast between garnet and olivine. Physics of the Earth and Planetary Interiors 166, 57–66.
Katsura, T., Ito, E., 1989. The system Mg_2SiO_4–Fe_2SiO_4 at high pressures and temperatures: precise determination of stabilities of olivine, modified spinel, and spinel. Journal of Geophysical Research 94, 15663–15670.
Katsura, T., et al., 2003. Post-spinel transition in Mg_2SiO_4 determined by high P–T in situ X-ray diffractometry. Physics of the Earth and Planetary Interiors 136, 11–24.
Katsura, T., et al., 2004. Olivine–wadsleyite transition in the system (Mg,Fe)2SiO4. Journal of Geophysical Research 109.
Katz, R.F., Spiegelman, M., Langmiur, C.H., 2003. A new parameterization of hydrous mantle melting. Geochemistry, Geophysics, Geosystems 9. http://dx.doi.org/10.1029/2002GC000433.
Kawai, K., Yamamoto, S., Tsuchiya, T., Maruyama, S., 2013. The second continent: existence of granitic continental materials around the bottom of the mantle transition zone. Geoscience Frontiers 4, 1–6.
Kawakatsu, H., Niu, F., 1994. Seismic evidence for a 920-km discontinuity in the mantle. Nature 371, 301–305.
Kawakatsu, H., Yoshioka, S., 2011. Metastable olivine wedge and deep dry cold slab beneath southwest Japan. Earth and Planetary Science Letters 303, 1–10.
Kay, R.W., Kay, S.M., 1993. Delamination and delamination magmatism. Tectonophysics 219, 177–189.
Kerrick, D.M., Connolly, J.A.D., 2001. Metamorphic devolatilization of subducted mid-ocean ridge metabasalts: implications for seismicity, arc magmatism and volatile recycling. Earth and Planetary Science Letters 189, 19–29.
Kerschhofer, L., Sharp, T.G., Rubie, D.C., 1996. Intracrystalline transformation of olivine to wadsleyite and ringwoodite under subduction zone conditions. Science 274, 79–81.
Kerschhofer, L., Rubie, D.C., Sharp, T.G., McConnell, J.D.C., Dupas-Bruzek, C., 2000. Kinetics of intracrystalline olivine–ringwoodite transformation. Physics of the Earth and Planetary Interiors 121, 59–76.
King, S.D., 2016. An evolving view of transition zone and midmantle viscosity. Geochemistry, Geophysics, Geosystems 17, 1234–1237.
King, S.D., Masters, G., 1992. An inversion for radial viscosity structure using seismic tomography. Geophysical Research Letters 19, 1551–1554.
King, S.D., Frost, D.J., Rubie, D.C., 2015. Why cold slabs stagnate in the transition zone. Geology http://dx.doi.org/10.1130/G36320.1 .
Kirby, S.H., Stein, S., Okal, E.A., Rubie, D.C., 1996. Metastable mantle phase transformations and deep earthquakes in subducting oceanic lithosphere. Reviews of Geophysics 34, 261–306.
Koper, K.D., Wiens, D.A., Dorman, L.M., Hildebrand, J.A., Webb, S.C., 1998. Modeling the Tonga slab: can travel time data resolve a metastable olivine wedge? Journal of Geophysical Research 103, 30,079–30,100.
Krystopowicz, N.J., Currie, C.A., 2013. Crustal eclogitization and lithosphere delamination in orogens. Earth and Planetary Science Letters 361, 195–207.
Kubo, T., Ohtani, E., Kato, T., Urakawa, S., Suzuki, A., Kanbe, Y., Funakoshi, K., Utsumi, W., Fujino, K., 2000. Formation of metastable assemblages and mechanisms of the grain-size reduction in the postspinel transformation of Mg_2SiO_4. Geophysical Research Letters 27, 807–810.
Kubo, T., Ohtani, E., Kato, T., Urakawa, S., Suzuki, A., Kanbe, Y., Funakoshi, K., Utsumi, W., Kikegawa, T., Fujino, K., 2002a. Mechanisms and kinetics of the post-spinel transformation in Mg_2SiO_4. Physics of the Earth and Planetary Interiors 129, 153–171.
Kubo, T., Ohtani, E., Kondo, T., Kato, T., Toma, M., Hosoya, T., Sano, A., Kikegawa, T., Nagase, T., 2002b. Metastable garnet in oceanic crust at the top of the lower mantle. Nature 420, 803–806.
Kubo, T., Ohtani, E., Kato, T., Kondo, T., Hosoya, T., Sano, A., Kikegawa, T., 2008. Kinetics of the post-garnet transformation: implications for density and rheology of subducting slabs. Physics of the Earth and Planetary Interiors 170, 181–192.
Kubo, T., Ohtani, E., Kato, T., Shinmaei, T., Fujino, K., 1998. Effect of water on the α-β transformation kinetics in San Carlos olivine. Science 281, 85–87.
Kubo, T., Kaneshima, S., Torii, Y., Yoshioka, S., 2009. Seismological and experimental constraints on metastable phase transformations and rheology of the Mariana slab. Earth and Planetary Science Letters 287, 12–23.
Kung, J., Li, B., Uchida, T., Wang, Y., 2005. In-situ elasticity measurement for the unquenchable high-pressure clinopyroxene phase: implication for the upper mantle. Geophysical Research Letters 32. http://dx.doi.org/10.1029/2004GL021661.
Kuroda, K., Irifune, T., Inoue, T., Nishiyama, N., Miyashita, M., Funakoshi, K., Utsumi, W., 2000. Determination of phase boundary between ilmenite and perovskite in $MgSiO_3$ by in situ X-ray diffraction and quench experiments. Physics and Chemistry of Minerals 27, 523–532.
Lawrence, J., Shearer, P., 2008. Imaging mantle transition zone thickness with SdS-SS finite-frequency sensitivity kernels. Geophysical Journal International 174, 143–158.
Lay, T., Garnero, E.J., 2013. Reconciling the post-perovskite phase with seismological observations of lowermost mantle structure. In: Hirose, K., Brodholt, J., Lay, T., Yuen, D.A. (Eds.), Post-Perovskite: The Last Mantle Phase Transition. American Geophysical Union, Washington, DC http://dx.doi.org/10.1029/174GM11 .
Lebedev, S., Chevrot, S., van der Hilst, R.D., 2002. Seismic evidence for olivine phase changes at the 410- and 660-kilometer discontinuities. Science 296, 1300–1302.
Li, W., Deschamps, F., Tackley, P.J., 2014. Effects of low-viscosity post-perovskite on the stability and structure of primordial reservoirs in the lower mantle. Geophysical Research Letters 41, 7089–7097.
Lin, J., Speziale, S., Mao, Z., Marquardt, H., 2013. Effects of the electronic spin transitions of iron in the lower mantle minerals: implications for deep mantle geophysics and geochemistry. Reviews of Geophysics 51, 244–275.
Litasov, K., Ohtani, E., 2003. Hydrous solidus of CMAS-pyrolite and melting of mantle plumes at the bottom of the upper mantle. Geophysical Research Letters 30. http://dx.doi.org/10.1029/2003GL018318.
Litasov, D.K., Ohtani, E., 2007. Effect of water on the phase relations in Earth's mantle and deep water cycle. In: Ohtani, E. (Ed.), Advances in High-pressure Mineralogy, pp. 115–156.
Litasov, K., Ohtani, E., Suzuki, A., Kawazoe, T., Funakoshi, K., 2004. Absence of density crossover between basalt and peridotite in the cold slabs passing through 660 km discontinuity. Geophysical Research Letters 31. http://dx.doi.org/10.1029/2004GL021306.
Litasov, K.D., Ohtani, E., 2005. Phase relations in hydrous MORB at 18–28 GPa: implications for heterogeneity of the lower mantle. Physics of the Earth and Planetary Interiors 150, 239–263. http://dx.doi.org/10.1016/j.pepi.2004.10.010.
Litasov, D.K., Ohtani, E., Sano, A., Suzuki, A., Funakoshi, K., 2005a. Wet versus cold subduction. Geophysical Research Letters 32. http://dx.doi.org/10.1029/2005GL022921.
Litasov, K., Ohtani, E., Sano, A., Suzuki, A., Funakoshi, K., 2005b. In situ X-ray diffraction study of post-spinel transformation in a peridotite mantle: implication for the 660-km discontinuity. Earth and Planetary Science Letters 238, 311–328.
Liu, X., Zhong, S., 2016. Constraining mantle viscosity structure for a thermochemical mantle using the geoid observation. Geochemistry, Geophysics, Geosystems 17, 17,895–17,913.
Liu, J., Topor, L., Zhang, J., Navrotsky, A., Liebermann, R.C., 1996. Calorimetric study of the coesite stishovite transformation and calculation of the phase boundary. Physics and Chemistry of Minerals 23, 11–16.

Liu, K.H., Gao, S.S., Gao, Y., Wu, J., 2008. Shear wave splitting and mantle flow associated with the deflected Pacific slab beneath northeast Asia. Journal of Geophysical Research 113. http://dx.doi.org/10.1029/2007JB005178.
Machetel, P., Weber, P., 1991. Intermittent layered convection in a model mantle with an endothermic phase change at 670 km. Nature 350, 55–57.
Marquardt, H., Miyagi, L., 2015. Slab stagnation in the shallow lower mantle linked to an increase in mantle viscosity. Nature Geoscience 8, 311–314.
Marquart, G., Schmeling, H., 2000. Interaction of small mantle plumes with the spinel–perovskite phase boundary: implications for chemical mixing. Earth and Planetary Science Letters 177, 241–254.
Marton, F.C., Bina, C.R., Stein, S., Rubie, D.C., 1999. Effects of slab mineralogy on subduction rates. Geophysical Research Letters 26, 119–122.
Marton, F.C., Shankland, T.J., Rubie, D.C., Xu, Y., 2005. Effects of variable thermal conductivity on the mineralogy of subducting slabs and implications for mechanisms of deep earthquakes. Physics of the Earth and Planetary Interiors 149, 53–64.
Matyska, C., Yuen, D.A., 2007. Lower mantle material properties and convection models of multiscale plumes. In: Foulger, G.R., Jurdy, D.M. (Eds.), Plates, Plumes, and Planetary Processes. Geological Society of America, pp. 137–163.
Matyska, C., Yuen, D.A., Wentzcovitch, R.M., Čížková, H., 2011. The impact of variability in the rheological activation parameters on lower-mantle viscosity stratification and its dynamics. Physics of the Earth and Planetary Interiors 188, 1–8.
Mishin, Y., Gerya, T.V., Burg, J., Connolly, J.A.D., 2008. Dynamics of double subduction: numerical modeling. Physics of the Earth and Planetary Interiors 171, 280–295.
Mitrovica, J.X., Forte, A.M., 2004. A new inference of mantle viscosity based upon joint inversion of convection and glacial isostatic adjustment data. Earth and Planetary Science Letters 225, 177–189.
Morishima, H., Kato, T., Suto, M., Ohtani, E., Urakawa, S., Utsumi, W., Shimomura, O., Kikegawa, T., 1994. The phase boundary between α- and β-Mg_2SiO_4 determined by in situ X-ray observation. Science 265, 1202–1203.
Mosenfelder, J.L., Marton, F.C., Ross, C.R., Kerschhofer, L., Rubie, D.C., 2001. Experimental constraints on the depth of olivine metastability in subducting lithosphere. Physics of the Earth and Planetary Interiors 127, 165–180.
Motoki, M.H., Ballmer, M.D., 2015. Intraplate volcanism due to convective instability of stagnant slabs in the mantle transition zone. Geochemistry, Geophysics, Geosystems 16. http://dx.doi.org/10.1002/2014GC005608.
Murakami, M., Hirose, K., Kawamura, K., Sata, N., Ohishi, Y., 2004. Post-perovskite phase transition in $MgSiO_3$. Science 303, 855–858.
Nakagawa, T., Buffett, B.A., 2005. Mass transport mechanism between the upper and lower mantle in numerical simulations of thermochemical mantle convection with multicomponent phase changes. Earth and Planetary Science Letters 230, 11–27.
Nakagawa, T., Tackley, P.J., 2004. Effects of a perovskite-post perovskite phase change near core–mantle boundary in compressible mantle convection. Geophysical Research Letters 31. http://dx.doi.org/10.1029/2004GL020648.
Nakagawa, T., Tackley, P.J., 2005. The interaction between the post-perovskite phase change and a thermo-chemical boundary layer near the core–mantle boundary. Earth and Planetary Science Letters 238, 204–216.
Nakagawa, T., Tackley, P.J., 2011. Effects of low-viscosity post-perovskite on thermo-chemical mantle convection in a 3-D spherical shell. Geophysical Research Letters 38, L04309. http://dx.doi.org/10.1029/2010GL046494.
Nakagawa, T., Tackley, P.J., Deschamps, F., Connolly, J.A.D., 2009. Incorporating selfconsistently calculated mineral physics into thermochemical mantle convection simulations in a 3-D spherical shell and its influence on seismic anomalies in Earth's mantle. Geochemistry, Geophysics, Geosystems 10. http://dx.doi.org/10.1029/2008GC002280.
Nakagawa, T., Tackley, P.J., Deschamps, F., Connolly, J.A.D., 2010. The influence of MORB and harzburgite composition on thermo-chemical mantle convection in a 3-D spherical shell with self-consistently calculated mineral physics. Earth and Planetary Science Letters 296, 403–412.
Nishi, M., Kato, T., Kubo, T., Kikegawa, T., 2008. Survival of pyropic garnet in subducting plates. Physics of the Earth and Planetary Interiors 170, 274–280.
Nishi, M., Kubo, T., Kato, T., 2009. Metastable transformations of eclogite to garnetite in subducting oceanic crust. Journal of Mineralogical and Petrological Sciences 104, 192–198.
Nishi, M., Kubo, T., Kato, T., Tominaga, A., Funakoshi, K., Higo, Y., 2011. Exsolution kinetics of majoritic garnet from clinopyroxene in subducting oceanic crust. Physics of the Earth and Planetary Interiors 189, 47–55.
Nishi, M., Irifune, T., Ohfuji, H., Tange, H., 2012. Intracrystalline nucleation during the post-garnet transformation under large overpressure conditions in deep subducting slabs. Geophysical Research Letters 39. http://dx.doi.org/10.1029/2012GL053915.
Nishi, M., Kubo, T., Ohfuji, H., Kato, T., Nishihara, Y., Irifune, T., 2013. Slow Si–Al interdiffusion in garnet and stagnation of subducting slabs. Earth and Planetary Science Letters 361, 44–49.
Nishihara, Y., Shinmei, T., Karato, S., 2006. Grain-growth kinetics in wadsleyite: effects of chemical environment. Physics of the Earth and Planetary Interiors 154, 30–43.
Nishihara, Y., Tinker, D., Kawazoe, T., Xu, Y., Jing, Z., Matsukage, K.N., Karato, S., 2008. Plastic deformation of wadsleyite and olivine at high-pressure and high-temperature using a rotational Drickamer apparatus (RDA). Physics of the Earth and Planetary Interiors 170, 156–169.
Nishiyama, N., Irifune, T., Inoue, T., Ando, J., Funakoshi, K., 2004. Precise determination of phase relations in pyrolite across the 660 km seismic discontinuity by in situ X-ray diffraction and quench experiments. Physics of the Earth and Planetary Interiors 143-144, 185–199.
Niu, F., Kawakatsu, H., 1997. Depth variation of the mid-mantle seismic discontinuity. Geophysical Research Letters 24, 429–432.
Oganov, A.R., Ono, S., 2004. Theoretical and experimental evidence for a post-perovskite phase of $MgSiO_3$ in Earth's D″ layer. Nature 430, 445–448.
Oguri, K., Funamori, N., Uchida, T., Miyajima, N., Yagi, T., Fujino, K., 2000. Post-garnet transition in a natural pyrope: a multi-anvil study based on in situ X-ray diffraction and transmission electron microscopy. Physics of the Earth and Planetary Interiors 122, 175–186.
Ohta, K., Hirose, K., Lay, T., Sata, N., Ohishi, Y., 2008. Phase transitions in pyrolite and MORB at lowermost mantle conditions: implications for a MORB-rich pile above the core–mantle boundary. Earth and Planetary Science Letters 267, 107–117.
Ohtani, E., Sakai, T., 2008. Recent advances in the study of mantle phase transitions. Physics of the Earth and Planetary Interiors 170, 240–247.
Okamoto, K., Maruyama, S., 2004. The eclogite–garnetite transformation in the MORB + H_2O system. Physics of the Earth and Planetary Interiors 146, 283–296.
Omori, S., Komabayashi, T., Maruyama, S., 2004. Dehydration and earthquakes in the subducting slab: empirical link in intermediate and deep seismic zones. Physics of the Earth and Planetary Interiors 146, 297–311.
Ono, S., Oganov, A.R., 2005. In situ observations of phase transition between perovskite and $CaIrO_3$-type phase in $MgSiO_3$ and pyrolitic mantle composition. Earth and Planetary Science Letters 236, 914–932.
Ono, S., Ito, E., Katsura, T., 2001. Mineralogy of subducted basaltic crust (MORB) from 25 to 37 GPa, and chemical heterogeneity of the lower mantle. Earth and Planetary Science Letters 190, 57–63.
Pankow, K.L., Williams, Q., Lay, T., 2002. Using shear wave amplitude patterns to detect metastable olivine in subducted slabs. Journal of Geophysical Research 107. http://dx.doi.org/10.1029/2001JB000608.
Peltier, W.R., Solheim, L.P., 1992. Mantle phase transitions and layered chaotic convection. Geophysical Research Letters 19, 321–324.
Pennacchioni, G., 1996. Progressive eclogitization under fluid-present conditions of pre-Alpine mafic granulites in the Austroalpine Mt Emilius Klippe (Italian Western Alps). Journal of Structural Geology 18, 549–561.
Piazzoni, A.S., Steinle-Nuemann, G., Bunge, H.P., Dolejs, D., 2007. A mineralogical model for density and elasticity of the Earth's mantle. Geochemistry, Geophysics, Geosystems 8. http://dx.doi.org/10.1029/2007GC001697.
Poirier, J.P., Peyronneau, J., Madon, M., Guyot, F., Revcolevschi, A., 1986. Eutectoid phase transformation of olivine and spinel into perovskite and rock salt structures. Nature 321, 603–605.
Powell, R., Holland, T.J.B., Worley, B., 1998. Calculating phase diagrams involving solid solutions via non-linear equations, with examples using THERMOCALC. Journal of Metamorphic Geology 16, 577–588.
Ricard, Y., Wuming, B., 1991. Inferring the viscosity and the 3-D density structure of the mantle from geoid, topography and plate velocities. Geophysical Journal International 105, 561–571.
Ricard, Y., Mattern, E., Matas, J., 2005. Synthetic tomographic images of slabs from mineral physics. In: van der Hilst, R.D., Bass, J.D., Matas, J., Trampert, J. (Eds.), Changing Views on the Structure, Composition, and Evolution of Earth's Deep. Geophysical Monograph Series Vol. 160. American Geophysical Union, Washington, DC, pp. 285–302.
Richard, G., Mattern, E., Matas, J., 2005. Synthetic tomographic images of slabs from mineral physics. In: van der Hilst, R.D., Bass, J.D., Matas, J., Trampert, J. (Eds.), Changing Views on the Structure, Composition, and Evolution of Earth's Deep. Geophysical monograph series Vol. 160. American Geophysical Union, Washington, DC, pp. 285–302.
Richter, F.M., 1973. Finite amplitude convection through a phase boundary. Geophysical Journal of the Royal Astronomical Society 35, 265–276.
Rickers, F., Fichtner, A., Trampert, J., 2013. The Iceland–Jan Mayen plume system and its impact on mantle dynamics in the North Atlantic region: evidence from full-waveform inversion. Earth and Planetary Science Letters 367, 39–51.
Riedel, M.R., Karato, S., 1997. Grain-size evolution in subducted oceanic lithosphere associated with the olivine-spinel transformation and its effects on rheology. Earth and Planetary Science Letters 148, 27–43.
Ringwood, A.E., 1982. Phase transformations and differentiation in subducted lithosphere: implications for mantle dynamics, basalt petrogenesis, and crustal evolution. Journal of Geology 90, 611–643.
Ringwood, A.E., 1991. Phase transformations and their bearing on the constitution and dynamics of the mantle. Geochimica et Cosmochimica Acta 55, 2083–2110.
Roberge, M., Bureau, H., Bolfan-Casanova, N., Frost, D.J., Raepsaet, C., Surble, S., Khodja, H., Auzende, A.L., Fiquet, G., 2015. Is the transition zone a deep reservoir for fluorine? Earth and Planetary Earth Interior 429, 25–32.
Rubie, D.C., 1984. The olivine–spinel transformation and the rheology of subducting lithosphere. Nature 308, 505–508.
Rubie, D.C., Ross, C.R., 1994. Kinetics of the olivine–spinel transformation in subducting lithosphere: experimental constraints and implications for deep slab processes. Physics of the Earth and Planetary Interiors 86, 223–241.
Rudolph, M.L., Lekic, V., Lithgow-Bertelloni, C., 2015. Viscosity jump in Earth's mid-mantle. Science 350, 1349–1352.
Samuel, H., Tosi, N., 2012. The influence of post-perovskite strength on the Earth's mantle thermal and chemical evolution. Earth and Planetary Science Letters 323-324, 50–59.
Sano, A., Ohtani, E., Litasov, K., Kubo, T., Hosoya, T., Funakoshi, K., Kikegawa, T., 2006. In situ X-ray diffraction study of the effect of water on the garnet–perovskite transformation in MORB and implications for the penetration of oceanic crust into the lower mantle. Physics of the Earth and Planetary Interiors 159, 118–126.
Schmeling, H., Monz, R., Rubie, D.C., 1999. The influence of olivine metastability on the dynamics of subduction. Earth and Planetary Science Letters 165, 55–66.
Schmidt, M.W., Poli, S., 1998. Experimentally based water budgets for dehydrating slabs and consequences for arc magma generation. Earth and Planetary Science Letters 163, 361–379.
Schubert, G., Yuen, D.A., Turcotte, D.L., 1975. Role of phase transitions in a dynamic mantle. Geophysical Journal of the Royal Astronomical Society 42, 705–735.

Shahnas, M.H., Peltier, W.R., Wu, Z., Wentzcovitch, R.M., 2011. The high-pressure electronic spin transition in iron: potential impacts upon mantle mixing. Journal of Geophysical Research 116. http://dx.doi.org/10.1029/2010JB007965.
Sharp, T.G., Rubie, D.C., 1995. Catalysis of the olivine to spinel transformation by high clinoenstatite. Science 269, 1095–1098.
Sidorin, I., Gurnis, M., Helmberger, D.V., 1999. Evidence for a ubiquitous seismic discontinuity at the base of the mantle. Science 286, 1326–1329.
Smyth, J.R., Frost, D.J., 2002. The effect of water on the 410-km discontinuity: an experimental study. Geophysical Research Letters 29. http://dx.doi.org/10.1029/2001GL014418.
Speziale, S., Milner, A., Lee, V.E., Clark, S.M., Pasternak, M.P., Jeanloz, R., 2005. Iron spin transition in the Earth's mantle. Proceedings of the National Academy of Sciences 102, 17918–17922.
Steinberger, B., Calderwood, A.R., 2006. Models of large-scale viscous flow in the Earth's mantle with constraints from mineral physics and surface observations. Geophysical Journal International 167, 1461–1481.
Stern, R.J., Scholl, D.W., 2010. Yin and yang of continental crust creation and destruction by plate tectonic processes. International Geology Review 52, 1–31.
Stixrude, L., Lithgow-Bertelloni, C., 2011. Thermodynamics of mantle minerals — II. Phase equilibria. Geophysical Journal International 184, 1180–1213.
Stixrude, L., Lithgow-Bertelloni, C., 2012. Geophysics of chemical heterogeneity in the mantle. Annual Review of Earth and Planetary Sciences 40, 569–595.
Sung, C., Burns, R.G., 1976. Kinetics of high-pressure phase transformations: implications to the evolution of the olivine + spinel transition in the downgoing lithosphere and its consequences on the dynamics of the mantle. Tectonophysics 31, 1–32.
Suzuki, A., Ohtani, E., Morishima, H., Kubo, T., Kanbe, Y., Kondo, T., Okada, T., Terasaki, H., Kato, T., Kikegawa, T., 2000. In situ determination of the phase boundary between wadsleyite and ringwoodite in Mg_2SiO_4. Geophysical Research Letters 27, 803–806.
Tackley, P.J., 1996. On the ability of phase transitions and viscosity layering to induce long wavelength heterogeneity in the mantle. Geophysical Research Letters 23, 1985–1988.
Tackley, P.J., 2012. Dynamics and evolution of the deep mantle resulting from thermal, chemical, phase and melting effects. Earth-Science Reviews 110, 1–25.
Tackley, P.J., 2015. Mantle geochemical geodynamics. In: Schubert, G. (Ed.), Treatise of Geophysics, second edition Elsevier, pp. 521–585.
Tackley, P.J., Stevenson, D.J., Glatzmaier, G.A., Schubert, G., 1993. Effects of an endothermic phase transition at 670 km depth in a spherical model of convection in the Earth's mantle. Nature 361, 699–704.
Tackley, P.J., Stevenson, D.J., Glatzmaier, G.A., Schubert, G., 1994. Effects of multiple phase transitions in a three-dimensional spherical model of convection in Earth's mantle. Journal of Geophysical Research 99, 15,877–15,901.
Tackley, P.J., Xie, S., Nakagawa, T., Hernlund, J.W., 2005. Numerical and laboratory studies of mantle convection: philosophy, accomplishments and thermo-chemical structure and evolution. In: van der Hilst, R.D., Bass, J.D., Matas, J., Trampert, J. (Eds.), Earth's Deep Mantle: Structure, Composition and Evolution. Geophysical Monograph Series. American Geophysical Union, Washington D.C. http://dx.doi.org/10.1029/160GM07 .
Tackley, P.J., Nakagawa, T., Hernlund, J.W., 2007. Influence of the post-perovskite transition on thermal and thermo-chemical mantle convection. In: Hirose, K., Brodholt, J.P., Lay, T., Yuen, D.A. (Eds.), Post-perovskite: The Last Mantle Phase Transition. Geophysical Monograph Series Vol. 174. American Geophysical Union, Washington D.C., pp. 229–248.
Tagawa, M., Nakakuki, T., Tajima, F., 2007. Dynamical modeling of trench retreat driven by the slab interaction with the mantle transition zone. Earth, Planets and Space 59, 65–74.
Tateno, S., Hirose, K., Sata, N., Ohishi, Y., 2009. Determination of post-perovskite phase transition boundary up to 4400 K and implications for thermal structure in D″ layer. Earth and Planetary Science Letters 277, 130–136.
Tetzlaff, M., Schmeling, H., 2000. The influence of olivine metastability on deep subduction of oceanic lithosphere. Physics of the Earth and Planetary Interiors 120, 29–38.
Tetzlaff, M., Schmeling, H., 2009. Time-dependent interaction between subduction dynamics and phase transition kinetics. Geophysical Journal International 178, 826–844.
Torii, Y., Yoshioka, S., 2007. Physical conditions producing slab stagnation: constraints of the Clapeyron slope, mantle viscosity, trench retreat, and dip angles. Tectonophysics 445, 200–209.
Tosi, N., Yuen, D.A., 2011. Bent-shaped plumes and horizontal channel flow beneath the 660 km discontinuity. Earth and Planetary Science Letters 312, 348–359.
Tosi, N., Yuen, D.A., Čadek, O., 2010. Dynamical consequences in the lower mantle with the post-perovskite phase change and strongly depth-dependent thermodynamic and transport properties. Earth and Planetary Science Letters 298, 229–243.
Tsuchiya, T., Tsuchiya, J., Umemoto, K., Wentzcovitch, R.M., 2004. Phase transition in $MgSiO_3$ perovskite in the Earth's lower mantle. Earth and Planetary Science Letters 224, 241–248.
Tsujino, N., Nishihara, Y., 2009. Grain-growth of ferropericlase at high-pressure. Physics of the Earth and Planetary Interiors 174, 145–152.
van den Berg, A.P., Hoop, M.V.D., Yuen, D.A., Duchkov, A., van der Hilst, R.D., Jacobs, M.H., 2010. Geodynamical modeling and multiscale seismic expression of thermo-chemical heterogeneity and phase transitions in the lowermost mantle. Physics of the Earth and Planetary Interiors 180, 244–257.
Van Hunen, J., van der Berg, A.P., Vlaar, N.J., 2001. Latent heat e¡ects of the major mantle phase transitions on low-angle subduction. Earth and Planetary Science Letters 190, 125–135.
van Keken, P.E., Ballentine, C.J., 1998. Whole-mantle versus layered mantle convection and the role of a high-viscosity lower mantle in terrestrial volatile evolution. Earth and Planetary Science Letters 156, 19–32.
van Keken, P.E., Ballentine, C.J., 1999. Dynamical models of mantle volatile evolution and the role of phase transitions and temperature-dependent rheology. Journal of Geophysical Research 104, 7137–7151.
van Keken, P.E., Karato, S., Yuen, D.A., 1996. Rheological control of oceanic crust separation in the transition zone. Geophysical Research Letters 23, 1821–1824.
van Mierlo, W.L., Langenhorst, F., Frost, D.J., Rubie, D.C., 2013. Stagnation of subducting slabs in the transition zone due to slow diffusion in majoritic garnet. Nature Geoscience 6, 400–403.
Vanacore, E., Niu, F., Kawakatsu, H., 2006. Observations of the mid-mantle discontinuity beneath Indonesia from S to P converted waveforms. Geophysical Research Letters 33. http://dx.doi.org/10.1029/2005GL025106.
Vaughan, P.J., Coe, R.S., 1981. Creep mechanism in $Mg2SiO_4$: effects of a phase transition. Journal of Geophysical Research 86, 389–404.
Vilella, K., Shim, S., Farnetani, C.G., Badro, J., 2015. Spin state transition and partitioning of iron: effects on mantle dynamics. Earth and Planetary Science Letters 417, 57–66.
Wang, Y., Martinez, I., Guyot, F., Liebermann, R.C., 1997. The breakdown of olivine to perovskite and magnesiowustite. Science 275, 510–514.
Wang, C., Yoneda, A., Osako, M., Ito, E., Yoshino, T., Jin, Z., 2014. Measurement of thermal conductivity of omphacite, jadeite, and diopside up to 14 GPa and 1000 K: implication for the role of eclogite in subduction slab. Journal of Geophysical Research 119, 6277–6287.
Wentzcovitch, R.M., Justo, J.F., Wu, Z., da Silva, C.R.S., Yuen, D.A., Kohlstedt, D., 2009. Anomalous compressibility of ferropericlase throughout the iron spin cross-over. Proceedings of the National Academy of Sciences 106, 8447–8452.
Wiens, D.A., McGuire, J.J., Shore, P.J., 1993. Evidence for transformational faulting from a deep double seismic zone in Tonga. Nature 364, 790–793.
Wookey, J., Stackhouse, S., Kendall, J.M., Brodholt, J., Price, G.D., 2005. Efficacy of the post-perovskite phase as an explanation for lowermost-mantle seismic properties. Nature 438, 1004–1007.
Xu, W.B., Lithgow-Bertelloni, C., Stixrude, L., Ritsema, J., 2008. The effect of bulk composition and temperature on mantle seismic structure. Earth and Planetary Science Letters 275, 70–79.
Xu, S., Shim, S., Morgan, D., 2015. Origin of Fe^{3+} in Fe-containing, Al-free mantle silicate perovskite. Earth and Planetary Science Letters 409, 319–328.
Yamazaki, D., Kato, T., Ohtani, E., Toriumi, M., 1996. Grain growth rates of $MgSiO_3$ perovskite and periclase under lower mantle conditions. Science 274, 2052–2054.
Yamazaki, D., Inoue, T., Okamoto, M., Irifune, T., 2005. Grain growth kinetics of ringwoodite and its implication for rheology of the subducting slab. Earth and Planetary Science Letters 236, 871–881.
Yamazaki, D., Matsuzaki, T., Yoshino, T., 2010. Grain growth kinetics of majorite and stishovite in MORB. Physics of the Earth and Planetary Interiors 183, 183–189.
Yanagisawa, T., Yamagishi, Y., Hamano, Y., Stegman, D.R., 2011. Mechanism for generating stagnant slabs in 3-D spherical mantle convection models at Earth-like conditions. Physics of the Earth and Planetary Interiors 183, 341–352.
Ye, Y., Gu, C., Shim, S., Meng, Y., Prakapenka, V., 2014. The postspinel boundary in pyrolitic compositions determined in the laser-heated diamond anvil cell. Geophysical Research Letters 41, 3833–3841.
Yoshino, T., Yamazaki, D., 2007. Grain growth kinetics of $CaIrO_3$ perovskite and post-perovskite, with implications for rheology of D″ layer. Earth and Planetary Science Letters 255, 485–493.
Yu, Y.G., Wentzcovitch, R.M., Tsuchiya, T., Umemoto, K., Weidner, D.J., 2007. First principles investigation of the postspinel transition in Mg_2SiO_4. Geophysical Research Letters 34. http://dx.doi.org/10.1029/2007GL029462.
Yu, Y.G., Wu, Z., Wentzcovitch, R.M., 2008. Alpha–beta–gamma transformations in Mg2SiO4 in Earth's transition zone. Earth planet. Science Letters 273, 115–122.
Yu, Y.G., Wentzcovitch, R.M., Vinograd, V.L., Angel, R.J., 2011. Thermodynamic properties of $MgSiO_3$ majorite and phase transitions near 660 km depth in $MgSiO_3$ and $Mg2SiO_4$: a first principles study. Journal of Geophysical Research 116. http://dx.doi.org/10.1029/2010JB007912.
Yuen, D.A., Monnereau, M., Hansen, U., Kameyama, M., Matyska, C., 2007. Dynamics of superplumes in the lower mantle. In: Yuen, D.A., Maruyama, S., Karato, S., Windley, B.F. (Eds.), Superplumes: Beyond Plate Tectonics. Springer Verlag, Heidelberg, pp. 239–268.
Zhang, J., Li, B., Utsumi, W., Liebermann, R.C., 1996. In situ X-ray observations of the coesite stishovite transition: reversed phase boundary and kinetics. Physics and Chemistry of Minerals 23, 1–10.
Zhong, S., Gurnis, M., 1994. Role of plates and temperature dependent viscosity in phase change dynamics. Journal of Geophysical Research 99, 15,903–15,917.
Zhong, S., Gurnis, M., 1995. Mantle convection with plates and mobile, faulted plate margins. Science 267, 838–843.